THE "SCHEI" SANDUR

HYDROLOGIC AND SEDIMENTARY ASPECTS OF THE "SCHEI" SANDUR, ELLESMERE ISLAND, N. W. T.

by

BRUCE GEORGE BENNETT

A Thesis

Submitted to the Department of Geography

in Partial Fulfilment of the Requirements

for the Degree

Bachelor of Arts

McMaster University

April, 1975

PREFACE

In late February, 1972, an oil find at Romulus Lake, near Eureka, Ellesmere Island, generated interest about future pipeline development in south central Ellesmere Island and the feasibility of pipeline construction to the eastern coastal area. The most suitable potential pipeline corridor through this region extends from the north shore of Bay Fiord to Irene Bay, along the western margin of the Ellesmere Island Ice Cap to the head of Vendom Fiord, and thence through the Vendom-Makinson isthmus to Makinson Inlet, leading to the navigable waters of Smith Sound (see McCann et al., 1972).

Sandur plains are numerous and constitute a dynamic element of the landscape within this corridor. Information was clearly required of the processes and responses operating in this distinctive environment. Accordingly, a small sandur was selected for detailed investigation in the primary study area, adjacent to the western margin of the Ellesmere Island Ice Cap at the head of Vendom Fiord (78^{o} 03' N, 82^{o} 17' W). During the summers of 1973 and 1974 a detailed study of the hydrologic regime and sedimentological characteristics of the "Schei" River sandur was carried out, the results of which constitute this thesis. This work was one part of a continuing research project initiated in 1972 by members of the Geography

Department, McMaster University, concerned with the broad range of hydrologic conditions operating along this corridor.

Principal rivers in the study area were named by J. G. Cogley (in McCann et al., 1972) after members of the O. Sverdrup Second Norwegian North Polar Expedition - the initial expedition to explore the area from 1898 - 1902. In this account, the "Schei" and "Sverdrup" rivers have not been designated in quotation marks, though they are unofficial piace names.

ABSTRACT

During the summers of 1973 and 1974 processes and related responses operating on a small High Arctic sandur (basin area 91 km^2) were studied. Several aspects related to the sandur were investigated, including the hydrologic regime of surface runoff, channel hydraulic conditions, sediment transport, and the morphology of the channels and sandur surface.

Summer climatic conditions strongly affected surface runoff due to their influence on snowmelt, glacial melt, and summer precipitation. There was a noticeable diurnal rhythm in streamflow in response to snowmelt and glacial melt. The influences of ice blockage effects on streamflow were also observable. A shallow active layer resulted in a rapid response of surface runoff to snowmelt, glacial melt, and rainfall sources.

These aspects of the hydrologic regime strongly affected the hydraulic conditions of the streams. The main hydraulic adjustment was produced by changes in velocity which led to rapid changes in flow resistance and resulted in large variations in the rates of sediment transport. Estimates of the stream load in the 1974 summer confirmed that the bulk of the sediment was carried as bedload.

Channel bar forms which reflected hydraulic conditions changed considerably over a summer period. On a long term basis, the form of the channel longitudinal profile indicated an adjustment to downstream hydraulic conditions while the surface morphology and sediment distribution over the sandur revealed the two-dimensional variations in channel processes.

ACKNOWLEDGMENTS

Gratitude is expressed to Dr. S. B. McCann, the author's thesis advisor, who provided an opportunity for the author to carry out the present study. He offered ample encouragement during all phases of this work. Dr. M. K. Woo is entitled to a special thanks for his constant interest and inspiration in the study. Graham Cogley was very helpful for providing considerable advice and assistance in the field.

Assistance in the field was also provided by Edward McTavish, Piotr Blachut, and Susan Wilkins in 1973, and by Richard Gillie, Randy Crispo, and Colin Ballantyne in 1974.

Appreciation is extended to John Smith for his assistance in the lab, and to Wendy Minor who performed part of the chore of data reduction. Dr. M. K. Woo and Colin Ballantyne provided some pertinent information based on their analyses of field data, and they collaborated in the interpretation of results. Ms. F. Hein and Dr. R. G. Walker also took part in many useful discussions pertaining to the study.

The preparation of some material for photographic re-

production was provided by Mr. J. Whorwood and Mr. R. Bignell.

The author is most grateful to Ms. V. Bennett for her patient and careful efforts in typing the manuscript, and my parents for their considerable support. A special thanks to Ms. K. Jaques for her encouragement and endurance during the many setbacks and frustrations during this undertaking.

The project, from which this thesis is a product, was funded by Glaciology Division of Environment Canada; the funding was arranged by Dr. O. Løken, head of Glaciology Division. Funds were also provided by National Research Council grants to Dr. S. B. McCann.

Any errors in this thesis must be attributed to the author, and not be a reflection on the project from which the study is derived from.

CONTENTS

FIGURES

TABLES

UNITS AND NOTATIONS

The following is a list of symbols used in this text. Abbreviations for measurement units include:

μm,mm,cm,m,km	micrometre, millimetre, centimetre, metre, kilometre
mg, g	milligram, gram
ml, l	millilitre, litre
s, hr(h)	second, hour
C	centigrade degrees

Other abbreviations are:

a.s.l.	(elevation) above sea level
B.P.	(years) before present
ppm	parts per million
Ø	phi ($-\log_2 D$)

Symbols are as follows:

A	area
a	coefficient in relation $W_s = aQ^b$ or $Y = aY^b$
a_1, a_2	exponent and coefficient respectively in relation $Y = a_2 e^{a_1 x}$
$\overline{B}$	mean cobble size
b	exponent in relation $W_s = aQ^b$ or $Y = aX^b$
c	conductivity; coefficient in relation $\overline{d} = cQ^f$
D, D_c, D_s, D_m	particle size; critical particle size, average particle size, mean particle size (D_{50})

D_{50}, (D_{90})	particle size where 50 (90) per cent of the material is finer
$\bar{d}$	mean water depth
E	evaporation; elevation
e	base of natural logarithms
e_{ij}	residual
f	exponent in relation $\bar{d} = cQ^f$
g	acceleration due to gravity
g'_s	specific rate of bedload sediment transported by submerged weight
H_t	total hardness
K_r	coefficient of particle roughness
K_t	coefficient of mean flow resistance
k	coefficient in relation $\bar{u} = kQ^m$
M	Folk and Ward's graphic mean
m	exponent in relation $\bar{u} = kQ^m$
N	sample number; number of counted clasts in photograph sediment analysis
n	Manning's roughness coefficient
p	precipitation
Q	discharge; runoff
R	hydraulic radius
r	correlation coefficient
S	water surface slope
s	suspended sediment concentration

$\bar{u}$, u_*, u_{*_c}	mean velocity; shear (friction) velocity; critical shear velocity
W_s	water surface width
$W_s/\bar{d}$	width-depth ratio
X,Y	discrete location coordinates of map area in trend surface analysis
x	distance in relation $Y = a_2 e^{a_1 x}$
Y	height in relation $Y = a_2 e^{a_1 x}$
y	stage
Z	observed value in trend surface analysis
ff	Darcy-Weisbach resistance coefficient (friction factor)
γ_f	specific gravity of fluid
γ_s	specific gravity of sediment
$\emptyset$	particle inertia
$1/\Psi$	entrainment function
θ	energy gradient of stream
α	coefficient of trend in trend surface analysis
β	Shield's beta
ρ_f	fluid density
ρ_s	sediment density
τ_o, τ_c	tractive force (shear stress) acting on channel bottom; critical tractive force

CHAPTER I

INTRODUCTION AND REVIEW

1.1 INTRODUCTION

Sandur (pl. sandar) is an Icelandic term which refers to an outwash plain. It has been widely accepted as glacial outwash deposits formed by meltwaters in a proglacial zone. Krigstrom (1962) distinguished two types of sandar: dalsandur (valley sandur) and slattlandssandur (plain sandur). In glacierized regions of the Canadian Arctic, sandur, as valley fill deposits, are the dominant contemporary fluvial landform in the lower portions of many arctic basins. To a lesser extent in some nonglacierized areas, similar deposits may also occur.

These extensive fluvial outwash plains are composed of coarse clastic sediment deposited as valley fills, and exhibit surfaces which possess gradients of usually less than 5^{o}. Sandar are generally areas of aggradation, with aggradation rates generally depending on the amount of sediment-water load carried by the braided streams. Sandur streams are usually characterized by considerable coarse sediment transport rates, high competence, and abundant sediment loads. These continually shifting high energy streams locally influence erosion and

deposition over the outwash, and hence affect the nature of the alluvial deposits. The absence of vegetation on the active outwash surfaces indicates the unstable and variable characteristics of the braided channels.

This study is concerned with the fluvial processes and deposits which characterize a small valley sandur (dalsandur) at the head of Vendom Fiord, Ellesmere Island (Fig. 1.1). The primary purpose of the investigation was to study aspects of the hydrologic and sedimentological environment of the Schei sandur, concentrating the study mainly in the upper portion of the outwash surface.

1.2 LITERATURE REVIEW

Texts dealing with fluvial processes in a periglacial environment have generally devoted only limited discussion to the importance of fluvial activity. Tricart (1969) has suggested that the Arctic possesses a distinctive environment due to the inhibition of geomorphic processes operating in this high latitude cold climate. Bird (1967) and Embleton and King (1968) give only a limited treatment of fluvial geomorphic processes, although they suggest its importance may be appreciable. Distinctive periglacial landforms usually discussed of the arctic environment include patterned ground,

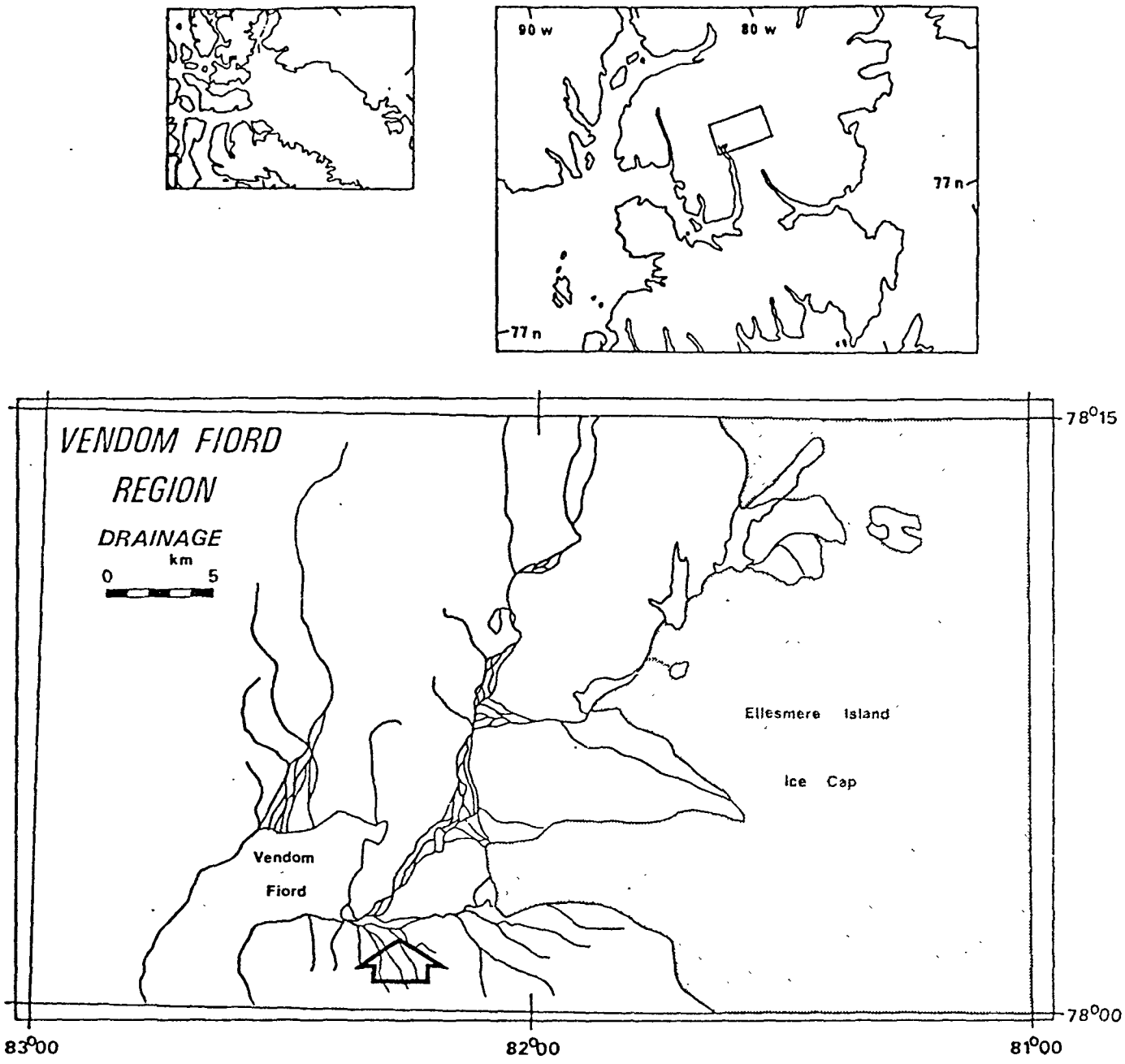

Figure 1.1 Location of the study area, marked by the arrow on the main map.

Inset maps show the general location within Ellesmere Island..

blockfields, antiplanation terrace features, frost cracks and frost-heaving phenomena, solifluction movement, and slope deposits.

Fluvial activity is significant with respect to erosion, transportation, and deposition of material, even though runoff only occurs during the brief summer season. Flow does not occur over the winter months. Runoff over the relatively bare ground surface, underlain by permafrost, is concentrated during the spring snowmelt freshet and leads to considerable sediment transport during this short period. Precipitation as summer rainfall, and in some basins, glacial meltwater, also provide considerable runoff during the summer season and hence provide an impetus for significant sediment transport and reworking.

The earliest High Arctic observations came from Tarr's (1897) research of fluvial erosion by meltwater channels on Baffin Island. Rudberg (1963) realized the importance of the effects of water as the major geomorphic agent acting on the ground in western Axial Heiberg Island. Cook (1967), working on the Mecham River, Cornwallis Island, concluded that the spring snowmelt freshet was primarily important in transporting the bulk of weathered products from other processes, although not in itself producing significant erosion. Pissart (1967) noted the importance of fluvial activity

and erosion on Prince Patrick Island, especially during heavy summer rainfall events (a conclusion similarly reached by Rudberg).

Rapp (1960) discovered that solution transport of salts were the most effective transport process in Karkevagge, northern Scandinavia. Østrem, Bridge, and Rannie (1967) have shown the importance of fluvial processes and sediment transport in arctic proglacial streams on Baffin Island. Arnborg, Walker, and Peippo (1967), working in northern Alaska, reported the bulk of runoff and sediment transport occurred during the spring flood. Adams (1966) and Maag (1969) have investigated in detail glacial drainage and runoff aspects in a proglacial zone on Axel Heiberg Island. Maag in particular discusses the effectiveness of concentrated fluvial processes, and a specific aspect of fluvial erosion by thaw action. Cogley (1971) studied solution and suspended transport in two non-glacierized arctic basins on Cornwallis and Devon Islands, and concluded appreciable quantities of solutes and detritus are removed during the annual thaw season. McCann, Howarth, and Cogley (1972) similarly have quantatively reported on the role of water as an agent of considerable sediment transport. The most comprehensive treatment of fluvial processes in arctic watersheds has been investigated by Church (1972) working in proglacial areas on Baffin Island. Church discusses the significance of sediment transport on sandur rivers,

especially the dominance of bedload transport influencing fluvial processes in this particular environment.

One of the first investigations of significance on sandur processes was carried out by Thorarinsson (1939) on Hofellsjokull, Iceland. Hjulstrom et al. (1954-57) reported on detailed morphologic and hydrologic studies carried out on the Hoffellssandur, Iceland, and also included discussions of the geology, geomorphology, and climate in the area. Krigstrom (1962) qualitatively discussed channel processes related to braiding and channel bar formation on sandar in Iceland, while Doeglas (1962) investigated structures in sedimentary deposits on proglacial braided outwash. Fahnestock (1963) presented the first detailed analysis of fluvial and morphologic processes on the dalsandur of Emmons Glacier, Washington. In 1971, McDonald and Banerjee reported on an investigation of sediments and bedforms of recent braided outwash plains and a braided valley fill, and compared the modern environments to Pleistocene outwash sediments. Williams and Rust (1969) have investigated sedimentary features of braided outwash in the Donjek River, Yukon.

Recent studies of sandur have provided further knowledge of sandur processes and associated features. Church (1972) has published perhaps the most authoritative investigation of hydrologic and sedimentary characteristics of sandur processes on two sandar on Baffin

Island. Numerous aspects of the hydrological and sedimentological environment of sandar have been discussed by Church, relative to a generalized process-response model. Boothroyd (1972) reported on deposition processes, and morphologic and sedimentary analyses, on portions of the coarse-grained outwash fan of the Scott Glacier, Alaska. Smith, D. (1973) examined sediment rates and processes of aggradation on the Alexandra - N. Saskatchewan outwash. Fahnestock and Bradley (1973) discuss channel features on the braided outwash of the Knik and Matanuska Rivers, in Alaska. Smith, N. (1974) investigated bar formation and sediment distribution patterns on the Kicking Horse outwash plain, B.C. Hein (1974) recently continued the earlier work of Smith, N., in studying shallow coarse-grained braided deposits and processes in the Kicking Horse outwash sediments.

1.3 A PROCESS-RESPONSE MODEL

A sandur surface can be treated as an open system where energy-mass exchanges with the surroundings are allowed to pass freely through the boundaries, relating the form to the process. Interactions between process and response elements are complicated. Conceptually, however, a process-response model for a sandur can be formulated as follows:

1. The hydrologic regime affects the temporal and spatial variations in the hydraulic parameters.
2. The hydraulic parameters in turn affect the rates of erosion, sediment transport, and depositional processes.
3. These processes rearrange the geometry of the sandur surface.
4. The geomorphology of the sandur represents a long term response to the above noted processes.

1.4 FIELD PROGRAM

This model provided a basis for planning a field program of data collection which allows process and response elements within the sandur to be related. The boundaries of the system are as follows: the upper limit of the sandur lies immediately below the hogback ridge where the Schei River emerges from a narrow gorge; the lower limit is at the confluence with the Sverdrup River and terraces form its lateral boundaries (Figs. 1.2 and 1.3).

Response elements are the easiest to examine, and the morphology and sediments of the whole sandur were investigated on a sample basis. A more detailed investigation of the processes and related responses was carried out in the upper part of the sandur, and involved a consideration of variations in stream discharge,

SCHEI VALLEY AREA: view east. flown August, 1950
photograph number T461R-131. National Air Photo Library
Surveys and Mapping Branch D.E.M.R.

Figure 1.2 Schei River sandur and vicinity, at the head of Vendom Fiord, Ellesmere Island.

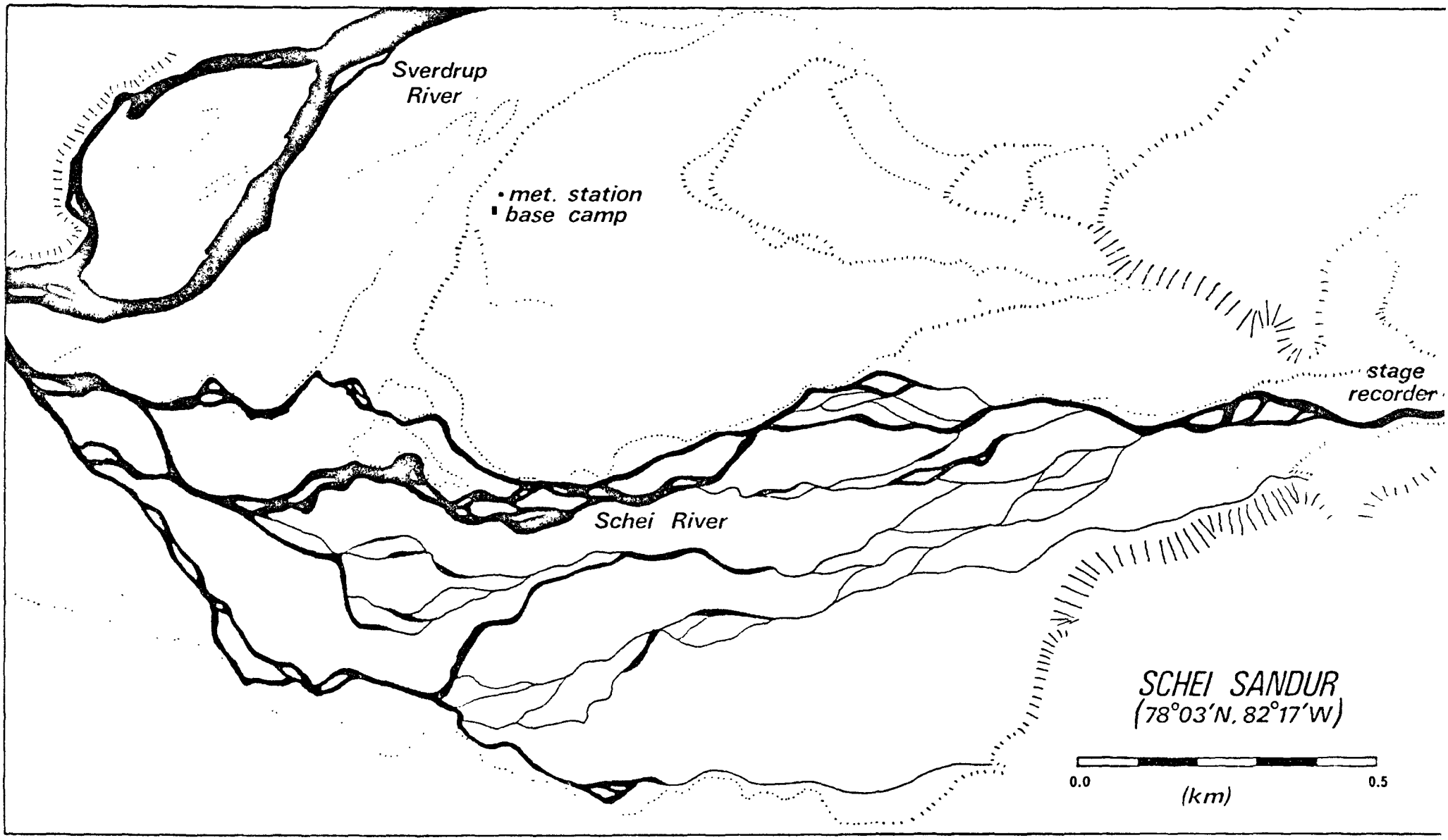

Figure 1.3 The field area showing location of the base camp and installations.

channel hydraulics and sediment transport; these processes induced changes in the channel pattern and form, resulting in channel bar alterations and braiding. The results from this detailed study have application to the overall sandur system.

1.5 OUTLINE

Chapter II examines the boundary conditions of the region and study area, discussing the bedrock geology and unconsolidated deposits, and commenting on the temporal variations in the weather which are viewed as energy inputs. The next two chapters outline the transfer processes studied. Chapter III reviews the hydrologic regime, while Chapter IV considers the sediment transported during the summer period. Chapter V discusses the hydraulics of the river as related to its influence on the response elements - the morphology and sediments of the sandur. Chapter VI summarizes the results of the study.

CHAPTER II

ENVIRONMENT CHARACTERISTICS OF SOUTH-CENTRAL ELLESMERE ISLAND

2.1 BEDROCK GEOLOGY

The geology of Ellesmere Island is mainly comprised of rocks of Phanerozoic age, underlain by the northern extension of the Precambrian Canadian Shield. The following geologic summary is based on accounts by Thorsteinsson and Tozer (1960) and Norris (in Fortier et al., 1963).

The southeastern section of Ellesmere Island is composed of Precambrian granite gneisses and migmatites. Overlying this Precambrian basement to the north and west occurs an unconformable succession of lower Paleozoic (Cambrian to Upper Devonian), Triassic, Cretaceous, and Tertiary sedimentary strata.

In the Vendom Fiord study area (Fig. 2.1) the lower Paleozoic sequence commences with the Middle Ordovician carbonates of the Thumb Mountain and Irene Bay Formations of the Cornwallis Group. This is succeeded by the Upper Ordovician, Silurian, and Lower Devonian carbonates of the Allen Bay and Read Bay Formations, which are disconformably overlain by the Lower Devonian carbonate, evaporite, and clastic rocks of the Vendom Fiord Formation. Occurring over the Vendom Fiord

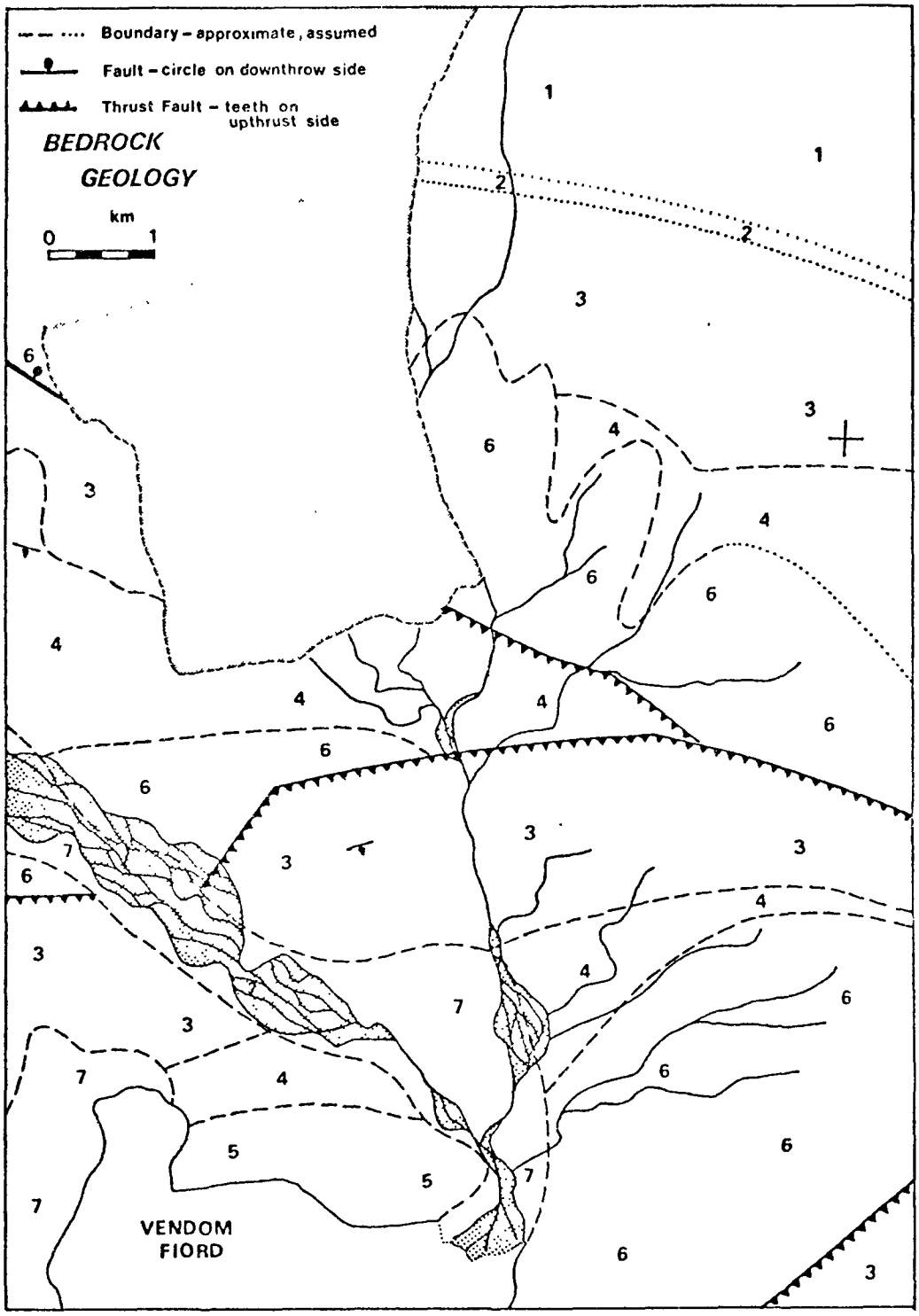

Figure 2.1 Geology of the Vendom Fiord area.

Formation is the Lower and Middle carbonates of the Blue Fiord Formation.

The Tertiary non-marine sediments of the Eureka Sound Formation rests unconformably as outliers over the Paleozoic Formations. Deposits of the Eureka Sound beds include sandstone, shale, conglomerate, and coal.

Structurally, the area is part of the Arctic Lowland and Franklinian Miogeosyncline provinces, and reveals a complicated structural history. The two major deformational events affecting the area were the late Devonian Ellesmerian Orogeny and the Eurekan Orogeny in the Cenozoic. The Ellesmerian Orogeny produced fold structures within the area and the more extensive Central Ellesmere Fold Belt. The Eurekan Orogeny resulted in thrust faults, with normal faulting probably postdating this tectonic event.

2.2 QUATERNARY EVOLUTION

Extensive glaciations of Ellesmere Island by the beginning of the Quaternary period resulted in the present form of the mountain, plateau, and lowland regions. The preglacial valleys and fiords have undoubtedly been reduced below former levels by glacial erosion during the Pleistocene epoch. All of Ellesmere Island was probably covered at the last glacial maximum about 17,000 to 20,000 years B.P. (Andrews, 1970).

Following the last major glacial maximum, ice retreat and decay of the Innuitian Ice Sheet resulted in an independent remnant ice cap in eastern Ellesmere Island. Hodgson (1972) suggests that a readvance and stillstand of the ice cap occurred about 7,500 to 8,500 years B.P., after the general deglaciation of west-central Ellesmere Island, and that it is comparable to the "Cockburn" phase of Baffin Island (Falconer et al., 1965). Hodgson (1972) and Ballantyne (personal communication) have summarized evidence to indicate that a readvance of the ice margin, and invasion of open water conditions, occurred in the Vendom Fiord area during this period.

Fluvial activity probably commenced in the valleys following further ice retreat and a drop in sea level about 7,000 years B.P. (Ballantyne, personal communication). Evidence of base level changes and rapid postglacial uplift since the occurrence of fluvial activity is given by the dissection of remnant alluvial fans and deltas. Numerous underfit gorges and gullies, and the extent and size of the older fluvial deposits in the Vendom Fiord region, suggest that fluvial activity and seasonal runoff were greater in postglacial time than at present. Church (1972), working in Baffin Island, concludes that fluvial sedimentation and erosion were particularly active during the warmer Hypsithermal period of postglacial time.

Portions of the ice margin have shown a late readvance about 200 to 400 years ago, as evidenced by recent moraine ridges adjacent to the ice cap, and now reveal a recession to the present position of the ice cap. The nature of the "sub-polar" ice cap and little change in

the extent of the present ice margin (as evidenced by early and recent aerial photographs) suggests that fluctuations have not been overly significant in recent times. Deglaciation is probably still in progress.

2.3 GENERAL CLIMATE

The general climate for Ellesmere Island is both cold and dry (McCann et al., 1972). Precipitation over the Canadian Arctic Archipelago is low, commonly decreasing from south to north. Summer temperatures are cool, with the bulk of total precipitation falling as rain during this short period.

Circulation during the winter months in the Canadian Arctic is marked by a persistent anticyclonic system, which develops over the western Arctic and remains until early spring. Snow accumulation occurs from late September to early June. In May this region of high pressure gives way to numerous disturbances which last through the summer. Open water conditions along the coasts in the latter part of the summer season result in considerable low cloud, fog, and drizzle. Cyclonic depressions moving over the Canadian Arctic produce maximum precipitation in July and August, with over 40 per cent of the annual total occurring as rainfall during this period (Meteorological Branch, C.H.S., 1970). In autumn increasingly frequent cold air invasions from the Arctic Ocean produce instabilities over the archipelago and result in intense storms in late September and early October.

The Eureka climatological station in west-central Ellesmere Island experiences a coastal climate, and its records provide an approximate indication of climatic conditions in the Vendom Fiord area. Precipitation and temperature data for the period between 1941-70 is summarized in Figure 2.2. Precipitation graphs for comparative purposes are also presented for Alert (Ellesmere Is.), Isachsen (Ellef Ringnes Is.), Resolute (Cornwallis Is.), and Thule (Greenland) (see map Fig. 2.3).

All stations show maximum precipitation in July, August, and September, with the bulk of precipitation occurring as rainfall. Eureka receives the lowest mean annual precipitation in Canada. The maximum 24-hour rainfall recorded at Eureka was 41.7 mm (Meteorological Branch, C.H.S., 1970), which represents an intense rainfall event accounting for 68 per cent of the annual total. The temperature graph for Eureka reveals the brief summer season from mid-June to late August, and average temperatures well below $0^{o}C$ for the majority of the year.

Generally summer temperature variability will affect the length of the summer season and the time of occurrence of the spring peak runoff, and hence the amount of runoff from snow and ice melt. Superimposed over the thermal conditions during the summer is the variability of summer precipitation affecting the total amount of runoff. This effect is more complex, as a warm, clear summer season with low precipitation may exhibit greater runoff from melt

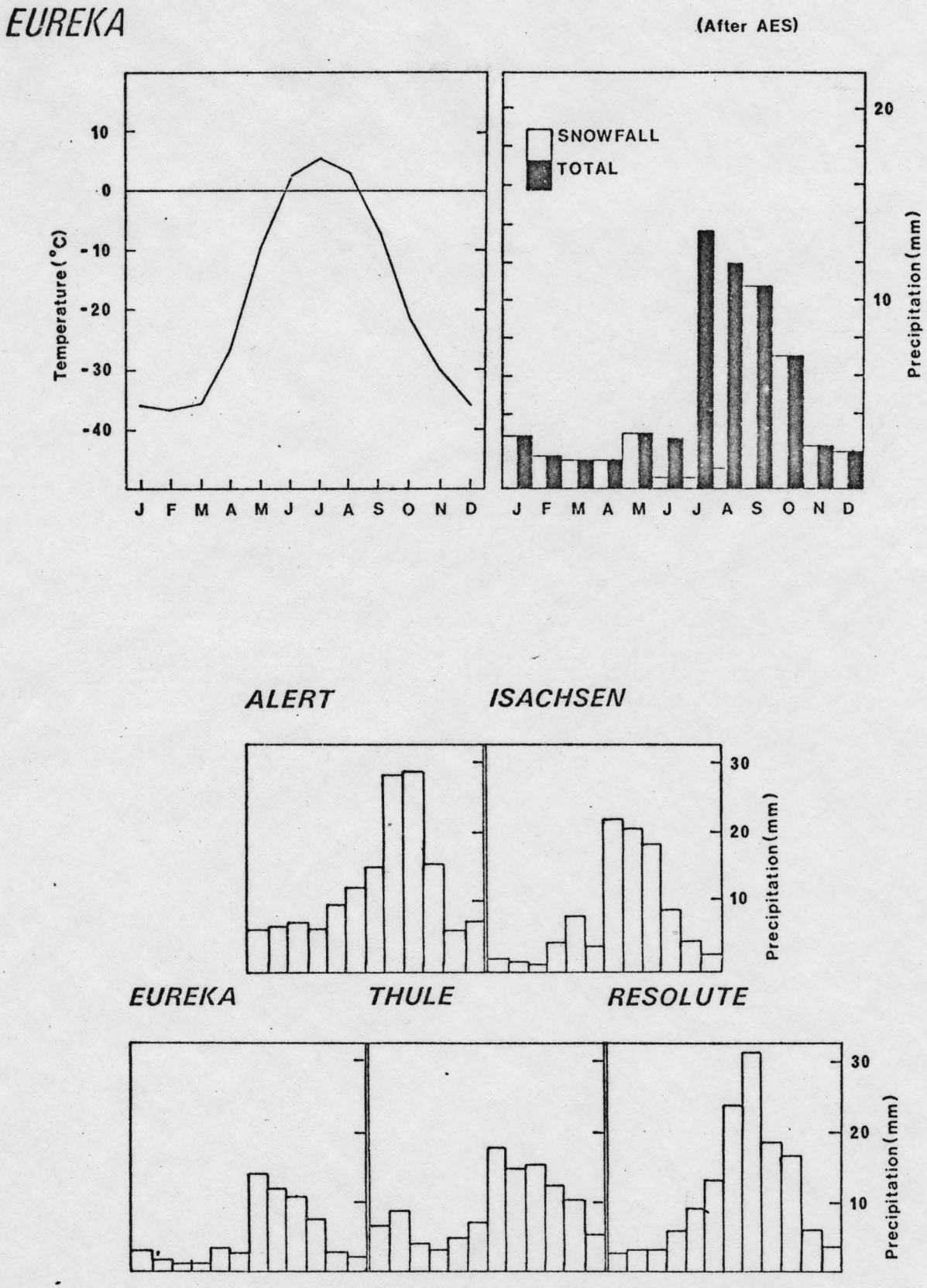

Figure 2.2 Mean temperature and precipitation values for Eureka and other weather stations between the period 1941-70.

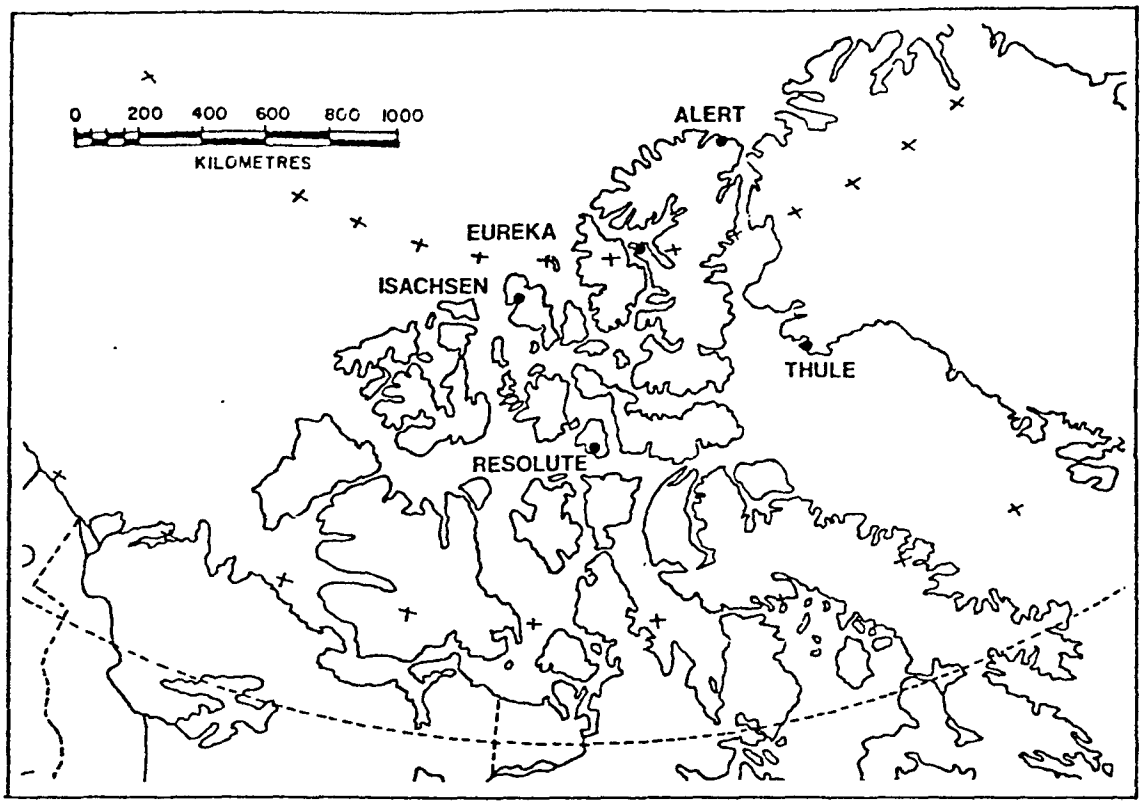

Figure 2.3 The Canadian Arctic Archipelago showing high Arctic weather stations.

than a cool, wet season which would dampen melt runoff, but may or may not provide an equal or greater amount of precipitation for runoff.

2.4 SCHEI RIVER BASIN

The Schei River basin is located in the interior of south-central Ellesmere Island at the head of Vendom Fiord. The Schei River is cut into the interior plateau as an easterly tributary of the Sverdrup River. The Schei basin drains the southwest sector of the Schei Glacier ice lobe of the Ellesmere Island ice cap.

The bedrock lithology is dominantly limestone and dolomite. Minor beds include conglomerate, sandstone, siltstone, shale, anhydrite, and coal. Beds generally dip moderately to the west in the area and show a complex structural history. Granite gneisses underlie the ice cap.

The postglacial history of the area has been discussed in detail by Ballantyne (1975, in preparation) and on a more regional basis by Hodgson (1972). Former outwash fans are located at the apex of the present active outwash surface. The earliest glacio-fluvial deposit was a major alluvial delta deposited from a melt-water channel between 6,000 to 7,000 years B.P., when ice had retreated behind the calcareous hogback ridge in the area. This Pleistocene outwash surface is composed of sand to boulder size material, showing considerable fluvial reworking, and has been

successively terraced during isostatic rebound and base level changes into a sequence of terrace remnants. The oldest deposit is now situated approximately 35 m above the present active surface.

The Schei basin, partially draining the Schei Glacier, is 91.2 km^2 in area, of which 32.4 km^2 or 35.5 per cent is glacierized. The Schei Glacier is a "cold" ice lobe and hence frozen to its bed along the margins. No detectable change in the position of the ice lobe could be observed since aerial photographs were taken of the area in 1950 and 1959. Drainage from the ice lobe to the Schei basin is mainly supraglacial (see Fig. 2.4) with marginal and submarginal drainage occurring along the south margin (Fig. 2.5). McCann et al., (1973) note that the ice lobe probably possesses a small mass budget, in which ablation during the summer season is balanced by accumulation occurring over the winter months. This produces a stability of the ice margin. Overall runoff rates today are probably similar to runoff in recent times.

The present outwash surface is primarily active along the central portion and northern margin of the sandur. It is approximately 2.5 km long and 0.7 km wide at its widest point. The sides of the surface are flanked by former glaciofluvial and alluvial deposits, and at the distal portions by estuarine flats. The south margin of the sandur is laterally bordered by deltaic deposits. The active surface is undoubtedly underlain by fine grained marine material.

Figure 2.4 Drainage conditions along the north-west margin of the Schei Glacier. Note the supraglacial channels on the glacier surface.

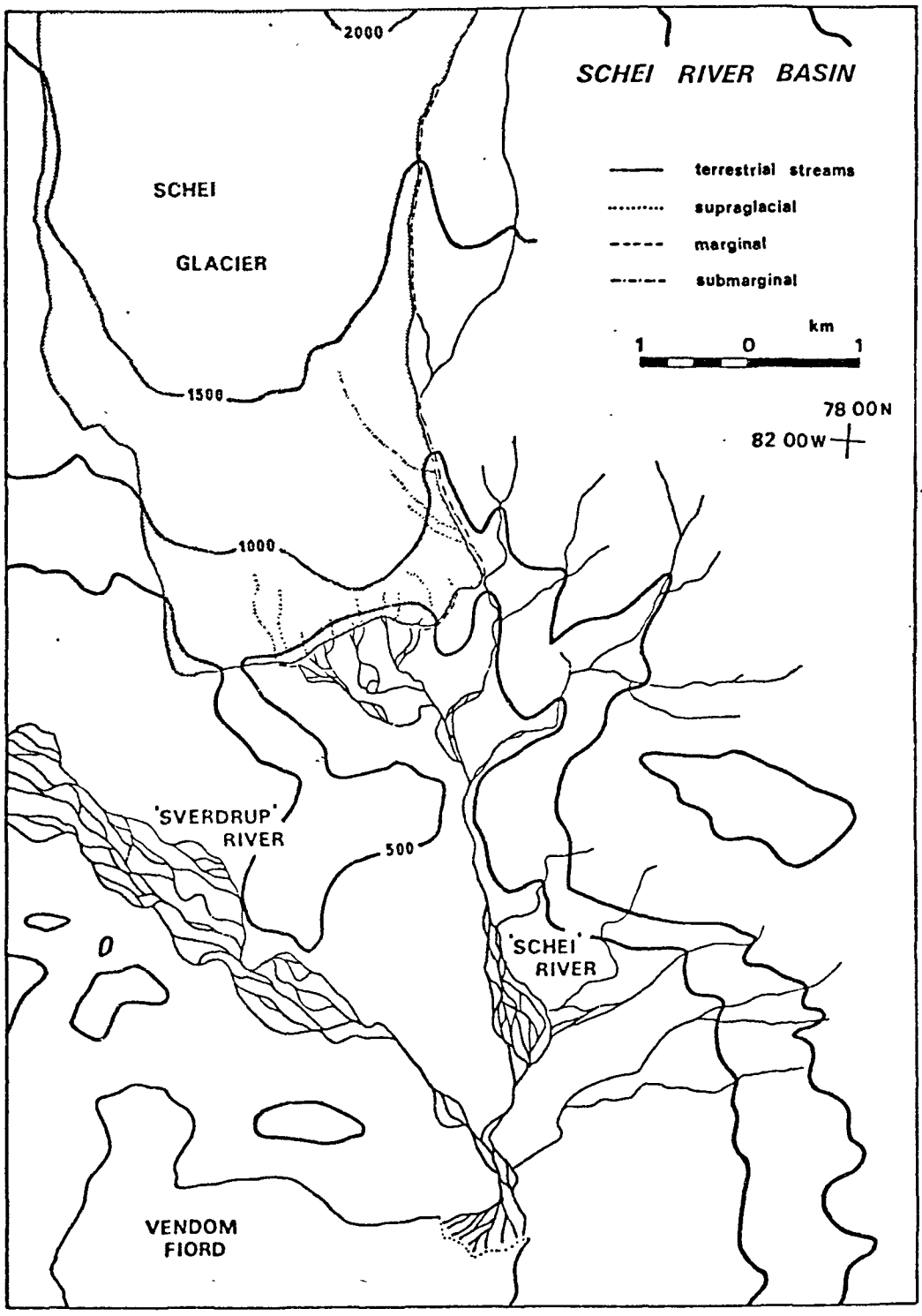

Figure 2.5 The Schei River drainage basin.

Sources of sediment available to the Schei River are mainly reworked alluvial material from the earlier terrace deposits and rock-fall and scree delivery from the hogback ridge. Other minor sources include nival erosion of fine grained material from earlier deltaic deposits along the sides of the sandur, and other material from the upper part of the basin transported to the lower sandur.

Polygonal frost cracks and solifluction lobes are evident in the older alluvial surfaces but appear to be mainly inactive at present, largely due to the widespread vegetation cover in the area. The active sandur surface is bare of vegetation except for portions that have been inactive for a considerable period of time. Usually these occur along the margins of the sandur, or older remnant sections of the previous terrace level. McCann et al. (1973) identified associations of SAXIFRAGA, PAPAVER, and grasses occupying the finer grained areas. The older inactive sets of terrace deposits are vegetated more heavily and are stabilized on the flat surfaces by DRYAS, PEDICULARIS, SAXIFRAGA, DRABA, grasses, mosses, and lichens. CASSIOPE, some DRYAS, and grasses are found in hummock depressions in nivation hollows and other moist areas.

CHAPTER III

HYDROLOGY

3.1 METEOROLOGICAL MEASUREMENTS AND SOURCES OF RUNOFF

Meteorological inputs to the Schei sandur system were monitored for the duration of the field investigation periods in both 1973 and 1974. All meteorological instruments were located at the base camp site (Fig. 3.1) adjacent to the Schei sandur (see Fig. 1.3). In addition to air temperature, precipitation, and incoming shortwave radiation measured in 1973, net allwave radiation and wind speed-direction were recorded in 1974.

Air temperature measurements were made using a Lambrecht thermohygrograph mounted in a Stevenson screen at a height of 1 m. Precipitation was recorded in an A.E.S. tipping-bucket rain gauge. No adjustment could be made for the occurrence of occult precipitation as cloud or fog vapour, although this probably represents a minor phenomena as a contribution of precipitation to the sandur surface. Incoming shortwave radiation was recorded with a Casella bimetallic actinograph. Wind direction was noted with twice daily measurements of wind speed on a Casella anemometer. Net allwave radiation was measured with a Swissteco net radiometer over a hummock surface.

Figure 3.1 Meteorological station at the base camp site, 1974.

Summer precipitation, glacial melt, and snowmelt from the winter accumulation of precipitation, are the major contributions to runoff. Groundwater discharge as a source of runoff was calculated to be minimal by both Hjulstrom (1955) and Church (1972). Only shallow percolation occurs through the active layer, due to the presence of the permafrost table. A maximum expected depth to the frost table of approximately 1 m would be reached only late in the summer season. Although groundwater discharge may be of minor importance in estimating runoff, considerable water exchange between channel flow and the subsurface of the sandur can be important. This is especially evident in the coarse sands and gravels in the lower portion of the Schei sandur where seepage occurs to a considerable extent (see Fig. 5.12). Church (1972) notes that the net exchange of water with permafrost storage is small, and evaporation low due to high humidities and low temperatures, although this last point may have been underrated in previous studies.

3.2 RUNOFF DATA AND HYDROGRAPHS

The daily runoff hydrographs of the Schei River for the seasons 1973-74 are illustrated in Figures 3.2 and 3.3, in addition to relevant meteorological data. It can be seen for both years that the data do not represent the complete seasons. In 1973, commencement of runoff began before flow could be recorded. Breaks in the hydrograph record are due to removal of the stilling well at the gauging site relocation, and removal by a rainfall flood event respectively.

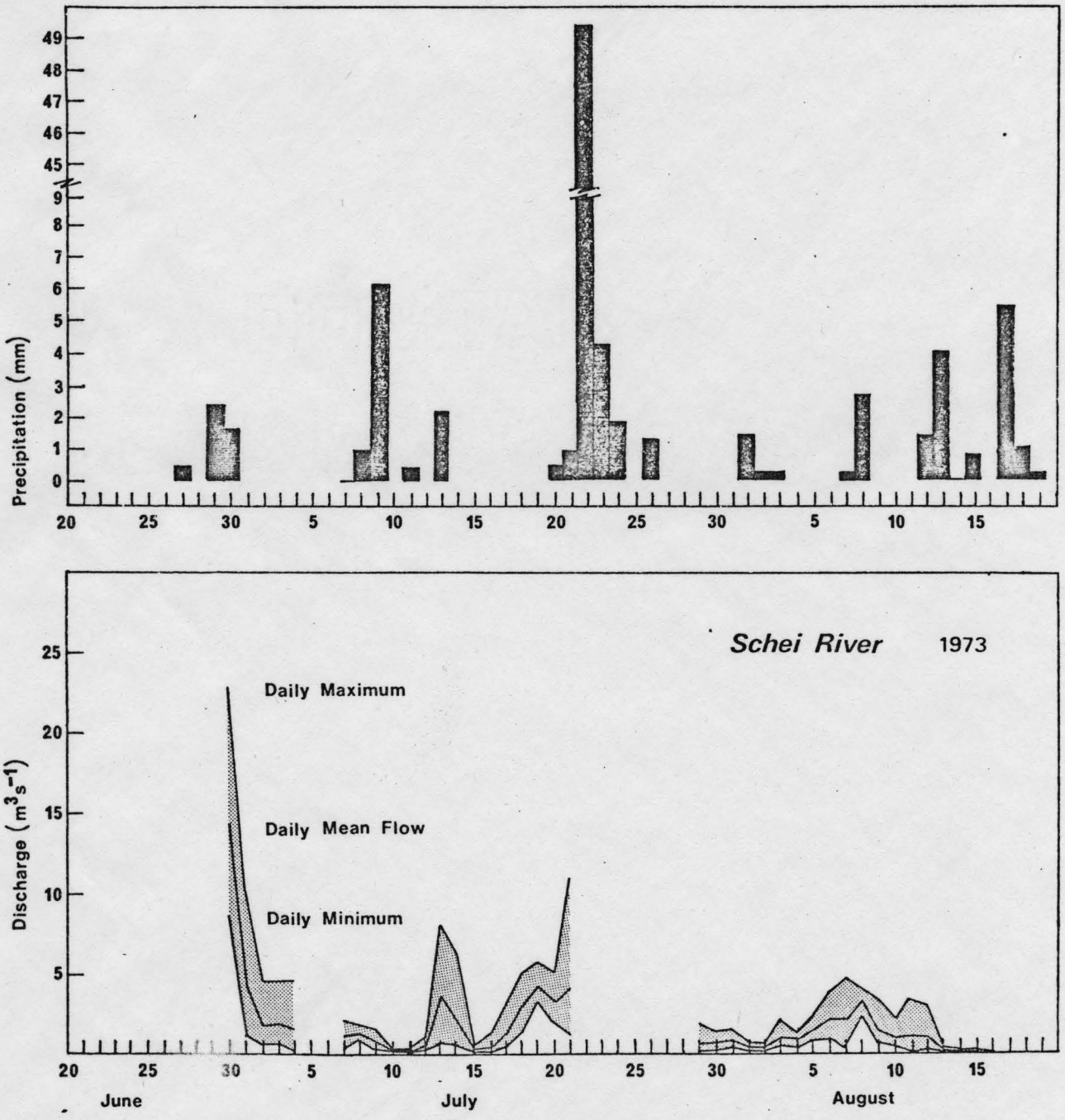

Figure 3.2 Summary of runoff and climatic data, 1973.

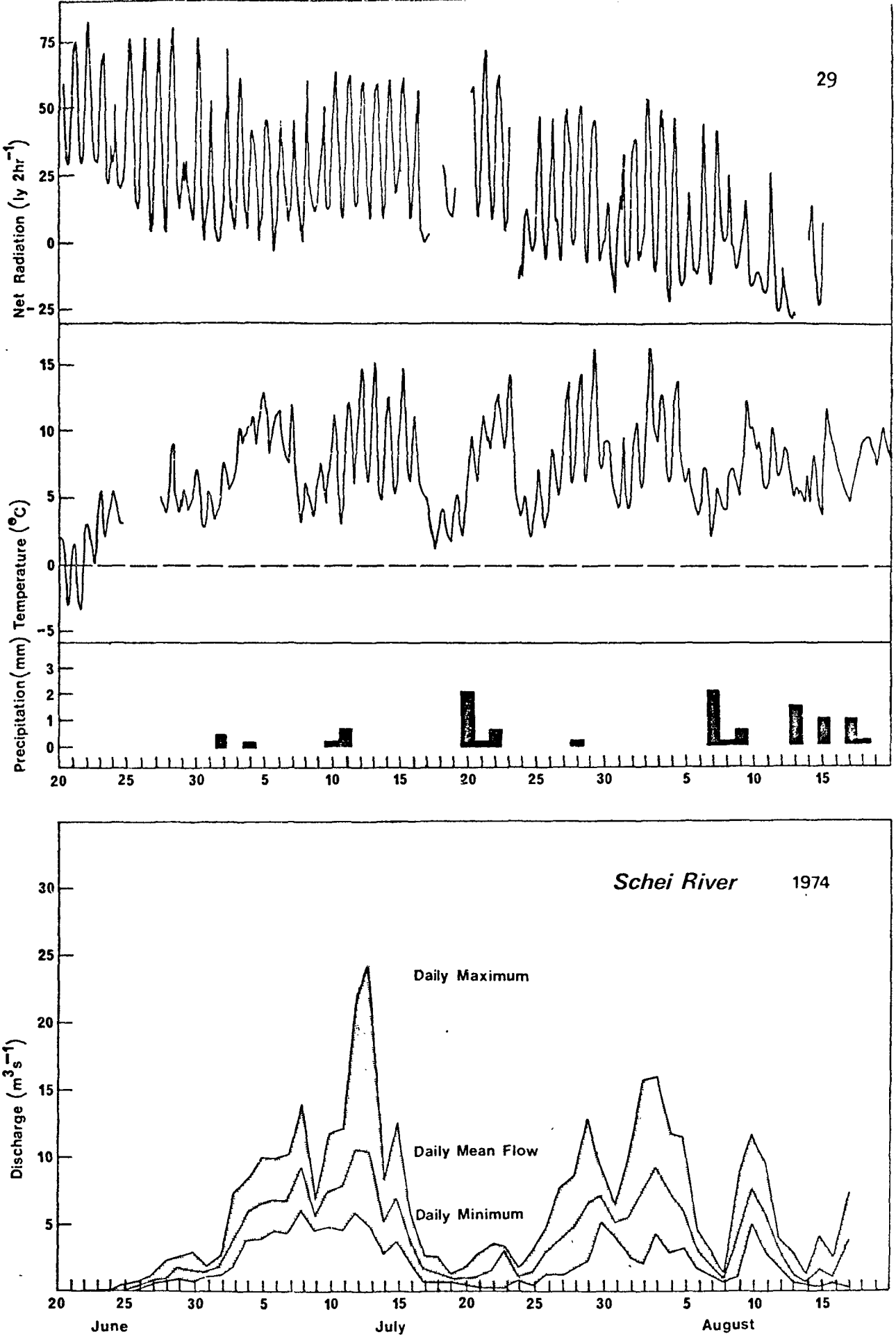

Figure 3.3 Summary of runoff and climatic data, 1974.

In 1974 a similar removal during the spring flood occurred, but water staff measurements of stage allowed a continuous trace to be made with interpolations. In both years, clear, warm climatic conditions at the end of the field investigation periods suggested runoffs from ice ablation continued into late August, or early September.

The runoff hydrograph for the 1973 season is in marked contrast to that in 1974. In 1973 discharge was lower and the hydrograph more suppressed under a greater influence from seasonal precipitation and snowmelt inputs. In 1974 the contribution from glacial ice ablation was more prominent than annual precipitation, and is reflected in significantly higher flows prevailing over the 1974 season from glacier melt due to maximum energy inputs during warmer, clear periods. Lower flows were experienced in the cooler, cloudy conditions of 1973, with precipitation at times falling as snow in the Vendom Fiord area, especially in the higher plateau regions. Clearly glacial ablation input is the most variable component of the runoff sources. It can also be seen that the seasonal precipitation inputs are highly variable over the two seasons. Which source of runoff will be more significantly important as a contributor to runoff over the summer season, will depend on the dominant climatic type(s) over the season.

A comparison of the precipitation and temperature aspects of the climate during the 1973-74 summers with the weather station at Eureka (cf. Fig. 2.2 and Figs. 3.2 and 3.3), suggests that the Vendom Fiord site experienced summer seasons resembling that of Eureka. Church (1972) discusses four types of summer weather patterns at Lewis River, Baffin Island:

1. Cyclonic storms of heavy overcast conditions and steady rain.
2. Weak circulation periods of low overcast cloud, drizzle, and fog.
3. Transitional weak circulation periods of high partial overcast, or broken cloud conditions.
4. Anticyclonic clear weather of either cool, or warm conditions; occasional local cooling from katabatic winds are evident.

These weather patterns produce a distinctive influence on runoff during the summer season, affecting the main contributors to runoff. These include direct precipitation, glacial ice ablation, and snowmelt runoff.

Measurements of runoff were made by conventional stream gauging and dye-injection techniques. Price type and Ott current meters were used to measure velocity and calculate discharge by the normal area-velocity method. Occasional discharge measurements were used to establish a stage-discharge rating curve (see Appendix B), with stage records of the Schei River maintained with a Leupold-Stevens type A35 stage recorder in 1973, and an Ott stage recorder in 1974 (see Fig. 3.9).

3.3 FLOW CHARACTERISTICS

A notable feature of the runoff hydrograph is the regular diurnal variability of discharge superimposed over the seasonal discharge trend (Fig. 3.4). The pattern of diurnal discharge variations are related to the diurnal nature of temperature and radiation intensities. As snowmelt and ice ablation to a high degree control runoff in the Schei basin, melt during good weather periods is related to diurnal fluctuations in available energy. A detailed diagram showing the diurnal variations related to heating inputs for a good weather period is illustrated in Figure 3.5. The diurnal cycles are evident due to rapid flow rates from overland flow to channel flow. Diurnal discharge ranges are more suppressed during cool, overcast conditions, with the pattern completely disrupted during stormy periods. McCann and Cogley (1972) using covariance and spectral analysis on diurnal variabilities in a non-glacierized basin, showed a stronger association between incoming shortwave radiation and discharge, than temperature and discharge, as an index of snowmelt discharge. A wide daily range in runoff is important in its influence on the sediment transport rate. Diurnal fluctuations in discharge have been reported by Arnborg (1955), Fahnestock (1963), McCann, Howarth, and Cogley (1972), Church (1972), and Smith (1974).

Over the summer season a number of recognizable trends can be observed in the runoff pattern. Referring to the 1974 season

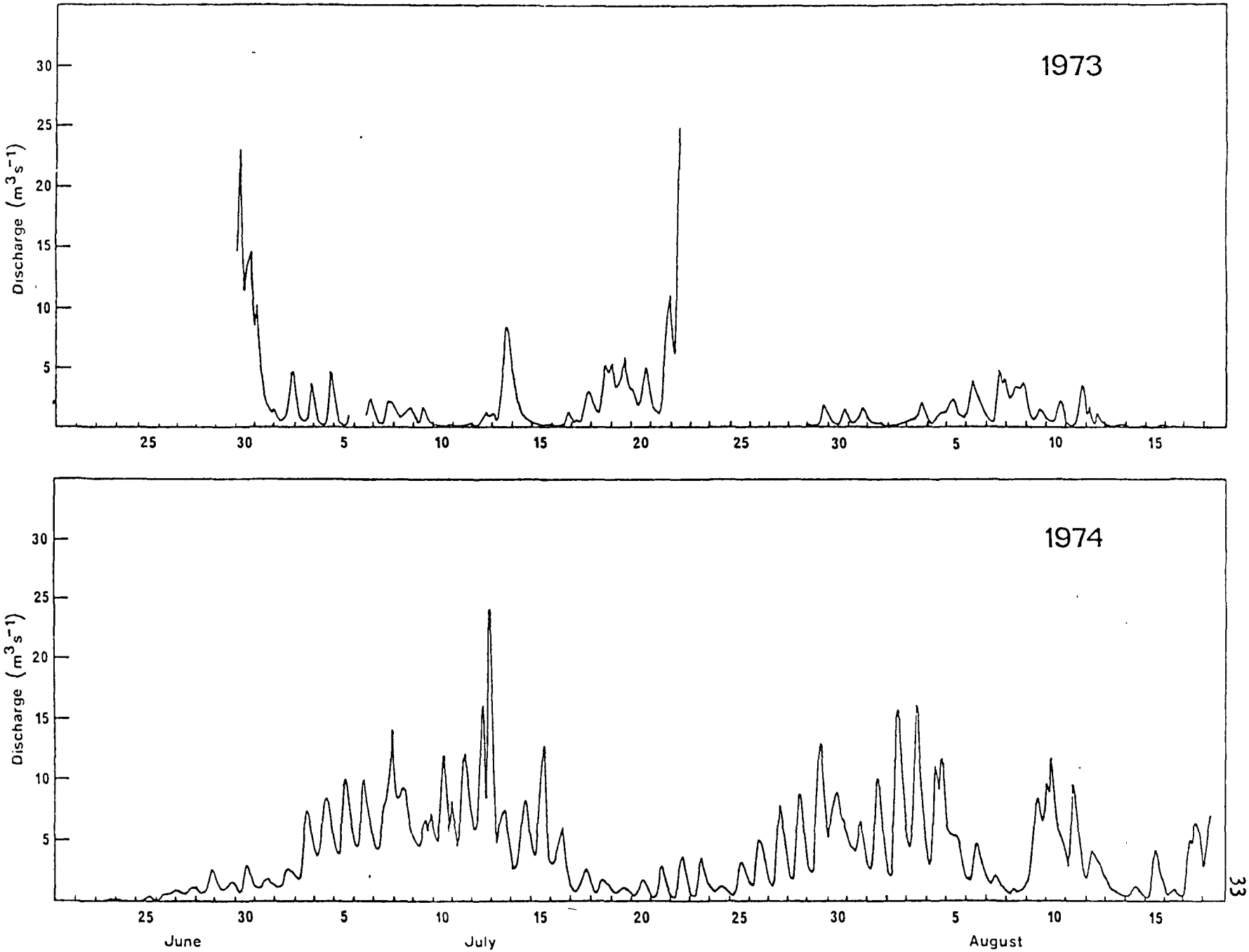

Figure 3.4 Seasonal discharge of Schei River, 1973-74.

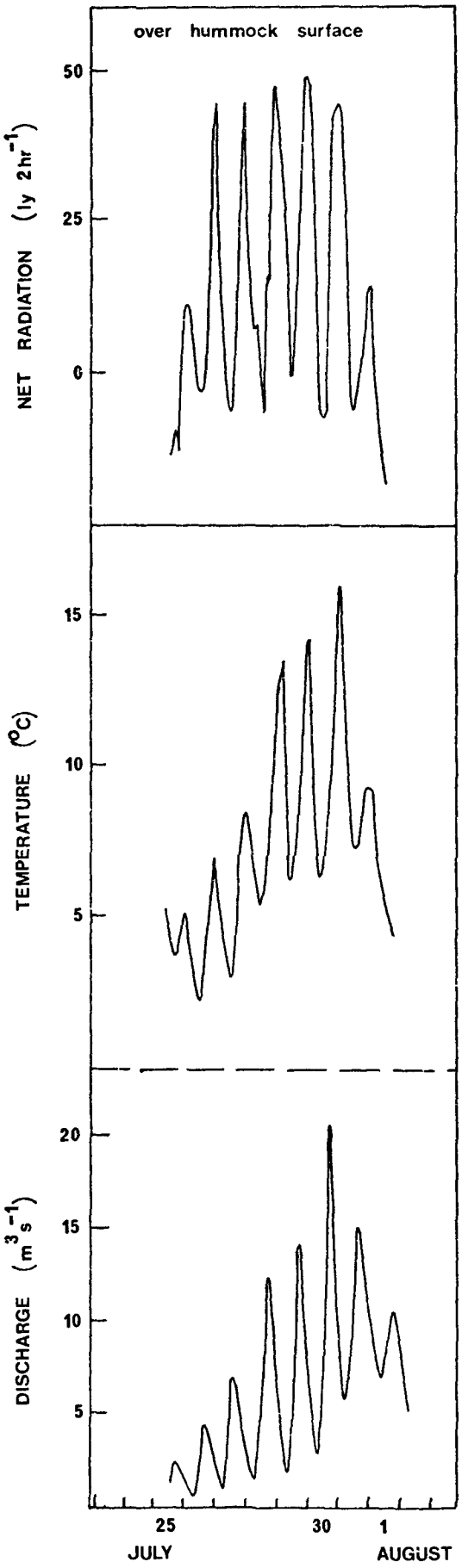

SCHEI RIVER
1974

Figure 3.5 Net radiation, temperature, and discharge graphs for a selected good weather period.

(see Fig. 3.3), mean daily air temperature and discharge increase successively with each day of radiation input during clear weather. Overcast conditions following a clear period, show a more rapid successive drop in overall daily temperature and runoff from a reduced energy input, usually accompanied by some precipitation. Intervening broken to clear conditions again show a gradual successive rise in mean daily air temperature and flow.

Within the diurnal discharge fluctuations are other irregular fluctuations in flow, due to the nature of the submarginal drainage along the Schei glacier which is affected by periodic ice falls and blockage of the channel. Subsequent release after a short period of ponding produces surging of water down the Schei River. This is evident in the two examples of perturbations on the stage trace of the Schei River illustrated in Figure 3.6. A sudden drop in the gauge level due to ice blockage is eventually followed by a surge of the stored water. In Figure 3.6a the range in the discharge variation is approximately 10 m^3s^{-1}, while in Figure 3.6b the discharge difference is approximately 4 m^3s^{-1}. The majority of the ice pondings show a consistent pattern, where initially the stage drops rapidly after the ice fall and damming of water. An equally rapid rise occurs when the water overtops the reservoir and resumes flow. Considerable leakage may be present (see Fig. 3.6a) before eventually the ice dam collapses and the stored water surges downstream with a concurrent rise in stage, although the length of blockage before bursting may vary considerably.

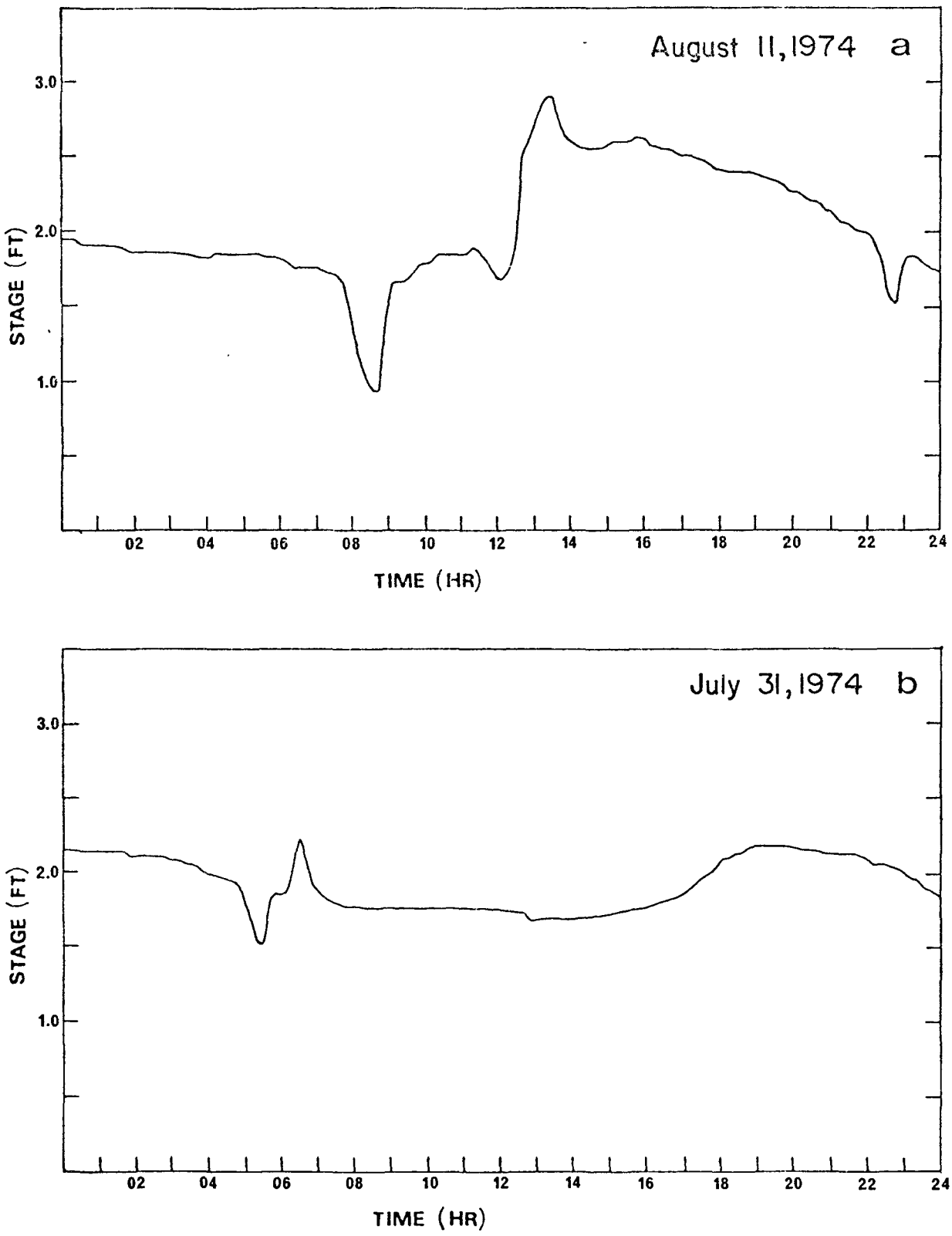

Figure 3.6 Schei River gauge trace showing flow interruptions.

If blockage of the channel remains while discharge decreases, the ponded water may gradually leak out and show an irregular decaying flow. The nature of the ice pondings produces a pronounced effect on irregularities in sediment transport and the diurnal variations in discharge, depending on flow conditions at the time of blockage, the effectiveness of the ponding, and the rate of water release.

3.4 SEASONAL RUNOFF PATTERN

The hydrologic regime in the high Arctic is distinctive and quite different from regimes in more southerly latitudes. During the winter season, which extends over most of the year, precipitation as snow accumulates prior to the spring flood, with no flow occurring. Runoff only occurs during the cool summer season of approximately three months. The runoff regimen of the Schei River exhibits both proglacial and nival influences.

During the summer runoff season at the head of Vendom Fiord, a sequence of three periods could be distinguished; the snowmelt period, summer flow, and freezeback. During the spring melt period, snow and ice melting produce a rapid increase in flow to a pronounced peak of discharge, usually in late June to early July. Runoff gradually decreases throughout the remainder of the summer as the amount of snow available for melt decreases. Runoff for the rest of the summer is supplied by local permanent snowpatches, ice ablation, and rainfall

storm events punctuating late season recessional flow. Effective renewed melting from the icefield may produce a second peak runoff in late July to early August, if warmer weather conditions prevail.

3.5 COMMENCEMENT OF RUNOFF

The commencement of flow from melt has been described by Pissart (1967), who divided the initiation of runoff during the snowmelt period into a sequence of four stages:

1. initial localized melt of the snowpack due to solar radiation, while air temperatures remained below $0^{o}C$.
2. general melt of the snowpack, with percolation of the meltwater to the snowpack base and into snow-choked stream channels, where refreezing occurs. (Storage of meltwater within snowpack).
3. commencement of flow over snow and ice in the streambeds.
4. runoff on the streambed with ice breakup and melt.

In 1973 initial snowmelt and flow had begun in early June and was not observed, while in 1974 initial melt occurred in the middle of June. From at least 19 June and onward in 1974, the first two stages were noted in the lower part of the Schei basin prior to early channel flow. Early conditions at the gauging site can be seen in Figure 3.7. It was not until several days later that the air temperature had risen and remained above the freezing point in

Snow conditions in the main channel;

view downstream at the gauging station.

a

Prior to the commencement of runoff on 20 June;

view upstream of the gauging section.

b

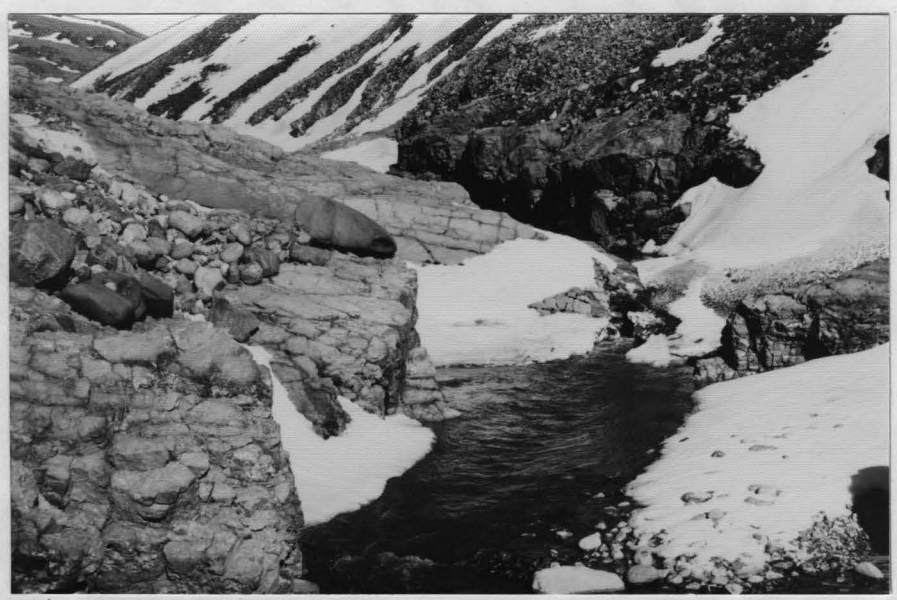

Commencement of flow on 22 June, carrying considerable suspended material.

c

Figure 3.7 a-b-c Illustrations of early channel conditions at the upper apex of the sandur, 1974.

conjunction with an extensive fine weather period. This led to a saturation of the snowpack and significant melt within the channels on 22 June. Initial low flow began to clear out snow along the thalwegs of the stream courses, with considerable localized melt occurring from the channel banks (Fig. 3.7c). Flow over snow (Pissart's third stage) was not observed. Continued fine weather eventually led to more extensive channel flow over the sandur. It appears the presence and amount of winter ice on the riverbeds is governed by the previous year's late season flow and freezeback conditions. Protection of the channelbeds by ice and snow was judged not to be considerable to any appreciable degree, as significant early flow would eventually break up the ice where flow was occurring.

The occurrence of initial spring flow is dependent on the climatic conditions and physiographic characteristics within the basin. Church (1972) proposes that an extended fair weather period, or a sufficient rainstorm event, will suffice in developing initial flow.

Although no effective coarse bedload transport occurred during this early low runoff period, significant concentrations of suspended material were evident in the Schei River during the first day of flow and onward. The early flow was heavily laden with a fine suspended load, due to the melting of snow laden with wind blown fines which had accumulated over the snow during the winter months.

The snowmelt flood which usually occurs in late June to early July may be the most important aspect of the hydrologic regime. The time of occurrence of the spring melt peak can be highly variable. This is evident in the hydrographs for the two seasons, and in Figure 3.8 which contrasts flow conditions on the Schei sandur on 19 June of 1973 and 1974. On this date in 1973 runoff had already commenced, with flow occurrence well into the spring nival flood. Snow on the sandur occurred only locally along the channel banks. In 1974, runoff did not begin until several days later as the channels of the sandur were snowchoked. Also a considerable amount of snow had accumulated in the lower portion of the outwash plain. Nival melt was only locally significant in other parts of the basin.

The spring flood usually accounts for the bulk of the runoff discharged over the summer season and implies an immense concentration of runoff and fluvial activity over a relatively short period of time. Rapid increased runoff from initial flow to the peak of the spring flood is evident in the 1974 hydrograph, compounded by the influence of glacial melt and icefall ponding. Figure 3.9 shows a comparison of the Schei River in flood and during low flow. Considerable diurnal variations in discharge occurred during the spring flood period and this exerted a definite influence on sediment transport. Coarse bedload transport dominated the total load movement during the flood period, with considerable sediment reworking occurring over the sandur.

1973.

1974.

Figure 3.8 Schei Sandur showing conditions over the outwash on 19 June of both seasons.

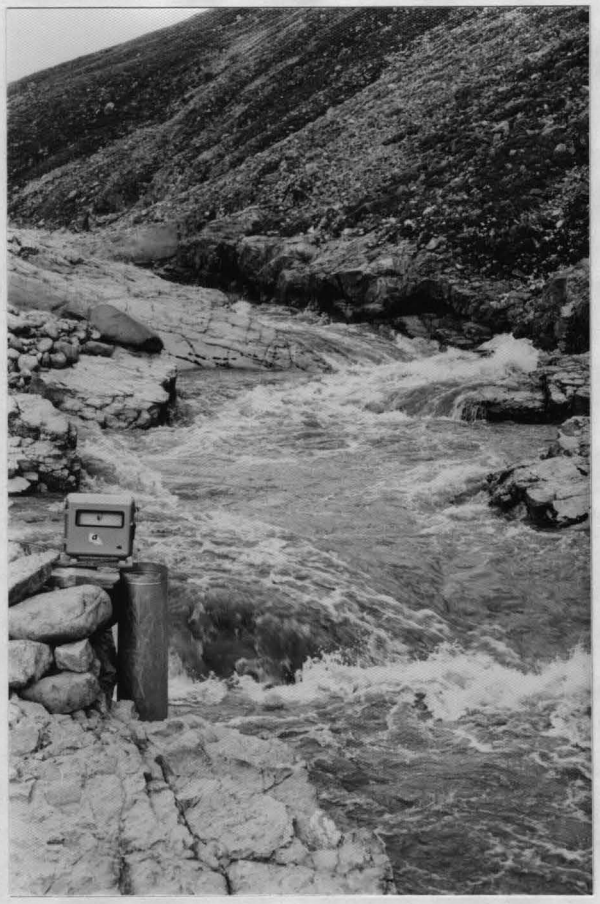

Schei River during spring flood on 10 July, 1974
discharge c. 14 $m^3 s^{-1}$

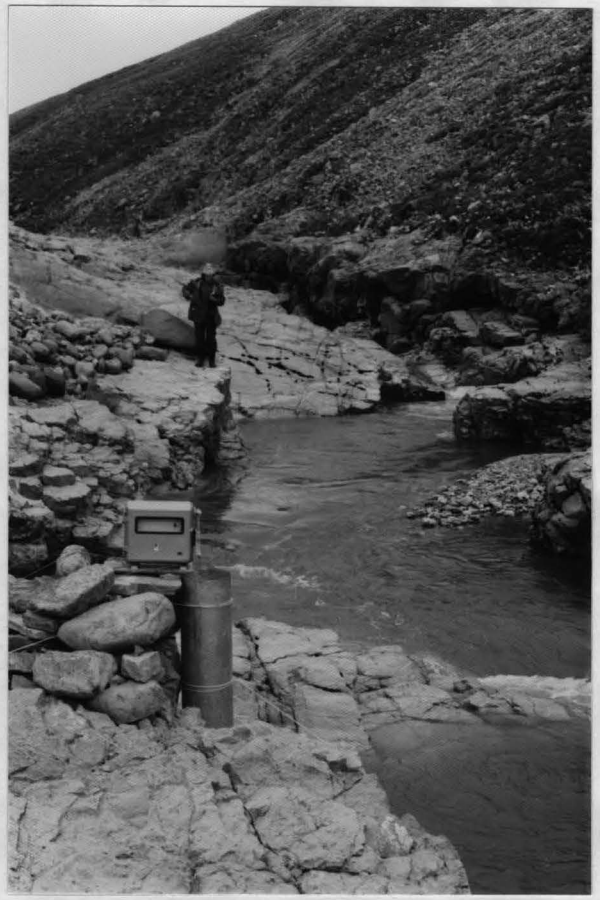

Schei River on 19 July, 1974
discharge c. 1 $m^3 s^{-1}$

Figure 3.9 Schei River at high and low flow conditions.

The suspended sediment load was also a significant component, with notable high concentrations occurring.

3.6 SUMMER RUNOFF

In both years following the spring flood, seasonal flow declined, being interrupted usually by runoff variations during good ablation periods, or rainfall flood events. Unless rainfall periods can provide significant precipitation to the basin, greater discharges can be expected from glacier melt during clear, warm weather conditions, than dampened and reduced runoff during overcast, cool periods. This becomes apparent in the 1974 hydrograph where a second flood peak from glacial melt occurred in early August, during fair weather. This peak is greater than the nival flood peak if the icefall ponding effect, which is superimposed over the spring flood, is removed. This latter event produced the maximum discharge for the season.

The development of a glacial melt peak is attributed to several causes by Church (1972):

1. early season heat deficit in the near-surface of the glacier has been counteracted.
2. lowering of the albedo of the surface and more effective melting, as the seasonal snow has been melted, exposing darker glacier ice.

3. extension of the drainage network over the entire watershed of the glacier.

An extended good weather period did not occur in 1973, and this is reflected in a more suppressed glacial melt peak during late July, or early August. Differences in the magnitude of the diurnal periodicity is also evident between the two peaks, contrasting the differences in radiative heating inputs.

Runoff is rapid in the dominantly high relief of the Schei basin. An example of rapid runoff response to a direct precipitation input is illustrated in Figure 3.10. McCann et al., (1973) reported general lag times of 5 h to runoff, in response to precipitation inputs over relatively small basins. This rapid runoff reflects little detainment of water in the active layer under the influence of continuous permafrost as an impermeable barrier. Thus for direct storm runoff events, the runoff ratio is given by:

$$\frac{Q}{p} = 1 - \frac{E}{p} \qquad \text{(III.1)}$$

(adapted from general formula given by Sellers, 1965)

where Q is the runoff; p is precipitation; and E is evaporation (values in mm hr^{-1})

$\frac{Q}{p}$ should approach unity with low evaporation rates, although the value may decrease over the summer. On a yearly basis runoff will be less than the total precipitation inputs.

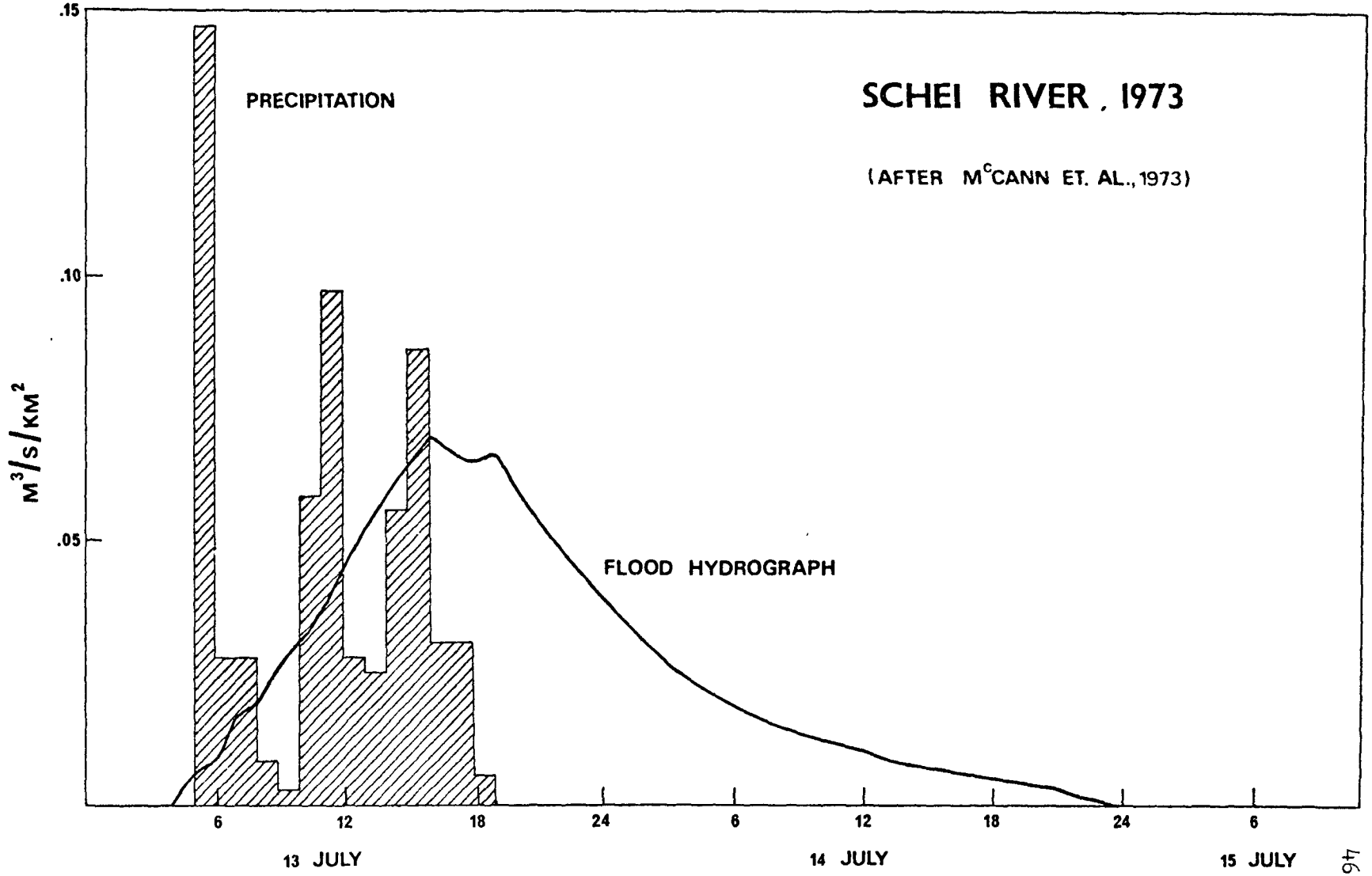

Figure 3.10 Illustration of the rapid response of discharge to precipitation.

3.7 FREEZEBACK AND SUMMARY

In 1973, runoff on the Schei River near the end of the season was derived almost entirely from groundwater flow. Discharge declined to a very low amount, with runoff periodically almost ceasing to flow. This was particularly noticeable during overcast weather near the end of August, when melt rapidly decreased. Water in the channels at times became trapped in the pool portions of the streams. This process may ultimately lead to percolation of the water into the bed, and the formation of naleds.

The occurrence of the peak runoff and runoff variability throughout the summer season is complex in a glacierized basin. Total runoff from melt is highly dependent on the length of the summer season (Church 1972) and rainfall inputs into the basin.

3.8 EXTREME FLOOD EVENTS

A number of extreme flood events occurred over the 1973-74 seasons which affected the normal flow pattern of the Schei River. Although precipitation is low over the Arctic, an intense storm event associated with frontal precipitation and high winds occurred on 22 July, 1973, and contributed to the most significant catastrophic runoff event during the season. This led to extensive sediment reworking

occurring over the sandur plain. Cogley and McCann (1975) discuss this particular storm event in further detail. The storm produced a rainfall rate of 49.4 mm in 24 hours, with a total recorded rainfall of 54.6 mm. This maximum 24 hour rainfall event exceeded the existing record at Eureka of 42.4 mm in 24 hours. The subsequent heavy storm runoff effectively removed the stage apparatus at the gauging site, and although no information could be gained on the total amount of water which passed through the gauging section, a peak discharge of approximately 50 m^3 s^{-1} was estimated for the event (McCann et al., 1973). The flood inundated a large portion of the sandur and completely altered the braided pattern (cf. Figs. 5.12 and 5.13).

An almost equally effective flood not related to climatic control occurred on 12 July, 1974, due to ice falls and ponding along the south margin of the Schei Glacier. Periodically, blockage of the flow and release of the stored water produces a flood of sufficient magnitude to cause considerable sediment transport and redistribution of material over the active outwash surface. The effectiveness of the flood on the Schei River depends on the length of effective blockage, amount of water ponded, and the rate of drainage. This is the case for the high peak discharge evident on the 1974 hydrograph on the above date, which is superimposed over the spring flood. Ice falls and ponding of this nature occurred frequently in both the 1973 and 1974 seasons, as noted by interruptions in stage, stranded ice blocks, and at times heavy ice and slush loads

carried by the Schei River. This accounts for irregular variations in discharge and the stream load, and will probably continue to exist in the near future due to conditions of submarginal drainage along the glacier and the position of the ice lobe.

CHAPTER IV

SEDIMENT TRANSPORT

4.1 INTRODUCTION

The transport of sediment may be subdivided into three fractions; the dissolved load, suspended load, and bedload. A sequence exists over the runoff season where the dissolved load is continuously present, the suspended load near continuous, and the bedload discontinuous occurring only at moderate to high flow conditions.

Sediment transport depends not only on the flow conditions but also on the availability of material for transport. The availability of former glacial debris, and present suitable conditions for producing considerable material, are the main factors in providing high sediment yields for transport. The several sources of material available to the Schei River sandur may be summarized in Table 4.1.

The results obtained of the sediment transported by the Schei River over the 1973-74 seasons are discussed in this section. As 1973 was primarily a reconnaissance study, the results from regular sampling are generally limited and discussed qualitatively. In addition to a sampling program, the 1974 season was augmented by a more theoretical approach in developing sediment rating curves for

TABLE 4.1

SOURCES OF MATERIAL AVAILABLE TO THE SCHEI SANDUR

Mode of Transport	Sources	Process of Delivery to Schei Sandur
Dissolved	Solutes derived from ground environment	Chemical solution of suitable material during surface and subsurface runoff
Suspended	Generally finer material from:	
	1. Alluvial material from the present outwash and former terraced deposits	1. Present reworking by fluvial activity and nival erosion; also fluvial-thermokarst undercutting
	2. Material from upper basin area	2. As above including transport by Schei River
Bedload	Generally coarser material from:	
	1. Alluvial material from the present outwash and former terraced deposits	1. Present reworking by fluvial activity and avalanching
	2. Material from hogback ridge	2. Rockfall and avalanching including transport by Schei River
	3. Material from upper basin area	3. As above

each segment of the total sediment load. Discussion, limitations, and some generalizations of the results subsequently follow.

4.2 DISSOLVED LOAD

The importance of solution processes has received minimal attention in recent studies of sediment transport in an arctic environment. Church (1972) indicated that the dissolved load, that portion of material transported in solution, was insignificant in Baffin Island streams draining granite gneiss terrains. Cogley (1971) and McCann, Howarth, and Cogley (1972) however, have emphasized that the transportation of material in solution may be the dominant transport component of fluvial erosion in carbonate rock areas of Cornwallis and Devon Islands (bedload estimates were not reported for comparison).

Lithology, vegetation, and the dominant type(s) of the runoff regimen influence this component of the total sediment load. Inconclusive statements on the effectiveness of solution rates in the Arctic are apparently due to overgeneralizations made of the results into other different Arctic environments.

The lower temperatures experienced in the Arctic increases the solubility of carbon dioxide, but the decrease in the rate of calcite solution more than counteracts the former effect and hence produces

relatively lower quantities of dissolved material. Also, the time that water spends in a subsurface environment, in mobilizing soluble materials, is reduced in areas of rapid runoff and drainage during the runoff season.

Water samples were taken on a regular daily basis during the 1973 and 1974 seasons. The sampling procedure is described on page 59. The dissolved sediment concentration from each filtered water sample was measured in the field with the use of a Barnstead PM-70CB conductivity bridge which assesses the effect of the dissolved material on electrical conductivity. Conductivity therefore provides an indication of the free ions in solution although the value also reflects other significant soluble ions. Temperature effects on conductivity were removed by exactly taking all readings at 25°C. The conductivity values ranged from 40 to 228 μ mho cm^{-1} over the two seasons.

A number of control water samples, comprising the complete range of the conductivity values, were taken following the filtering procedure and were stored in airtight polyethylene bottles of 250 ml capacity for later shipment back to the laboratory and an analysis of the total hardness of each sample (Ca^{++} and Mg^{++}). Dissolved calcium and magnesium were analyzed by titration using E.D.T.A. The range in the total hardness of the water quality control samples varied from 17 to 82 ppm. Two obviously anomalous results due to contamination of the samples were removed from the analysis. The concentration of

calcite in the water samples generally amounted to 50 to 80 per cent of the total solute concentration.

The variation in specific conductivity for the Schei River in 1973 and 1974 is shown in Figures 4.1 and 4.2. The conductivity values, as an indication of the solution load of the Schei River waters, generally reveal low values in total hardness, although Ca^{++} and Mg^{++} ions are present continuously.

To provide a comparison of the importance of the solution load to the total transport of material on the Schei River, a computed dissolved load was derived for the 1974 season. An assumed sediment density of 2.77 g cm^{-3} was used in the computation. The conductivity (c) values revealed an inverse relationship with discharge, yielding a derived regression relationship of:

$$c = 75.3\ Q^{-0.22} \qquad r = -.78 \quad (IV.1)$$

This conductivity rating curve is illustrated in Figure 4.3. For the 1973-74 season, the concentration of total dissolved solids (H_t) also reflected a significant correlation with the conductivity values, and can be expressed as:

$$H_t = 2.64 + 0.47\ c \qquad r = .92 \quad N = 20 \quad (IV.2)$$

Therefore the high correlation of total dissolved solids concentration with conductivity, and the inverse relationship of conductivity with discharge, suggests a dilution effect where discharge increases more rapidly than decreasing total solute concentration due to a smaller

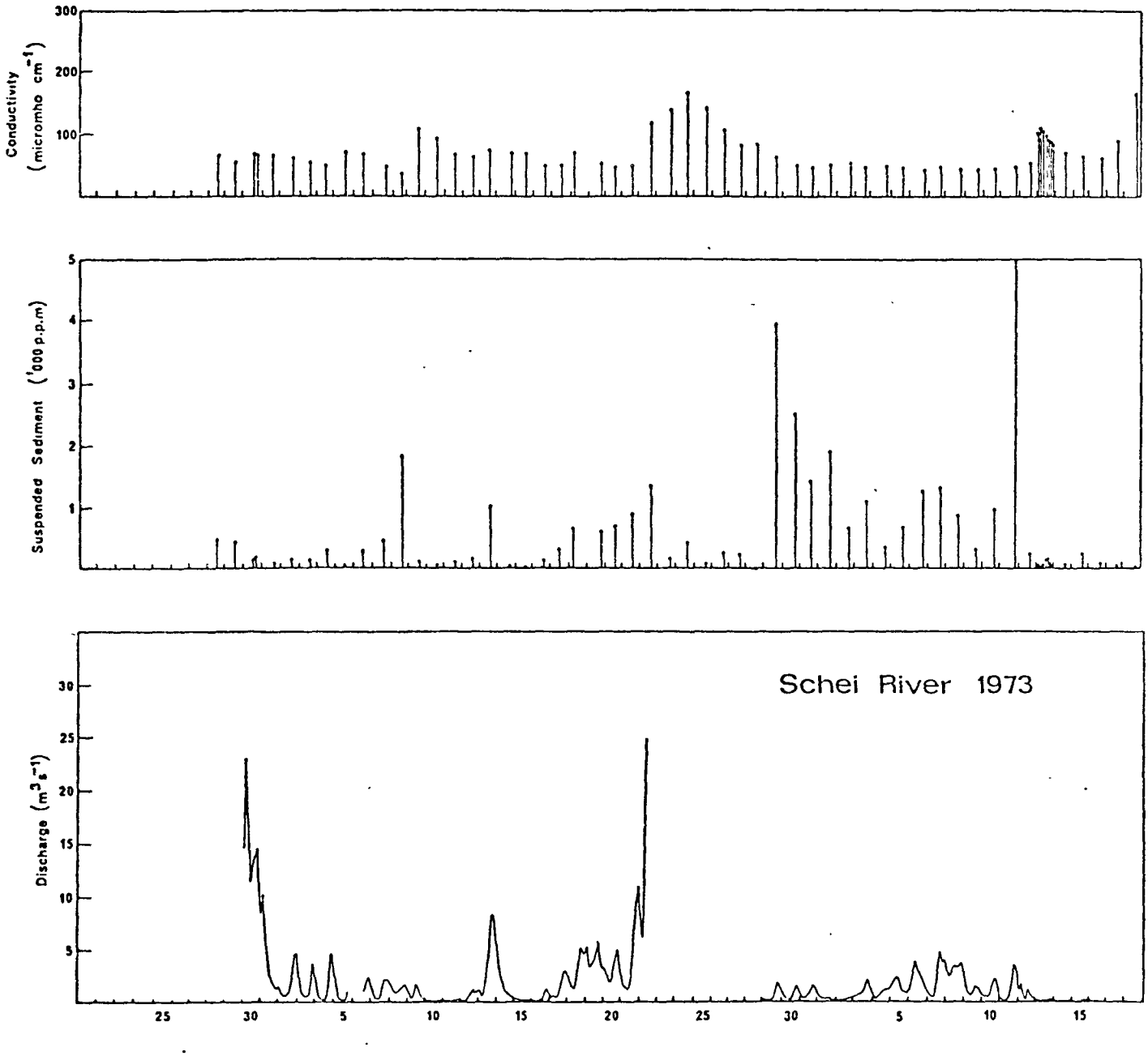

Figure 4.1 Conductivity and suspended sediment concentrations compared with discharge, 1973.

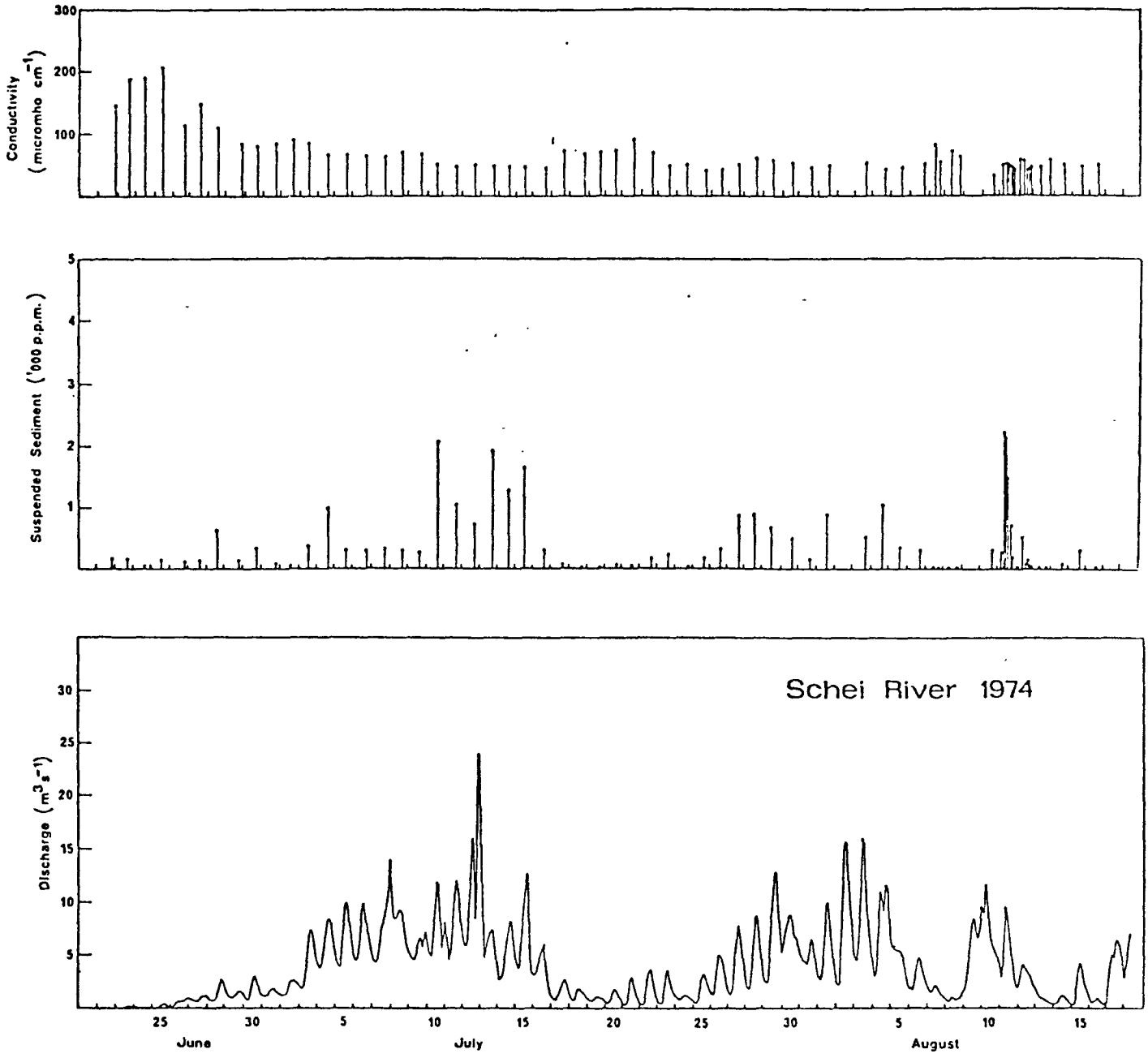

Figure 4.2 Conductivity and suspended sediment concentrations compared with discharge, 1974.

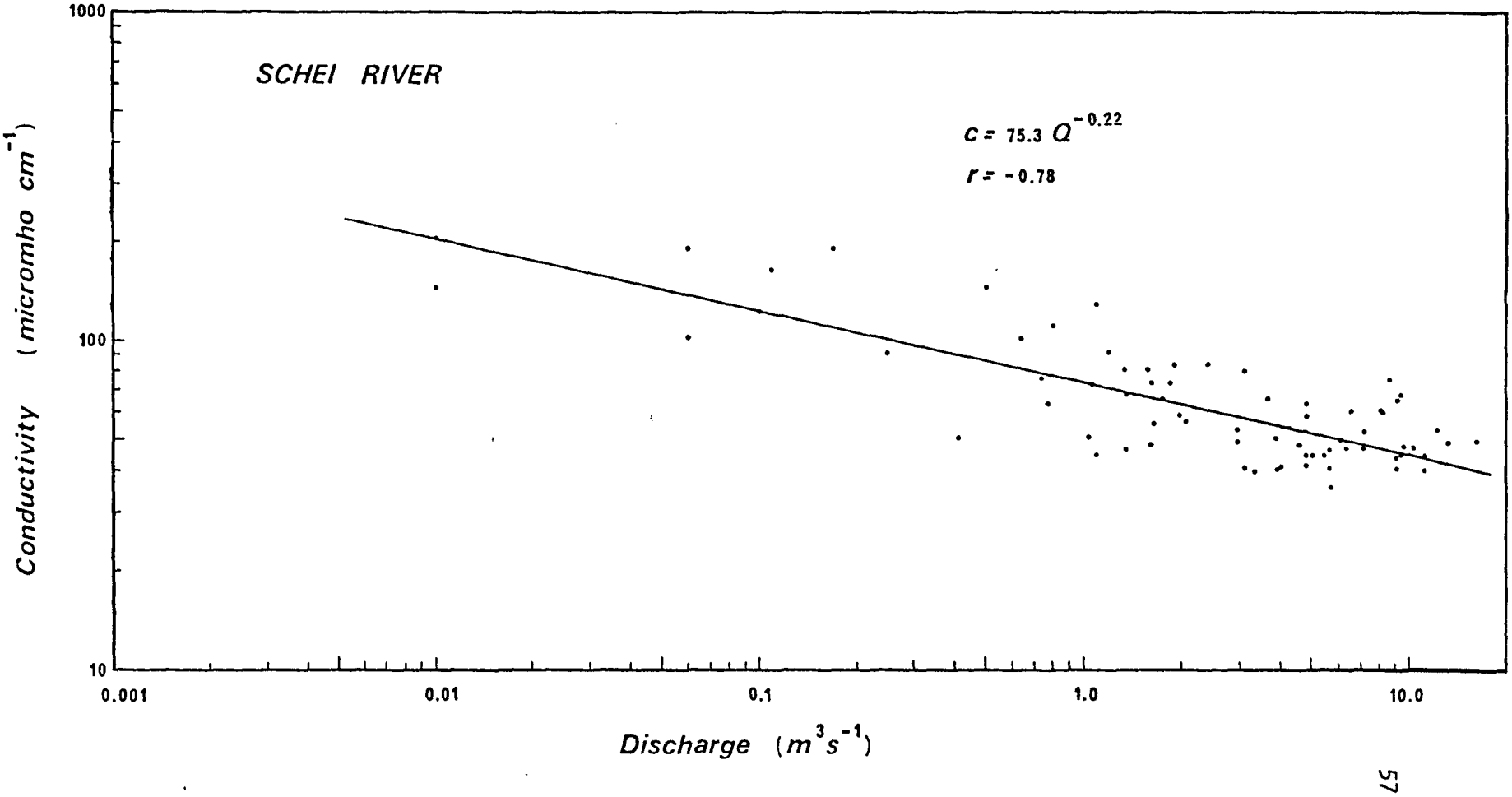

Figure 4.3 Relationship between conductivity and discharge, 1974.

amount of the total water in contact with a given surface area with increasing discharge (reduced solution reactions). Together these relationships were used to form a calculated discharge of total dissolved solids for the 1974 season on the Schei River, presented in Figure 4.6.

Only a small variation in the magnitude of the dissolved load occurs over the runoff season. A maximum value of 60.0 metric tons/day was reached during the snowmelt freshet, with the second highest computed load (53.3 metric tons/day) occurring during the late season glacial-melt peak.

4.3 SUSPENDED LOAD

The turbulent suspension of sediment can be viewed as an advanced state of bed-load movement and saltation (Raudkivi, 1967). The suspended sediment concentration is highly affected by viscosity, which in turn is affected by temperature. Thus the low temperatures of arctic streams possibly provide a unique situation of potentially increasing the suspended sediment load through an increased drag on small particles (hence entrainment), and an enhanced turbulence. This may be especially important on turbulence characteristics near the bed where the concentration is greatest, and on the influence on clay and

silt size material as the drag is also influenced by the size of the particle.

Water samples were taken throughout the 1973 and 1974 season to determine the suspended sediment concentrations. The sampling procedure generally involved taking the water samples at the occurrence of the daily high stage on the Schei River. All samples were taken in the main channel in the upper fan area of the sandur. Generally the water samples were retrieved with a U.S.G.S. Type DH-48 suspended sediment sampler yielding an integrated sample (approximately 350 ml) through the vertical. On occasions a wide open-mouthed polyethylene container (1000 ml capacity) was used for the sampling. During low flow conditions the samples were taken as far as possible out in the stream by wading. At higher restricting discharges, the sampler was immersed beside a bank of the stream where suspended sediment was assumed to be distributed fairly uniformly across the channel owing to sufficient turbulence generated in the stream.

The suspended sediment from each water sample was filtered in the field using a modification of a technique described by Østrem and Stanley (1969) and Østrem, Ziegler, and Ekman (1970) (see McCann et al., 1973, for a brief description of the device and method used). The filter papers used in the field were a cellulose acetate filter of 47 mm diameter and a mean pore size of 0.45 μm. It was presumed that only a negligible amount of extremely fine suspended sediment

material would pass through the filter paper during any given filtering procedure. The sediment filters were stored in plastic bags and shipped to the laboratory for analysis. The bulk of the suspended sediment sampled was comprised of clay to medium silt size material, with some sizes as large as coarse sand in samples taken from highly turbulent flows.

Observations of the ice margin in the upper part of the Schei River basin revealed that the bulk of runoff draining the icecap was sediment-free and that considerable fine material was rapidly entrained adjacent to the ice margin in flowing over glacial detritus. Therefore the glacier was viewed as a negligible source of sediment. The considerable distance and amount of glacial detritus which occurs between the ice margin and measurement site at the upper part of the Schei sandur generally assures an abundant supply of sediment for suspendent transport.

For both the 1973 and 1974 seasons, suspended sediment concentrations were considerable. The actual variations in the concentration of suspended material over the two seasons is displayed in Figures 4.1 and 4.2. The higher concentrations (greater than 2000 ppm) which occurred were:

	Date	Local Time (hr)	Concentration (ppm)	Discharge ($m^3 s^{-1}$)
1973	11 August	1745	4900	5.4
	29 July	1640	3950	3.6
	30 July	1830	2500	3.7
1974	11 August	1230	2204	9.7
	11 August	1305	2139	11.2
	10 July	1750	2051	12.3

The value recorded on 11 August, 1973, is an anomalous result as the discharge at the sampling time is only a moderate flow. This possibly reflects a high concentration due to material slumping upstream. The rainstorm flood of 22 July, 1973, provided a sampled concentration of 1350 ppm. For the duration of the flood it is possible that concentrations exceeded 3000 ppm. The three values quoted above for 1974 were the only concentrations over 2000 ppm. Only nine samples produced concentrations over 1000 ppm, with concentrations of 50 to 350 ppm more common. The highest concentration reported in a sandur environment was by Fahnestock (1963), quoting a value of 17200 ppm.

It is evident over the two seasons of record that in 1973 suspended sediment concentrations were, on occasions, higher than in 1974, especially during the latter part of the runoff season. However, discharge was more suppressed and reduced in 1973. This suggests variability in the availability, or supply of material to the Schei

River. This influence on supply is partially inherent in the greater amount of precipitation recorded in 1973, effectively increasing the sediment yield to the Schei River and resulting in greater concentrations of material entrained into suspension. This effect on the supply of sediment appears to be minimal during the drier 1974 season, with suspended sediment concentrations showing a greater dependence on turbulence generated by the flow (hydraulic factors have a greater influence than hydrologic factors). This is evident in a greater association and regularity between suspended concentrations and discharge in 1974 (see Fig. 4.2).

Previous investigations have shown relationships between suspended sediment concentrations and discharge (Fahnestock, 1963; Østrem, Ziegler, and Ekman, 1970; Church, 1972). The relationship between the suspended sediment concentration(s) and discharge (Q) was computed for the Schei River in 1974 to establish a calculated suspended sediment rating curve for predictive purposes. The derived equation is as follows:

$$s = 45.7\, Q^{1.22} \qquad r = .77 \quad (IV.3)$$

Figure 4.4 illustrates the relationship. The exponent in the equation implies that the concentration of suspended material increases more rapidly than increasing discharge.

The moderate significance of the relationship suggests that other factors affect the concentration of suspended material. A number of possible aspects which influence the above relationship are discussed as follows:

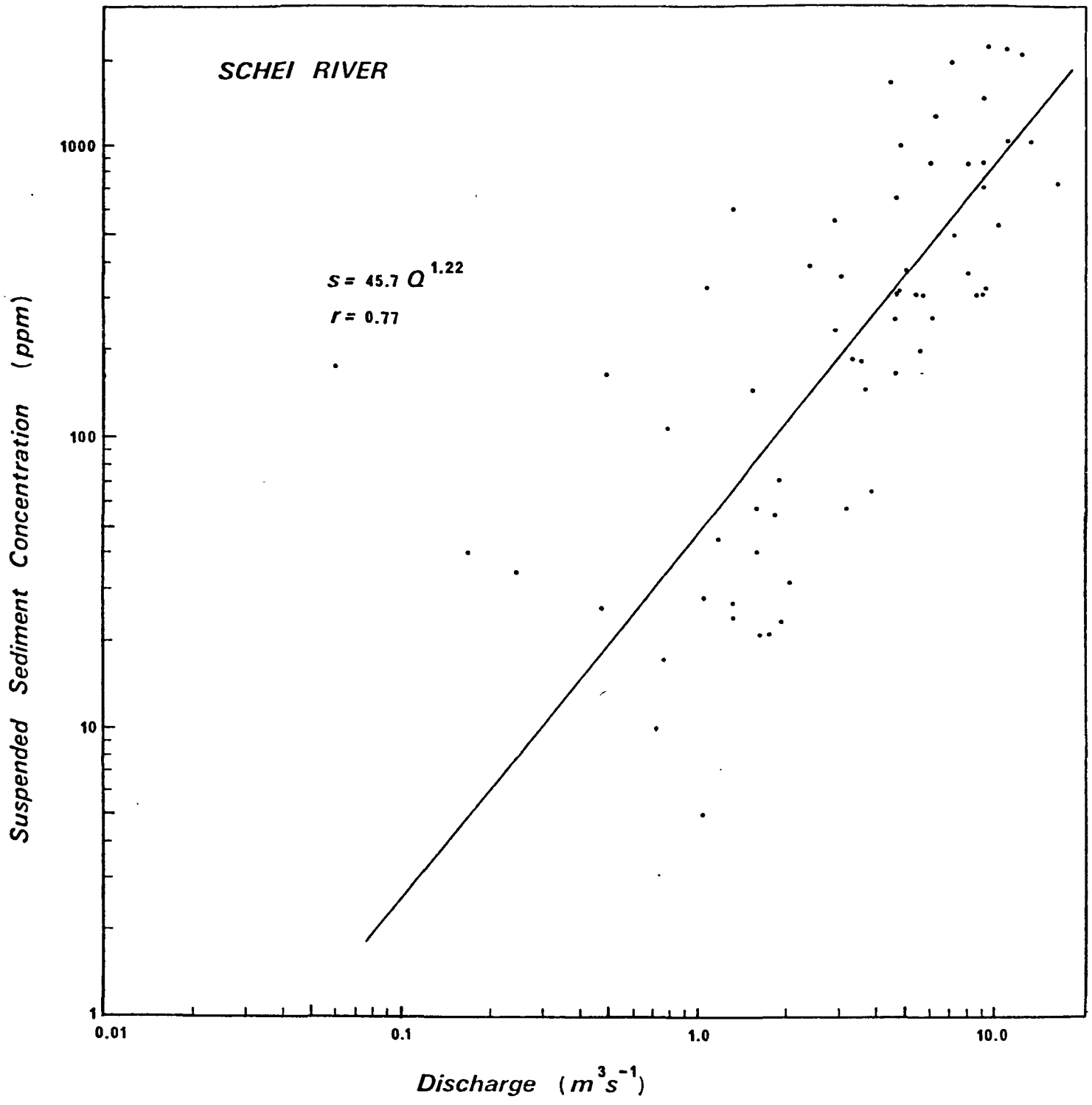

Figure 4.4 Relationship between suspended sediment concentration and discharge, 1974.

a. Sampling method. Possibly the largest error arises in the assumptions made in the field procedure of sampling, due to the flow pattern and distribution of suspended sediment across the channel; possibly occurs as longitudinal bands depending on the width-depth relationship (ratio).

b. Hysteresis effect (differences in the time of arrival of the peak discharge and the suspended sediment peak). This effect has probably provided an influence on the concentration of a sample for a given discharge due to differences in the concentration between the rising and falling limbs of the hydrograph. This effect was reduced as sampling usually occurred on the rising limb.

c. Precipitation effects. Scatter in the relationship suggests that in part the relationship is affected by the supply of material. Church (1972) performed a number of correlations between suspended sediment concentrations and a number of other factors likely to influence the concentrations of material. Church concluded that the concentration was a function of discharge and precipitation effects (affecting sediment yield). Although rainfall over a basin increases the sediment yield, the lack of rainfall events during the 1974 season suggests this exerts only a minor influence on the resultant concentrations although clearly an influence is evident during the 1973 season.

d. Water temperature. Water temperatures were conservative over the runoff seasons and the effects on kinematic viscosity (and hence the concentrations) were probably minimal, although in comparison to other fluvial environments are possibly significant due to an increased drag on small particles effectively increasing the competence of the stream.

e. Anomalous results. This is evident in the early runoff season of 1974, with high concentrations experienced at low flows due to aeolian sediments accumulating over the snow during the winter period. Anomalous results would also occur from local slumping which would increase the concentration and disrupt the relationship.

Despite the influences other than that due to hydraulic factors, the relationship was used for computing the suspended sediment load of the Schei River for the 1974 season, exemplified in Figure 4.6.

A marked increase in the amount of material carried in suspension occurs at discharges in excess of about 3 m^3s^{-1}. Therefore high loads carried in suspension occur frequently over the summer. The highest computed load was 993.3 metric tons/day during the snowmelt freshet. Other prominent peaks in the suspended load are mainly evident during the snowmelt freshet and glacial-melt flood.

4.4 BEDLOAD

Most studies define bedload as that portion of the total sediment load which moves at or near the bed by rolling, sliding, or saltation. It can be assumed that the amount of sediment moved as bedload is a function of the flow conditions, as the bed material provides an adequate supply of material for transport. However this assumption becomes complex due to packing and imbrication of the particles (underloose state; Church, 1972).

Hein (1974) discusses a number of difficulties which arise in applying transport formulae to a coarse material - shallow flow system. This includes the nature of the interactions between the flow, the roughness elements, and the particles in transport. Disruption of the flow by turbulent eddies shed from the bed particles have considerable effect on the initiation and continuing movement of sediment. Bed material size has a pronounced effect on the type of flow and velocity profile (Briggs and Middleton, 1965), and hence the assumption of a logarithmic velocity profile may no longer be valid in these systems (Hein, 1974). Other difficulties include the fact that the particles and the flow do not move at the same velocities, and variations in the rate of movement occur due to the effects of the bed shape.

An understanding of some aspects of open channel hydraulics

is required for a theoretical approach to bedload sediment transport. This includes a consideration of the following:

1) The measurement of certain flow parameters and the exceedence of threshold conditions, before bedload transport occurs.

2) The establishment of the hydraulic relationships and application of transport formulae to the motion of coarse sediments.

A. Initial sediment movement

The threshold of particle motion is defined as the moment of occurrence when fluid forces overcome the material resisting forces. Particles remain in a stable position when the condition is reached where the resisting forces become dominant. However particle motion, as a balance between these two forces, becomes complicated with grain interactions during movement. Movement of large particles in non-cohesive sediments depends on the numerous individual properties of each particle (i.e. density, size, shape).

In order to determine the flow conditions necessary for incipient movement of particles, measurements of the stream competence were attempted by a procedure employed by Church (1972). Size graded pebbles, cobbles, and boulders, were marked and set on the channel bed in phi groupings immediately downstream of the gauging site where the hydraulic geometry of the channel section was determined. The b-axis lengths were size graded at whole phi intervals from -5 phi to -10 phi

(20 to 600 mm actual range), comprised of material of various lithologies and densities. The marked particles set on the bed were completely exposed and were not protected by the bed itself. The particles were periodically checked for movement and the maximum previous stage was noted from the adjacent water level stage recorder (yielding the discharge and hydraulic parameter values for the stage condition). The hydraulic data obtained from the gauging section which was used as a basis for formulating the subsequent calculations is displayed in Table 4.2. Tractive force, or the shear stress acting on the channel bottom, was estimated by the equation

$$\tau_o = \rho_f g R S \qquad (IV.4)$$

Where τ_o is the tractive force acting on the bottom, ρ_f the fluid density (1.00 g cm^{-3}) g the acceleration due to gravity (9.83 m s^{-2}), R the hydraulic radius (approximated by the mean depth $\overline{d}$), and S the slope (0.0122).

The largest clast moved was assumed to represent the competence limit for the observed maximum stage.

Flow conditions required for the initial motion of coarse material on the channel bed were also determined using the Shield's entrainment function. Assuming the Shield's relations hold for a sandur system, the shear stress required for initial grain movement can be determined from the relationships (Raudkivi, 1967):

TABLE 4.2

HYDRAULIC DATA OF SCHEI RIVER, 1974

	Date	Measurement Time	Stage y (m)	Discharge Q ($m^3 s^{-1}$)	Surface Width W_s (m)	Mean Depth $\bar{d}$ (m)	Mean Velocity $\bar{u}$ ($m\ s^{-1}$)
(1)	2 July	1050-1120	0.27	1.43	15.06	0.15	0.65
(2)	4 July	1030-1110	0.55	** 4.54	17.28	0.28	* 1.06
(3)	5 July	To = 1950	0.80	10.05	* 18.55	* 0.34	* 1.64
(4)	10 July	To = 1155	0.67	4.37	* 17.21	* 0.25	* 1.04
(5)	27 July	1130-1215	0.38	2.91	17.15	0.19	0.92
(6)	27 July	1230-1305	0.47	3.15	17.20	0.23	0.79
(7)	27 July	1400-1430	0.61	6.48	17.70	0.30	1.20
(8)	27 July	1500-1535	0.64	7.62	17.95	0.32	1.31
(9)	14 August	1600-1625	0.34	1.30	15.20	0.12	0.69

* computed from equations (V.2a,b,c)

** computed from relationship in Appendix B

$$\tau_c = \beta g (\rho_s - \rho_f) D_s \qquad \text{(IV.5a)}$$

$$\tau_c = \rho f u_{*_c}^2 \qquad \text{(IV.5b)}$$

Where τ_c is the critical shear stress

g the acceleration due to gravity

ρ_s the mass density of the sediment

ρf the mass density of the fluid

D_s the average sediment particle size

β Shield's beta

and u_{*_c} the critical shear velocity

The Shield's criterion was used to estimate the smallest grain size which would resist entrainment, given the shear velocity. As the value of is 0.06 for fully turbulent flow, substitution and equating equations IV.5a,b gives:

$$D_c = \frac{\rho f u_*^2}{0.06\, g\, (\rho_s - \rho f)} \qquad \text{(IV.6)}$$

The shear velocity was estimated by rearranging equation IV.5b. This can be expressed as:

$$u_* = (g\, RS)^{1/2} \qquad \text{(IV.7)}$$

An average density of the sediment was assumed to be 2.65 g cm^{-3} and an average fluid density of 1.00 g cm^{-3}.

The critical grain size can also be expressed as a function of the tractive force by rearranging equation IV.5a. Substituting the constants in the equation yields:

$$D_c = \tau_c / 0.885 \qquad \text{(IV.8)}$$

Unfortunately only three sets of results were obtained from the competence tests and the results differed from that predicted by the Shield's criterion (Table 4.3). The results also differed from observations made on the Schei River for the initial motion of sediment, and hence remain unsatisfactory. For the three competence tests the Shield's criterion predicted a size of sediment smaller than that actually moved. However Church (1972) notes that differences in the actual competence and that predicted by the Shield's criterion arises from material openly exposed on the channel bed and material incorporated within the bed. Hein (1974) also suggests that discrepancies may be due to the fact that the critical shear velocity for initial sediment movement may be highly influenced by the interaction between the particles in motion and the bed roughness elements. A diagrammatic comparison of the results is given in Figure 4.5.

B. Transport Formula Computations of Bedload

Raudkivi (1967) discusses and compares various sediment transport formulae and notes that any of the published transport formulae can be transcribed in terms of establishing a functional relationship between particle inertia ($\emptyset$) and stream power ($1/\psi$). However, many of the bedload formulae have been developed for the transport of sand-size material and may not be applicable to coarse-grained sedim[illegible].

Hollingshead (1971) proposed a method of calculating bed load sediment transport rates in coarse bed material. The method is

TABLE 4.3

STREAM COMPETENCE AND TRACTIVE FORCE ESTIMATES
FROM FIELD MEASUREMENTS AND SHIELD'S CRITERION

	Discharge Q ($m^3 s^{-1}$)	Mean Velocity $\overline{u}$ ($m\ s^{-1}$)	Shear Velocity (1) u_* ($m\ s^{-1}$)	Tractive Force (2) τ_c ($N\ m^{-2}$)	Particle size moved: Observed D (mm)	Particle size moved: Predicted by Shield's criterion (3) D_c (mm)
(1)	1.43	0.65	0.134	17.99		20
(2)	4.54	1.06	0.183	33.58		38
(3)	10.05	1.64	0.202	40.77		46
(4)	4.37	1.04	0.173	29.98		34
(5)	2.91	0.92	0.151	22.79		26
(6)	3.15	0.79	0.166	27.58		31
(7)	6.48	1.20	0.190	35.98		41
(8)	7.62	1.31	0.196	38.38		43
(9)	1.30	0.69	0.120	14.39		16
(10)	$\overline{2.71}$	* 1.73	0.156	24.46	< 32	28
(11)	$\overline{14.8}$	* 1.97	0.214	45.81	~ 64	52
(12)	$\overline{23.55}$	* 2.62	0.236	55.77	~ 512	63

(1) computed by equation IV.7
(2) computed by equation IV.4
(3) computed by equation IV.6
* calculated from equation V.2c
— overbar notation denotes the maximum discharge over the measurement period

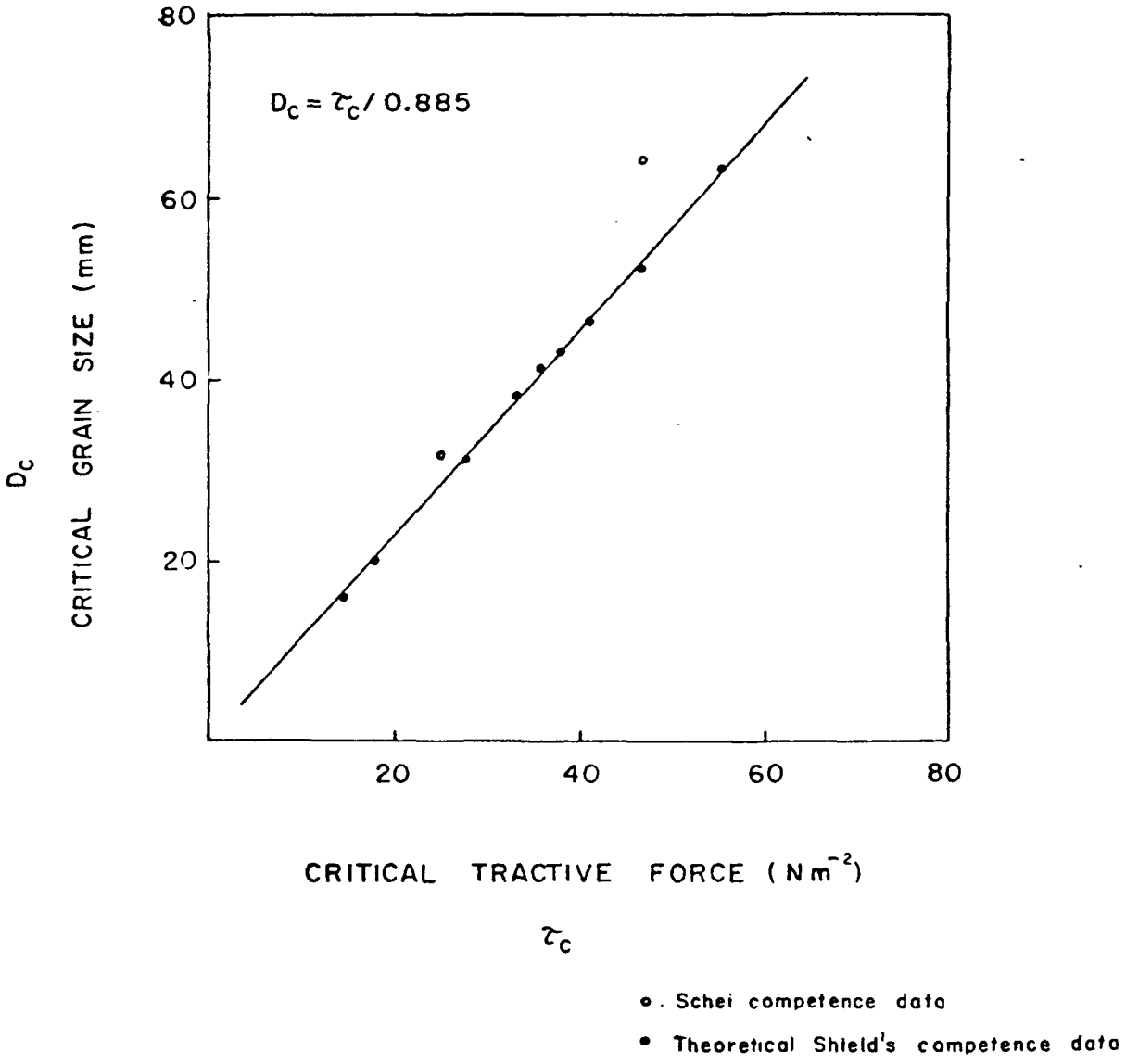

Figure 4.5 Sediment size entrained as a function of critical tractive force.

* Note that the observed value from the third field measurement (No. 12) has not been plotted.

based on an assessment of the river width contributing to the bedload transport, velocities occurring over the width, and R. H. Cooper's (discussed in Hollingshead, 1971) flume data analysis. Hollingshead found good agreement between adjusted sampler bed load estimates and calculated bed load rates for the gravel beds of the Elbow River, Alberta. Hein (1974), in an application of the Hollingshead method, also found close correspondence with measured bed load discharges in the Kicking Horse River. However, due to a lack of familiarity with the method as proposed by Hollingshead, the Meyer-Peter and Muller transport formula (in Chein, 1954) was selected. In addition, the Meyer-Peter and Muller formula provides a more conservative estimate of bed load transport than does the Hollingshead method (Hollingshead, 1970), and was empirically developed for a wide range in the parameters $\overline{d}$, S, D_s, and γ_s suitable for application to coarse bed material streams.

A brief discussion of the Meyer-Peter and Muller bedload equation, based on the account by Chein (1954), follows. The formula is based on a calculation of the bed shear stress from the total energy slope (with a correction made for that portion of the total flow resistance caused by grain size resistance effects). The average unit bed shear stress, exceeding the threshold condition, is then applied to the channel cross section for a calculated transport rate.

The equation is expressed as:

$$\gamma_f \, (K_t/K_r)^{1/3} \, RS - 0.047 \, (\gamma_s - \gamma_f) \, D_m = 0.25 \, (\gamma_f/g)^{1/3} \, g'_s{}^{2/3} \quad (IV.9)$$

Where γ_f is the specific gravity of the fluid

γ_s the specific gravity of the sediment

R the hydraulic radius; equals the mean depth ($\bar{d}$) with negligible bank resistance

S the water surface slope; approximates the energy gradient of the stream

D_m the mean particle size (D_{50})

g the acceleration due to gravity

and g'_s the specific rate of bedload sediment transport by submerged weight

K_r is the coefficient of particle roughness; equals $26/D_{90}{}^{1/6}$ where D_{90} is the particle size in which 90 per cent of the material is finer

K_t is the coefficient of mean flow resistance; equals $1/n$, where n is Manning's roughness coefficient.

The entrainment function ($1/\Psi$) can be expressed as:

$$1/\Psi = \frac{\tau_c}{\rho_f \, g \, [(\rho_s - \rho_f)/\rho_f] \, D_c} \quad (IV.10)$$

The value at the threshold of sediment movement was calculated to be 0.055, based on the results in Table 4.3. This is a slightly higher value of 0.047 in the Meyer-Peter and Muller value used in the bedload computation.

The values for the Meyer-Peter and Muller equation (IV.9) are as follows. The value of γ_f is 1.00, γ_s is an assumed value of 2.65, S an assumed constant of 0.0122, D_m is 35 mm, D_{90} is 295 mm, g is 9.83 ms^{-2}, and n is assumed to be 0.035. The values of D_m and D_{90} were obtained from a grain size distribution curve of the bed material at the gauging section. The parameters $\bar{d}$ and W_s (surface width) were calculated for each flow condition from the hydraulic geometry relationships (see p. 93). All values were adjusted to the proper units in the equation.

By transposing the terms, the unit transport rate was calculated for each flow condition and converted to a dry weight by the factor $\gamma_s/[\gamma_s - \gamma_f]$. The product of this value with the channel width then gives the bedload transport rate. This was then summed with the computations for the other flow conditions to give the sediment bedload for each day. The critical discharge given by the formula for incipient motion of the average size of the bed material is 5.2 m^3s^{-1}. This is in reasonable agreement with observations made of the initial grain movement on the Schei River. The derived load by bedload transport for the 1974 season is illustrated in Figure 4.6.

The bedload reveals the most abrupt change in the amount of material carried with a change in the flow conditions. Once initial sediment motion begins high loads occur at moderate to high flow conditions. Several peaks discontinuously occurring over the summer

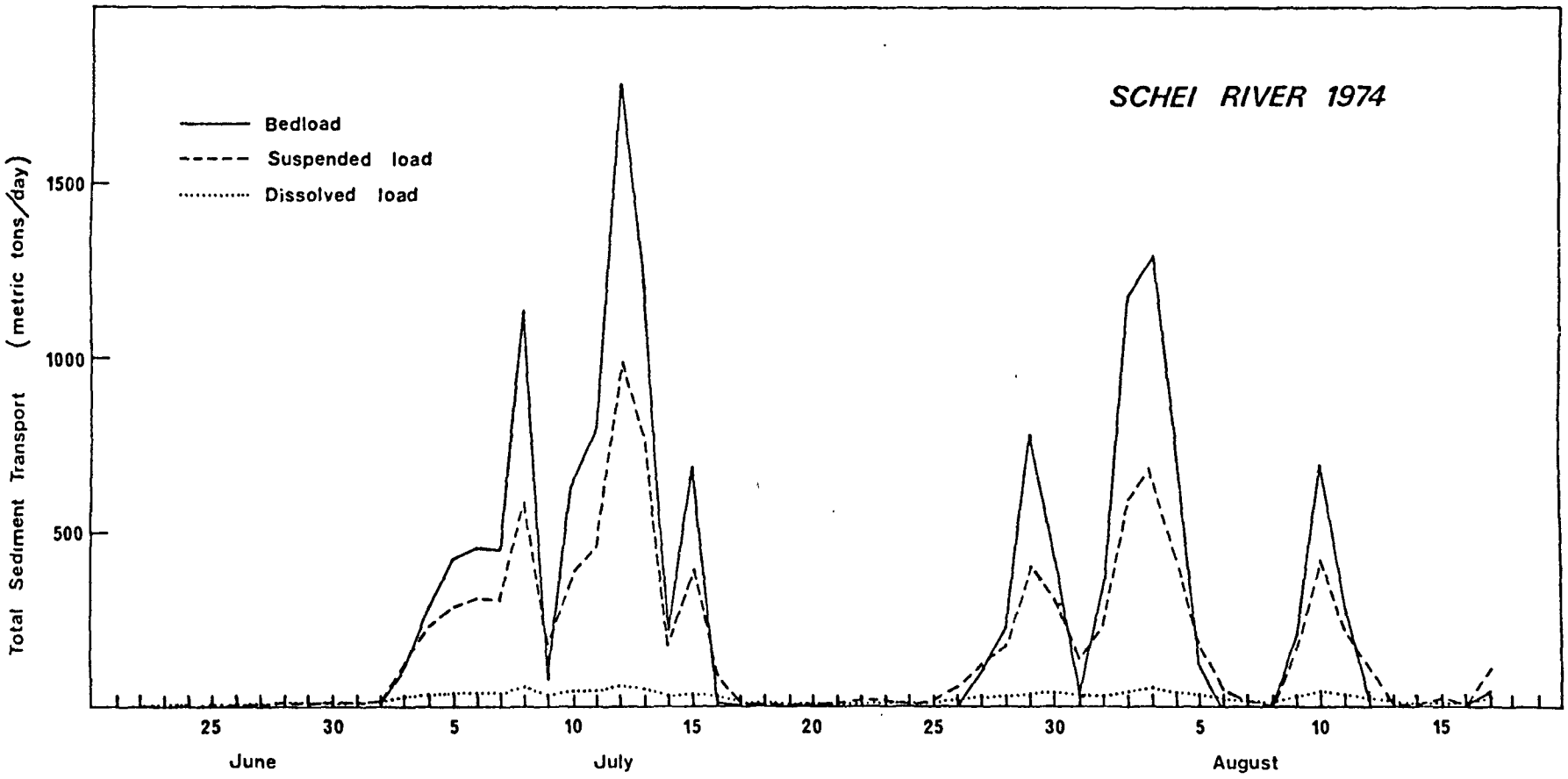

Figure 4.6 Daily total sediment loads of Schei River, summer of 1974.

runoff season are evident. The two highest loads yielded calculated values of 1783.5 and 1299.3 metric tons/day during the snowmelt freshet and late season glacial flood respectively.

4.5 SUMMARY AND DISCUSSION

A summary of the total daily sediment load by dissolved, suspended, and bedload transport, reveals that during the field investigation period in 1974, 15,014 metric tons of material were removed by bedload transport, 9,984 metric tons by suspended transport, and 1,419 metric tons by dissolved transport.

The study of the sediment transported by the Schei River may be summarized as follows:

1. The dissolved load is of only minor importance, accounting for approximately 5 per cent of the total load in 1974. However, during the lower flow season of 1973 the dissolved load was probably of greater significance.

2. The suspended load is an important component of the total sediment load and accounts for 38 per cent of the sediment removed in 1974. In 1973, the suspended load was probably the dominant mode of transport.

3. Sediment was mainly transported as bedload in 1974, with 57 per cent of the total load transported by this component. Also the Meyer-Peter and Muller transport formula was viewed as yielding a conservative estimate of bedload transport, so that the amount of material removed by this fraction may be higher. Bedload may have been only moderately important in 1973, occurring mainly during the higher flow events (22 July rainstorm flood; snowmelt freshet).

This suggests that the large variations in the magnitude of discharge recorded over the two runoff seasons, has a pronounced affect on the distribution of the load and the amount removed by each component. The flow frequency curve for the Schei River in 1974 (Fig. 4.7), indicates that although flow conditions necessary for any significant transport by bedload occurs less frequently than that required for suspended or dissolved transport, a considerable proportion of the total load is transported as bedload over a relatively short period of time (a conclusion similarly reached by Church, 1972). The sediment removed by each fraction of the total load is dependent on the duration and magnitude of the flow conditions, inherent in the influence by hydrologic factors.

The results obtained of the sediment transported in 1974 refer to conditions which occurred in the upper proximal area of the sandur, viewed as an input to the sandur system. Observations of the

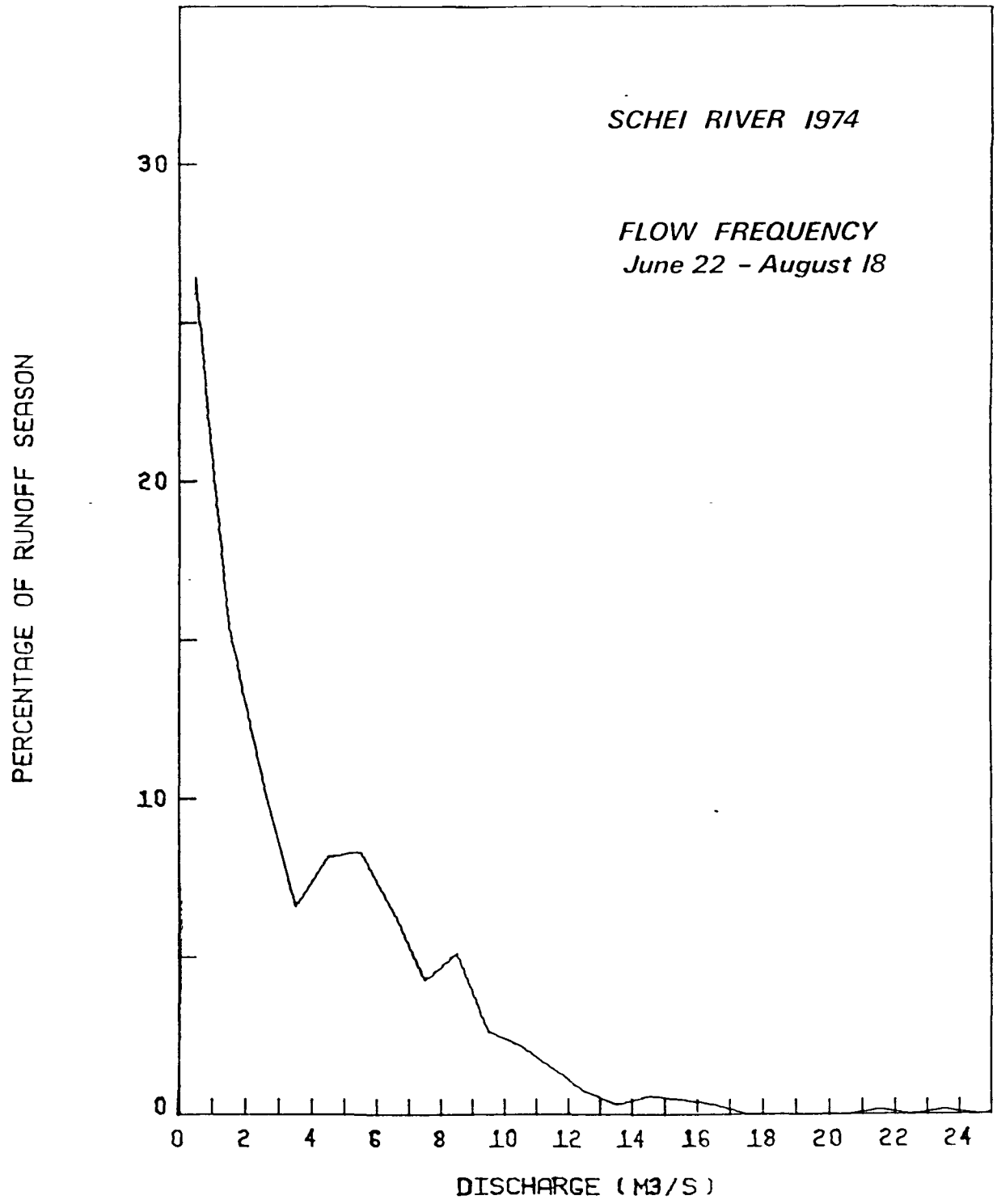

Figure 4.7 Flow frequency curve for Schei River, summer of 1974.
(after Ballantyne, 1975)

sediment transported out of the system suggested all the solutes were removed together with the bulk of the suspended material and some finer fraction of the bed transported sediment. It is unlikely that any dissolved material is precipitated out once taken into solution. However, considerable fine materials carried in suspension may be deposited over the sandur during declining flow (Fig. 4.8). The coarseness of the sandur sediments implies deposition of material moved as bedload, with a downfan gradation in the size of the material due to decreasing downstream competence. In this regard, the sandur system as a valley fill deposit, is mainly comprised of material which is carried as bedload and remains as temporary storage in transit through the system.

Veneer of silt in an abandoned channel area.

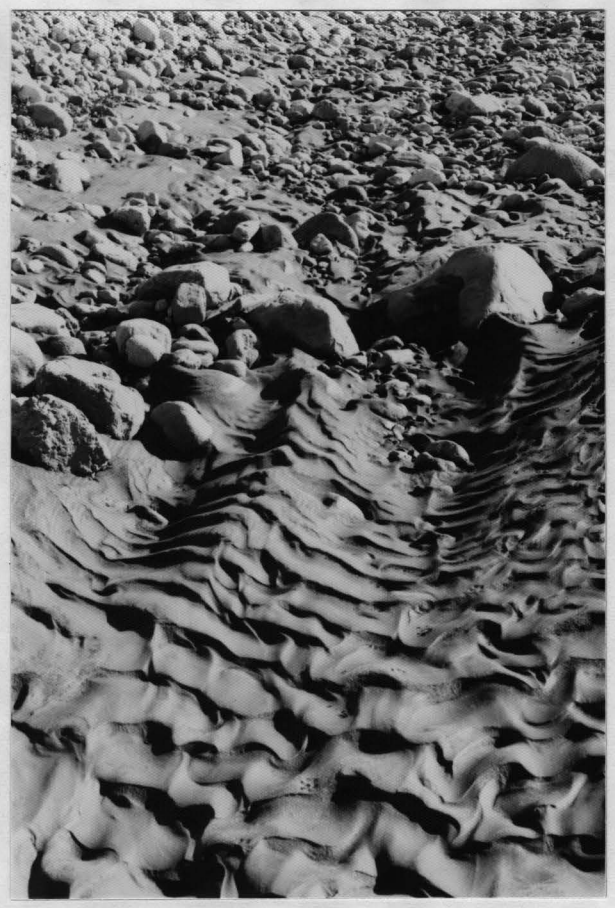

Silt and sand deposited in a minor channel.

Figure 4.8 Examples of fine material storage on the sandur.

CHAPTER V

HYDRAULICS AND SEDIMENT CHARACTERISTICS OF THE SANDUR

5.1 INTRODUCTION

This section considers the nature of the braided stream channels and the general surface characteristics of the Schei sandur. A discussion of the channel geometry and hydraulic conditions leads to a description of the bar forms developed within the channels, and an analysis of the changes which took place in the channel network during the two seasons of field observations. This consideration of process-form relationships, based on detailed field measurements in the upperfan area of the sandur, provides an understanding of the surface form and sediments of the sandur as a whole. Discussion of this latter aspect is based on the long profile of the main channel and sample information over the sandur, which has been analyzed and presented by an application of trend surface analysis.

The coarse noncohesive materials of sandur deposits are relatively easily eroded. Channel shape is related to the bed and bank materials (Wolman and Brush, 1961) and to the amount of sediment-water load transported by the stream. Channel stability is reached for flows below the competence level of the material comprising the

bed and banks (Church, 1972), with channel armouring from selective transport of the bed and bank material, imbrication, and packing, possibly raising the competence value. Flows above this competence value govern and alter the channel shape through local erosion and deposition, in accordance with the changing water and sediment discharge. The majority of channel adjustments occur by bank erosion, which gives the braided channels their characteristic wide and shallow channel shape.

Various mechanisms have been proposed to explain the causes of braiding. These include rapid fluctuations in discharge and sediment load, high channel slopes or change in slope, bank erodability, aggradational conditions, considerable sediment load, and high flow velocities.

Aggradational conditions in a fluvial environment are not the sole cause of braiding, for Leopold and Wolman (1957) and Fahnestock (1963) have reported that braided channels can also occur under equilibrium conditions. A steep channel slope, or change in slope, and sediment-water discharge fluctuations do appear to be associated with a braided regimen, but are dependent variables and are unlikely to be a cause of braiding per se.

Church (1972) and Smith, D. (1973) have cited both bank erodability, due to the noncohesive nature of coarse, clastic materials,

and a considerable coarse sediment load as the causes of braiding in coarse outwash deposits. Fahnestock (1963) has also asserted that significant bed load transport in these high energy streams is characteristic of the river mechanics operating in a braided environment. Other variables such as slope, flow velocities, variation in discharge, and changes in channel width and depth, influence lateral erosion in the noncohesive sediments and channel bar development, eventually leading to the development of multiple channels.

Smith, D. (1973) has suggested that braiding occurs in two distinct situations, based on different hydraulic conditions:

a. Channel anastomosis - channel division in a low energy gradient situation in stable channels.

b. Braiding - unstable multiple channels in noncohesive material, where high energy streams carry substantial sediment loads.

The second case describes the conditions of the Schei sandur.

5.2 CHANNEL GEOMETRY

To provide some indication of the shape of a number of sandur channels in the detailed study area (Fig. 5.1), width-depth

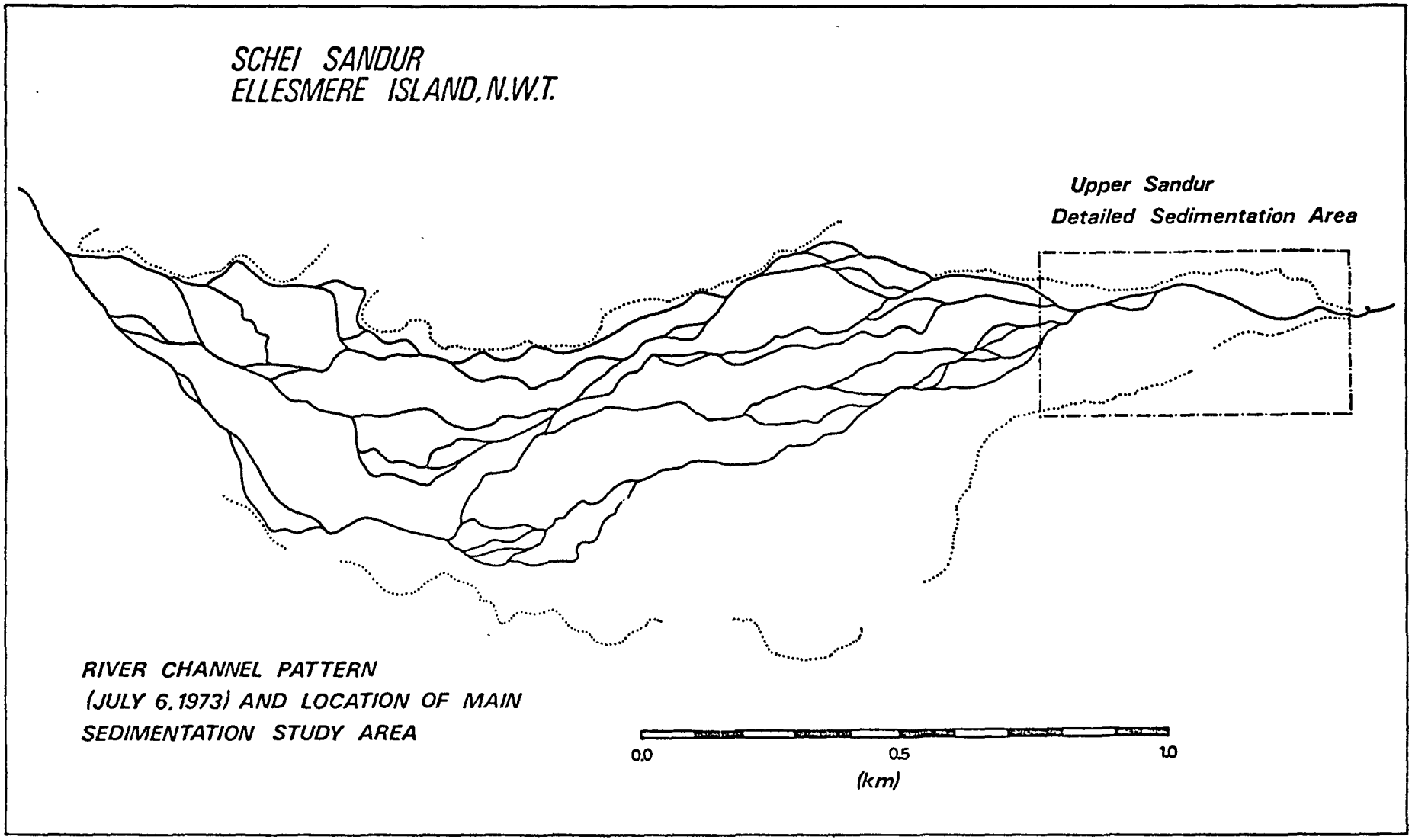

Figure 5.1 Location of the detailed study area on the Schei sandur, and principal channel pattern on 6 July, 1973.

ratios ($W_s/\bar{d}$; surface width to mean depth) were determined for comparative purposes to express channel cross-sectional shape as a function of the bed and bank materials. Eight channel cross-sections (P1 to P8) in this area, representing single or braided sections, were analyzed between sections for the comparisons, with the results presented in Table 5.1. Figure 5.3 illustrates some of the channel cross-sectional shapes under consideration. The sections are located at regular downstream intervals in the detailed study reach (Fig. 5.2).

Schei River channels, developed in noncohesive material, exhibit geometries which are generally shallow and wide. It can be seen that considerable variation in the channel geometries and width-depth ratios occur between channels for a given discharge. Generally, higher width-depth ratios were experienced in minor channels at-a-section, due to a lesser proportion of flow in the minor channels. Overall, for a given discharge, there appears to be no significant difference between width-depth ratios in a single channel and a corresponding braided channel, although braided channels may possess slightly lower $W_s/\bar{d}$ values.

In addition to comparing $W_s/\bar{d}$ ratios between sections, due to different channel types and shape, $W_s/\bar{d}$ ratios were compared at-a-section for variations due to discharge(Q) at the gauging

TABLE 5.1

Summary of the width-depth ratio values measured in the different channel cross-sections

(discharge approximately 2.6 $m^3 s^{-1}$)

Cross-Section		W_s (m)	$\bar{d}$ (m)	$W_s/\bar{d}$	A (m^2)	
S	P1	16.10	0.21	76.67	3.31	
S	P2	9.80	0.24	40.83	2.33	
S	P3	6.56	0.39	16.82	2.58	
S	P4	9.19	0.28	32.82	2.57	
S	P5	8.77	0.27	32.48	2.34	
	P7	7.70	0.25	30.80	1.95	
	P7m	1.40	0.03	46.67	0.04	
B	P7m	5.26	0.04	131.50	0.21	2.40
	P7m	2.00	0.02	100.00	0.03	
	P7m	1.60	0.04	40.00	0.07	
	P7m	3.00	0.03	100.00	0.10	
B	P8	7.07	0.26	27.19	1.83	2.22
	P8m	4.00	0.10	40.00	0.39	

S - single channel type

B - braided channel type

m - minor channel in braided cross-section

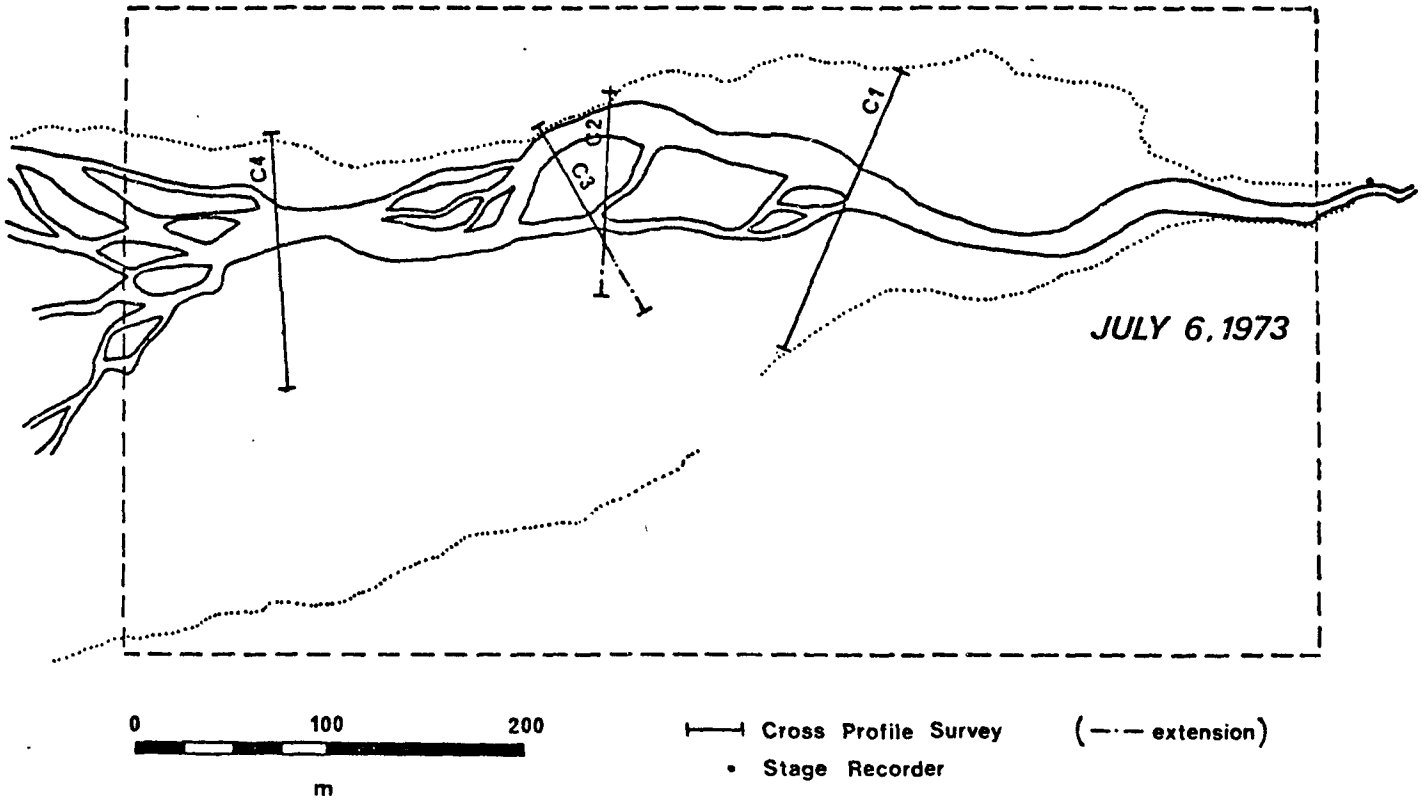

Figure 5.2 Schei Sandur detailed study reach.

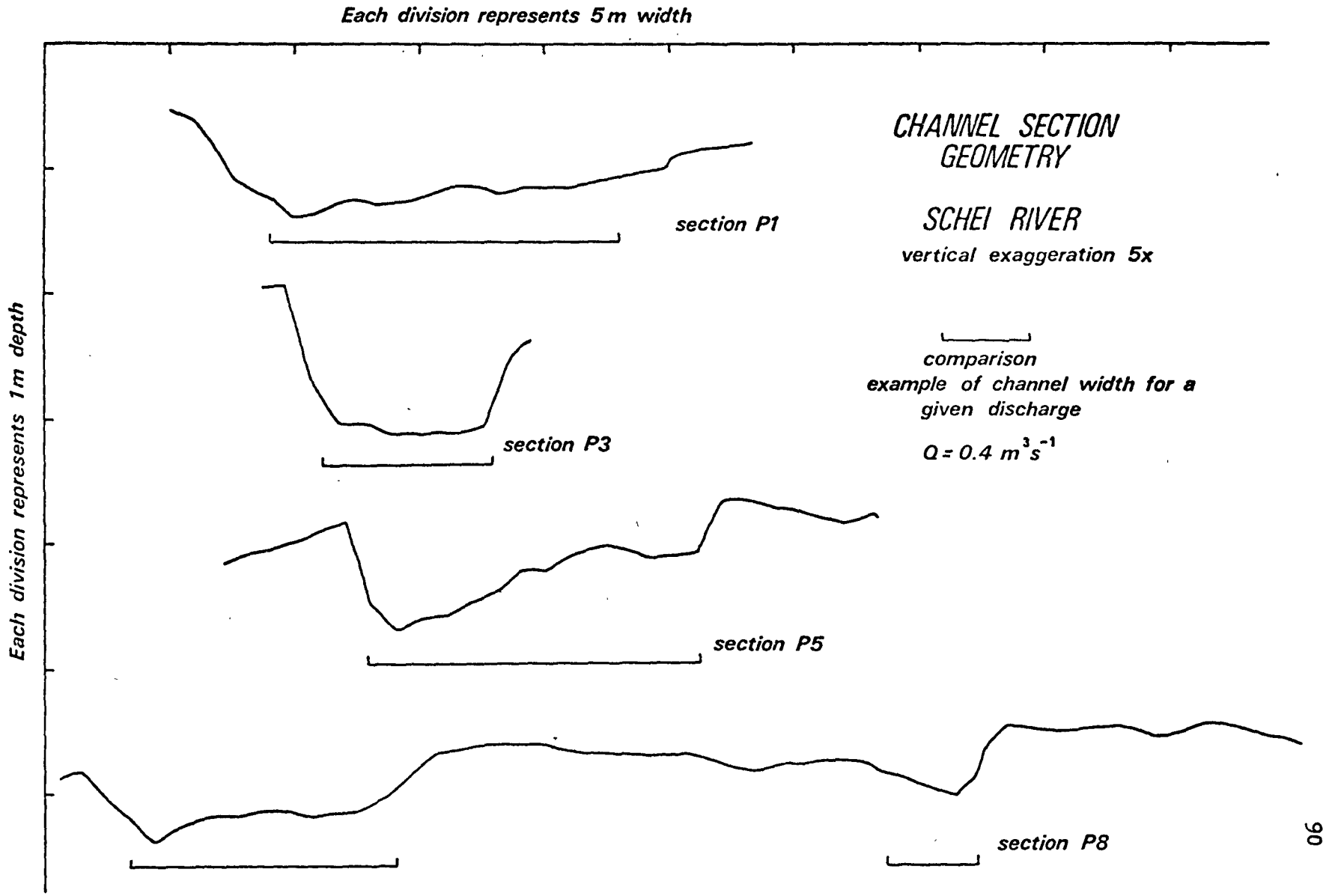

Figure 5.3 Geometry of some of the channel sections used in the $W_s/\bar{d}$ calculations. Section P1 represents the gauging section where the hydraulic geometry was determined.

section (P1). Table 5.2 summarizes the relation between $W_s/\bar{d}$ and discharge for this single channel type section. Although the exact relationship between changing width/depth and changing discharge depends on the channel geometry, the relationship reveals that ratios for this section generally increase with decreasing flow.

Over the two field seasons, sections P1 to P3 remained generally stable sections, while sections P4 to P8 revealed considerable reworking of the sediment, and alteration in cross-section. Sections P1 to P3 remained stable, even though it was observed that at higher flow conditions, general motion of the bed occurred. Channel section P1, following minor alterations in channel shape, appears to have adopted a slightly different relationship between increasing width/depth and increasing discharge, to the initial ratio. This partly reflects scatter in the stage-discharge rating curve (see appendix B). However, the width-depth ratio relationship (and hydraulic geometry relationships) with discharge are not significantly different for this similar channel type. Similar relationships following channel alterations, but resembling the same channel type, suggest a preservation of balanced fluctuations and regulation between fluid and material resisting forces (steady state conditions).

TABLE 5.2

Summary of changing width-depth ratio values with discharge at gauging section P1

	W_s (m)	$\overline{d}$ (m)	$W_s/\overline{d}$	A^2 (m)	$\overline{u}$ (m s^{-1})	Q $m^3 s^{-1}$)
*	17.95	0.32	56.09	5.81	1.31	7.62
*	17.70	0.30	59.00	5.34	1.20	6.48
	17.28	0.29	59.58	4.98	0.96	4.79
*	17.20	0.23	74.78	4.01	0.79	3.15
*	17.15	0.19	90.26	3.18	0.92	2.91
	16.10	0.21	76.67	3.31	0.79	2.61
	15.06	0.15	100.40	2.19	0.65	1.43
**	15.20	0.12	126.67	1.89	0.69	1.30
*	14.00	0.12	116.67	1.73	0.21	0.37

* Values measured after a minor alteration in cross-sectional shape, following snowmelt freshet.

** Value measured during low flow of late season glacial runoff period.

5.3 HYDRAULIC GEOMETRY

Channel adjustments to discharge were investigated by determining the hydraulic geometry of a single channel type at site P1, where the channel cross-section was stable and revealed minimal changes in shape. This section was selected as the stream gauging site due to the stability of the channel form, and for the purpose of establishing the stage-discharge rating curve. From this, relationships were derived for the three parameters of mean velocity ($\bar{u}$), surface width (W_s), and mean depth ($\bar{d}$) as a function of discharge (Q), of a modified form (Leopold and Maddock, 1953):

$$W_s = aQ^b \qquad \text{(V.1a)}$$

$$\bar{d} = cQ^f \qquad \text{(V.1b)}$$

$$\bar{u} = kQ^m \qquad \text{(V.1c)}$$

Note that, as the product of surface width, mean depth, and mean velocity equals discharge, that ideally $a \cdot c \cdot k = 1$ and $b+f+m = 1$. Mean depth was calculated by dividing the computed area of the section (A) by surface width, for a given discharge. The derived relationships are:

$$W_s = 15.07\ Q^{0.09} \quad r = .97 \qquad \text{(V.2a)}$$

$$\bar{d} = 0.14\ Q^{0.38} \quad r = .93 \qquad \text{(V.2b)}$$

$$\bar{u} = 0.46\ Q^{0.55} \quad r = .96 \quad N = 9 \qquad \text{(V.2c)}$$

$$A = 2.17\ Q^{0.46} \quad r = .94 \qquad \text{(V.2d)}$$

The exponents of the $\bar{u}$, W_s, and $\bar{d}$ equations sum to 1.02, while the product of the coefficients equals 0.97 (near unity in both cases).

A comparison of the exponent values measured at this cross-section with data from the Lewis River, Baffin Island, studied by Church (1972), and the Hoffellssandur, studied by Arnborg (1955), reveals that the exponent values of the Schei River are similar (Table 5.3), and that sandur channels commonly show a greater adjustment to changing discharge by changing velocity, while width and depth changes are more conservative. Also, depth increases more readily in response to changing discharge, than does width. Hydraulic data reported by other studies were not compared, as the published values are presented mainly as a mean for numerous channels in the particular study areas.

The rapid adjustment of velocity to discharge at the Schei River gauging section implies two associated phenomena:

a. Assuming an unlimited supply of material, an increasing sediment load occurs with higher flow conditions.

b. Resistance to flow, due to the lower boundary bed resistance, rapidly decreases due to a reduced form resistance at higher discharges, and possibly a dampening of turbulence by an increased suspended sediment load.

TABLE 5.3

Exponent Comparisons of Hydraulic Geometry

River	W_s	$\overline{d}$	$\overline{u}$	A	Source
Schei River	0.09	0.38	0.55	0.46	This study
Hoffellssandur : Gauge 1	0.17	0.39	0.44	0.66	Arnborg (1955) (computed by Church, 1972)
Upper Lewis River	0.18	0.40	0.42	0.58	Church (1972)
Middle Lewis River	$\overline{0.41}$	$\underline{0.10}$	0.49	0.51	
Lower Lewis River	0.10	0.30	$\overline{0.60}$	$\underline{0.40}$	
Lewis Base River	0.17	0.32	0.51	0.49	
Upper Triangle River	$\underline{0.09}$	$\overline{0.56}$	$\underline{0.35}$	$\overline{0.65}$	
Lower Triangle River	0.32	0.21	0.47	0.53	

maximum and minimum values indicated by over-bar and under-bar notations respectively

Assuming a fully developed turbulent flow and all flow resistance to be due to the boundary roughness, the Darcy-Weisbach friction factor (ff) can be determined as (Blatt, Middleton, and Murray, 1972):

$$ff = \frac{8gR\theta}{\bar{u}^2} \qquad (V.3)$$

Where θ is the energy gradient of the stream (approximated by the water surface slope, S), g the acceleration due to gravity (9.83 m s^{-2}), and R the hydraulic radius (approximated by $\bar{d}$ in the wide channels of the Schei River).

For the Schei gauging section (P1), the derived relationship between ff and discharge, Q (based on the parameter values in the above equation used at each flow condition), is:

$$ff = 0.675\ Q^{-.742} \qquad r = -.83 \qquad (V.4)$$

The exponent reveals an extremely rapid decrease in flow resistance with increasing discharge. The measured ff values ranged from 0.178 to 2.878, with an assumed constant water surface slope, S, of 0.0122, for all flows. However, extrapolation of the ff curve for higher discharges should be approached with caution, as the relationship no longer holds with mobile bed conditions (Blench, 1966). Similarly the extremely high friction factor at low flow conditions suggests a lower limit may exist in the relationship as flow occurs between the particles. Flow resistance at higher discharges can mainly be attributed to form resistance (channel shape;with changes in channel shape affecting flow resistance), while the particle roughness elements, determined

by the bed material characteristics, are probably the dominant resistance elements at low flow conditions. Church (1972) also notes that the boundary resistance is not only determined by the particle size characteristics, but also by the spacing.

With a constant slope through a given reach, a changing sediment-water load is transported by an adjustment of the channel geometry and of the friction factor. It appears that the more stable channels (P1 to P3) are capable of generally transporting all the imposed sediment-water loads normally experienced without altering the sections appreciably. In the more unstable channel sections of P4 to P8, the transport of an increased discharge and sediment load is accommodated by not only a change in the friction factor, but also by a change in the channel geometry due to localized scour and fill. Differences in the mode of adjustment are probably inherent in the nature of the bed and bank material and local slope. Church (1972) notes that with a limiting range of ff, unstable channels may have to adjust slope and cross-sectional geometry to carry the imposed sediment and discharge loads.

Initial braiding and channel division occurs when single channel adjustments cannot reduce an increased flow resistance (Church, 1972). For wider channels (as implied by higher $W_s/\overline{d}$ values) shear on the bed is increased. At high discharge and sediment load conditions, widening in the weak noncohesive banks, and alteration in cross-sectional channel geometry, may occur until the channel section is adjusted to transport the increased load and maintain critical

tractive forces slightly above those required to carry the load (assuming slope remains constant). However, channel adjustments from widening may also be accompanied by a reduced friction factor, inherent in an increased velocity and possible particle size change to carry the load. This results in a reduced depth from deposition of sediment on the bed and possibly a local increase in slope. This is concurrent with a localized adjusting development of two relatively narrow and deep (through scour) channels across a section, which possibly with a depositional adjustment, may then possess higher frictional factors but more efficient channels. Further minor re-adjustments occur with falling stage, although the net result of the braiding processes is not readily apparent until flow declines. Channel form then largely reflects a response to high flow conditions, with the shape determined by, and partially indicative of, recent flow history.

5.4 CHANNEL BAR FORM

Regularly spaced accumulations of coarse material generally occur in an oscillatory manner in the channel beds of the Schei River. These major morphologic components of the Schei River channels are a pool and riffle sequence, or pool and bar sequence, as termed by Smith, D. (1973). Smith, N. (1974) notes that bars reveal a wide

variety of sizes, shapes, and stages of alteration, reflecting complex erosional and depositional modifications.

Riffle bed forms comprise bars which occur in several distinctive 'unit bar' (Smith, N., 1974) types (Fig. 5.4). The more common types occurring over the Schei sandur may be classified as:

1. Left diagonal bars, deflecting flow to the left across the bar surface.
2. Right diagonal bars, diverting flow to the right.
3. Spool bars (Krigstrom, 1962), with relatively equal flow deflection on either side of a mid-channel accumulation, and resembling longitudinal bars.

The various types of bars occurring in the Schei River channels are illustrated in the photographs of Figure 5.5. Diagonal bars are the most prominent of the bar forms in the Schei River, occurring at channel bends, or downstream of channel junctions. Spool bars are a less commonly occurring type. Transverse, and point bars are uncommon in the Schei sandur, reflecting more simpler depositional formations. Transverse bars appear when sediment loads are deposited at lower discharges, and probably represent temporary deposition from a single cycle of discharge. Point bars become apparent when discharge is sufficient to permit flow into the minor channel which

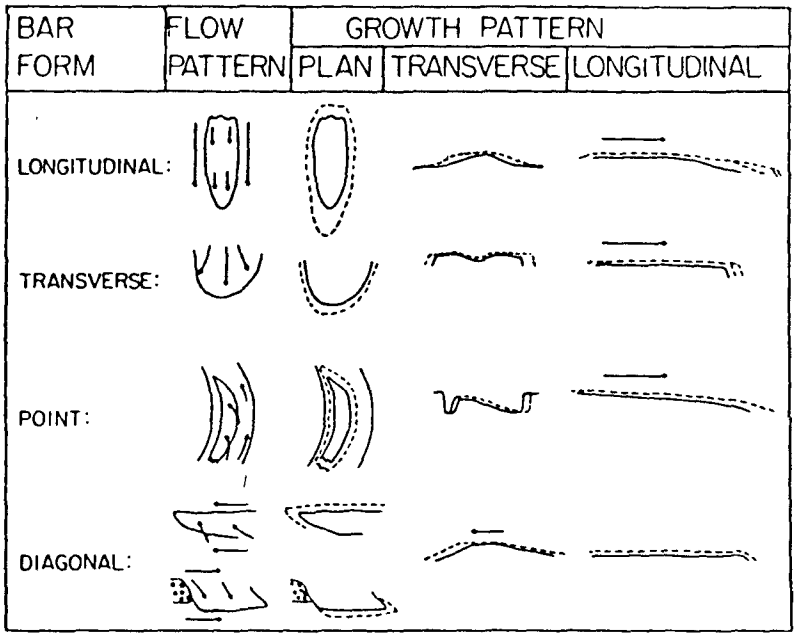

Generalized flow and growth patterns for typical unit bar forms. In each case a small amount of vertical accretion is assumed, although each bar may grow laterally without vertical deposition. *Dashed lines* indicate accretion.

Figure 5.4 Unit channel bar types.

(after Smith, N., 1974)

Spool bar
(longitudinal bar)
at low flow

a.

Right diagonal bar.
This, and the bar
type below, are the
dominant bar forms
on the Schei sandur.

b.

Left diagonal bar -
at section P8.
Note right diagonal
bar immediately
downstream.

c.

Figure 5.5 Channel bar types on the Schei sandur.

occurs on the inner convex margin of a channel bend. Diagonal bars develop with bar long axes oblique to the main flow, while spool, transverse, and point bars possess long axes relatively parallel to the main flow.

Diagonal bars usually represent an altered form from spool bar types, following the development of one of the channels due to increasing channel depth and area by scour. Deflected lateral flow across the bar is important in erosive activity on adjacent channel banks. Spool bars appear to represent a temporary bar form, developed from previous bar alterations at higher flows. This bar type usually becomes reworked and altered into another bar form.

Pool and bar forms are highly active during high flow conditions. With increasing discharge, flow into the converging pool reach scours the channel bed as a form of channel adjustment, with downstream diverging flow over the riffle portion (submerged bar) as a site of deposition. This is due to a higher boundary resistance over the riffle and a decreasing flow velocity. Deposition may occur on the bar surface, or the sediments may be transported to the next bar in the sequence and deposited there, depending on the flow conditions. With decreasing discharge, flow over the bar becomes shallow and diverging, with flow possibly supercritical over the

bar surface. This may lead to the development of erosion scour chutes which dissect the bar edges (Fig. 5.6,b) and with further development may form minor channelways through the bar, dividing it into a number of components (Fig. 5.6,a). Rapid alterations in the morphology and type of the bars can occur during the flood periods, with only the resultant form emerging after the flood peak(s). Complete depositional forms (unit bar) are rare over the Schei sandur, usually only being present as submerged, active bed forms. Unit bar types are suggested to occur as a potential complete bar form for a short period of time. The majority of bar forms occur as some alteration of the unit bar type, which causes diversion of flow while submerged or exposed, and leads to a braided pattern.

To examine changes in bar type, development, and location in the upper sandur area (see Fig. 5.2), plane-table maps of an active channel area were surveyed during the spring flood period of 1974. Rapid variations in flow conditions produced difficulties in traversing and mapping, preventing the monitoring of detailed changes. Only initial and final bar configurations were mapped over the period, during the occurrence of relatively low flows. The net change in the bar survey area is illustrated in Figure 5.7. The most significant changes over the season occurred during peak discharges of the snowmelt freshet and late season glacial peak, with considerable

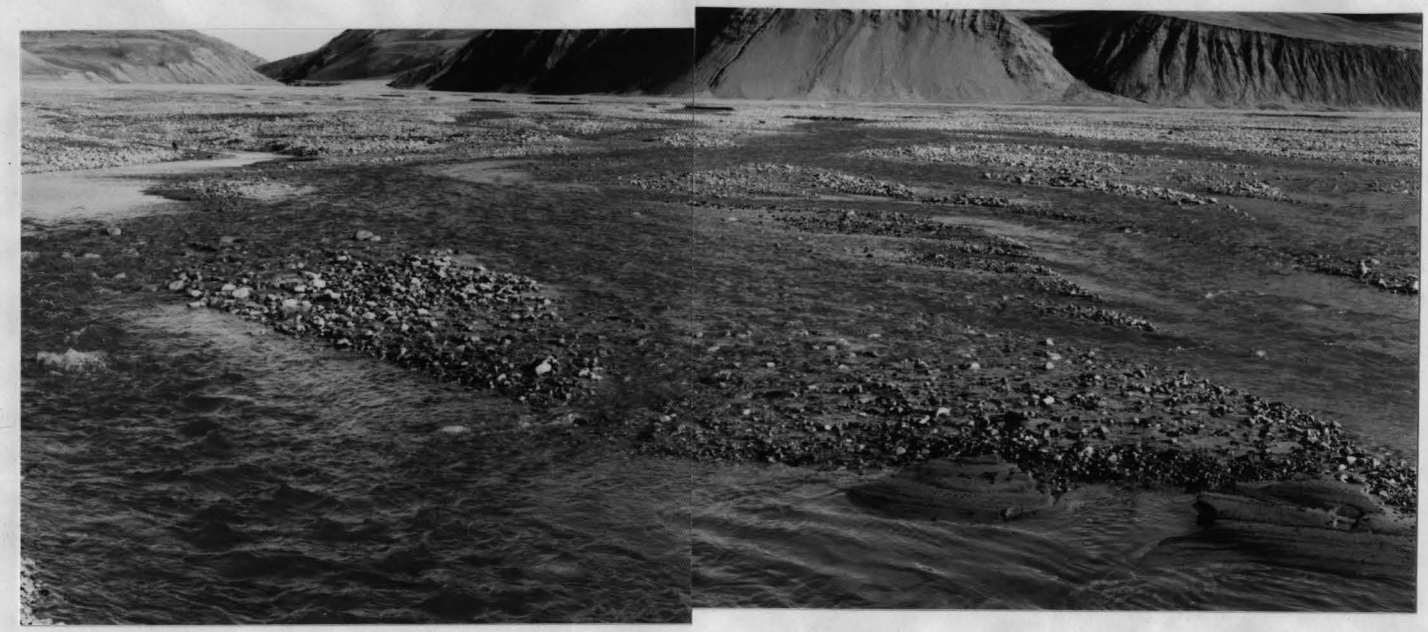

a. Detailed complexity of bar types and chutes in the medial portion of the Schei sandur.

Considerable temporary storage of coarse sediment occurs as bar forms. Note the fine material storage in the foreground, which was carried in suspension at high flow and deposited along the edge of the bar during decreasing discharge.

b. Close-up view of chutes developed on the edge of the bar.

Figure 5.6 a-b Detailed bar morphology on the sandur.

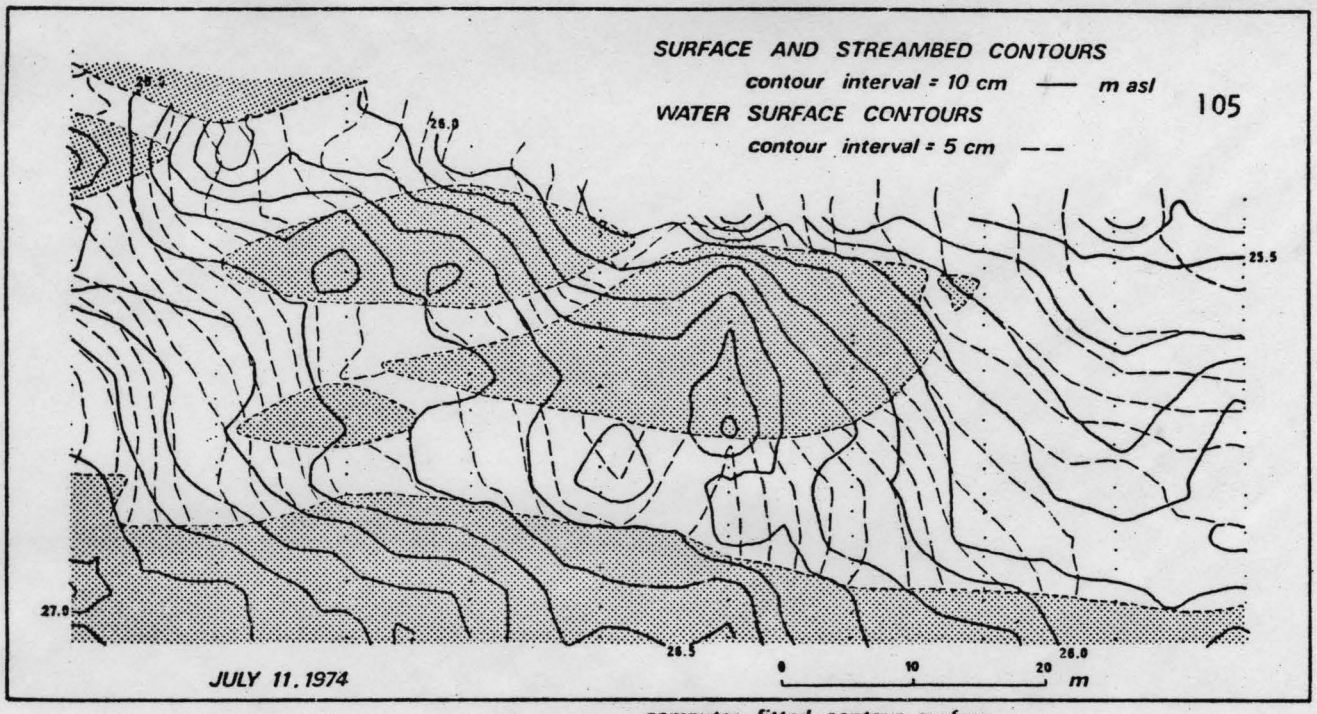

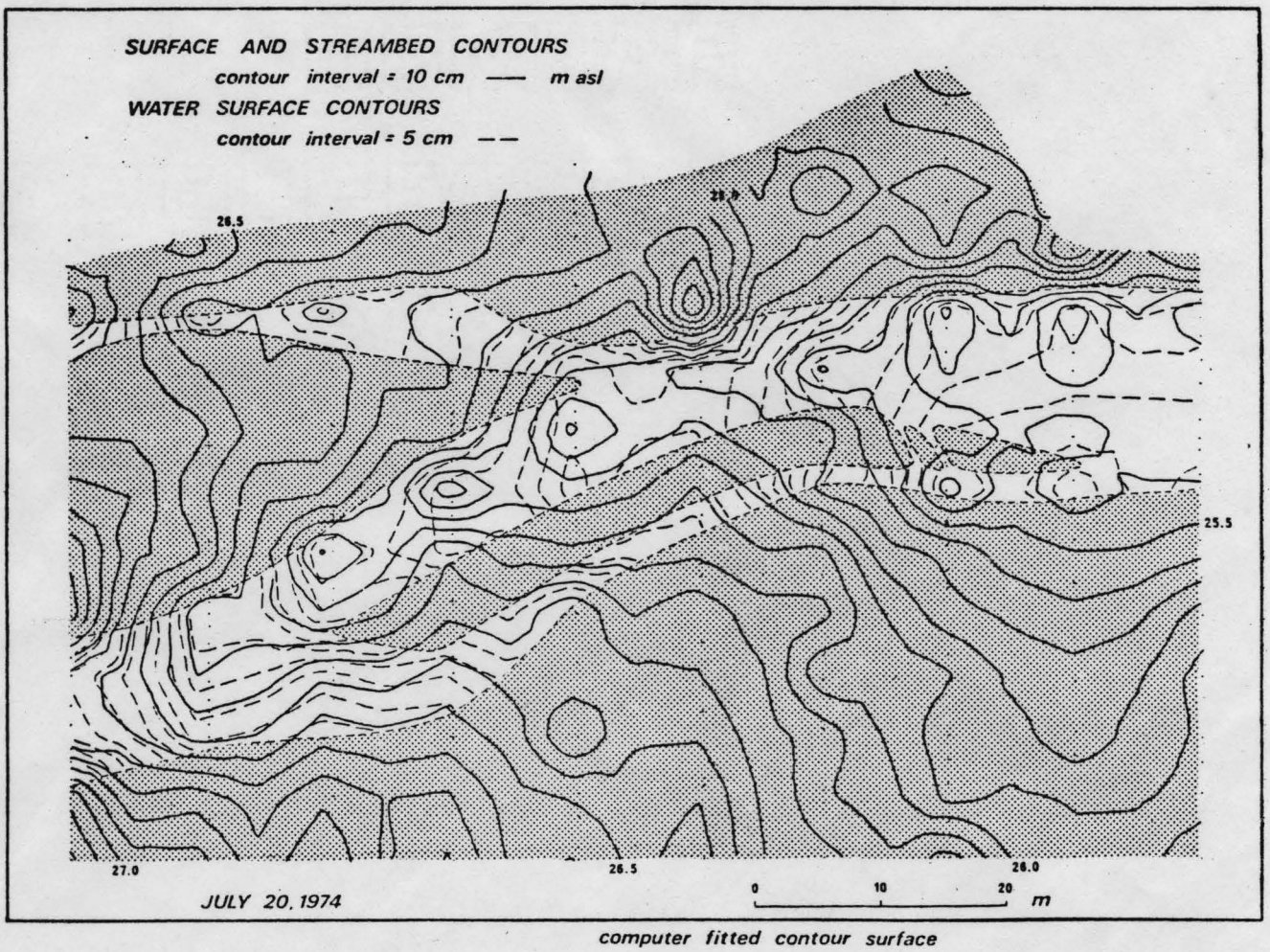

Figure 5.7 Survey results of the change in bar form during the latter part of the snowmelt freshet.

alteration in the bar form occurring between the original and resultant forms during the mapping sessions.

Between 11 and 19 July, 1974, erosion and deposition in the survey area developed the initial spool and left diagonal bar types into a temporary spool bar at high discharge conditions. This probably reflects an adjusted form due to geometry and friction factor alterations at these flow conditions. Further channel-bar alterations, channel bank erosion, and sediment reworking during the latter stages of the spring flood eventually transformed the spool bar into a point bar deposit (see Fig. 5.8), concurrent with a significant lateral shift in the main channel. Although considerable bar material was reworked and transported out of the survey area during the flood period, the bar location essentially remained stationary (an observation similarly noted by Church, 1972). Church (1972) suggests that bar stability in many channels reflects equilibrium with the water and sediment flow conditions.

12 July -
Left diagonal and spool bar types at low flow during snowmelt freshet.

a.

13 July -
Temporary unstable spool bar type at low flow. Developed from previous bar type.

b.

20 July -
Point bar type which developed following the snowmelt freshet.

c.

Figure 5.8 Channel bar changes at the channel bar survey site, 1974.

5.5 SANDUR CHANNEL CHANGES

Profiles across the active surface of the upper sandur area were repeatedly surveyed during the 1973 and 1974 seasons, to obtain some measure of the local variations in depth of scour, accretion, and cross sectional geometry. Survey results of the cross profiles (C1, C2, C3, and C4) are illustrated in Figure 5.9 (for the location of the profiles, see Fig. 5.2).

The hydrologic event associated with the considerable alterations in channel geometry and reworking of sediment between 11-14 July and 9 August, 1973, evident in profiles C1 to C4, was the extreme rainstorm of 22 July, 1973, which produced very high stream discharges. Minor changes also occurred with the higher flows associated with the 13 July rainstorm. All cross-sections reveal a lateral shift in the main channel due to adjustments during the high flow conditions of the 22 July flood. Changes in the area of each cross-section during the period from 11-14 July to 9 August are given below:

Section	A (m^2)
C1	- 3.1
C2	- 2.8
C3	+ 0.8
C4	- 8.7

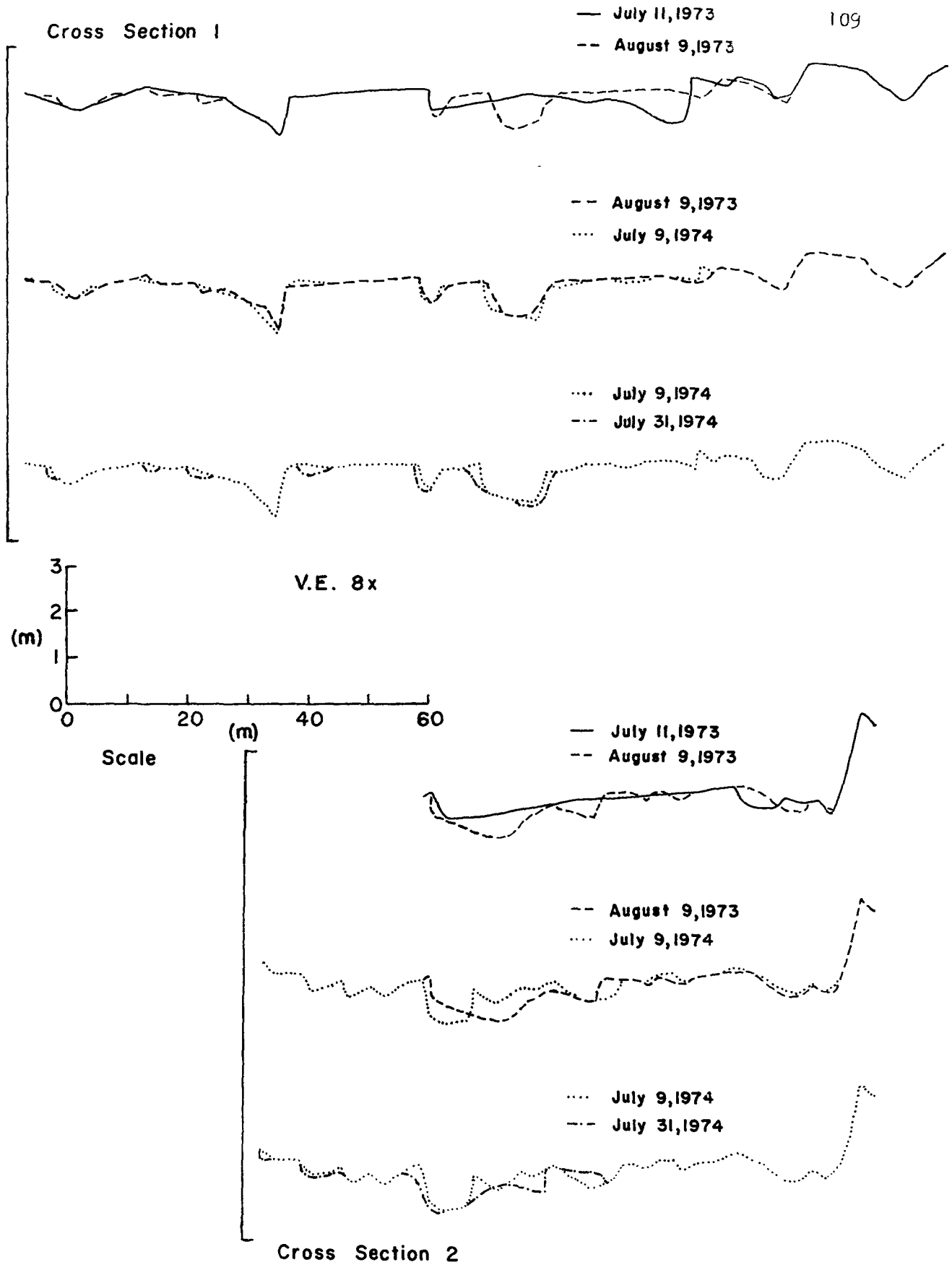

Figure 5.9 Changes in cross profiles (C1, C2, C3, C4) across the main channel(s) of the upper fan portion of the sandur over the two field seasons.

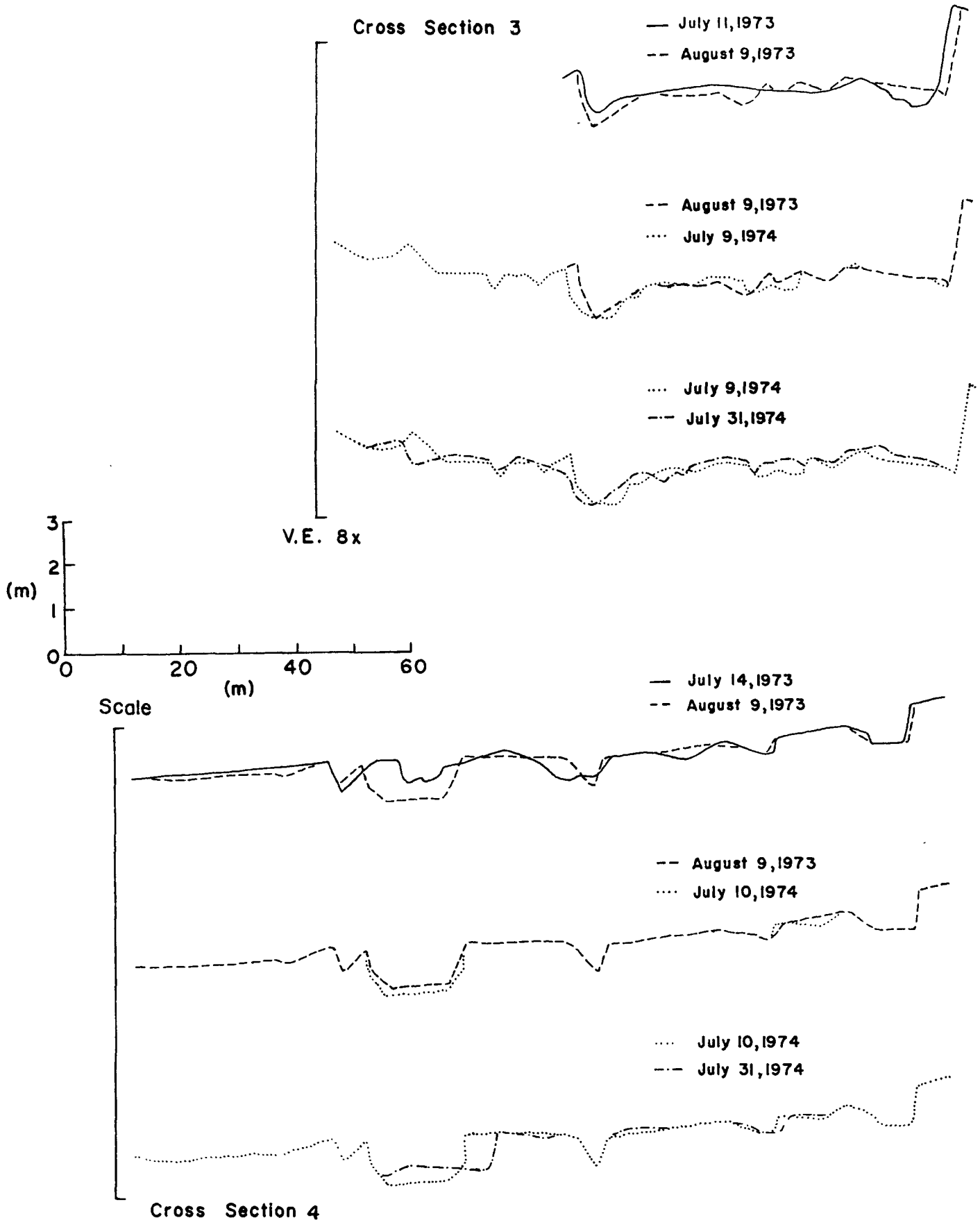

Figure 5.9 ... Continued

Overall the figures revealed a net loss in material over the short term, but may not be indicative of longer term trends (see Fahnestock, 1963). A resurvey, on 9-10 July, 1974, revealed that only minor erosional and depositional redistributions of sediment had occurred during the latter part of the 1973 season, and early part of the 1974 season, although significant accretion had occurred at profile C2 during the early phase of the 1974 spring flood.

The period between 9-10 July and 31 July, 1974, was characterized by local changes mainly due to the high flows of the latter part of the spring snowmelt freshet (especially the ice ponding and release effect on 12 July). Extension of the end marker of profile C2-3 was required, due to continuing bank erosion at this locale by flow deflection in the channel bar survey area. Generally it may be concluded that continuous small alterations occurred throughout both seasons, but that the more significant changes were restricted to higher flow periods.

In plan view, the pattern change in the upper sandur detailed study area mainly due to the rainstorm flood of 1973, and encompassing sections C1 to C4, can be seen in Figure 5.10. The period covers the first two cross section survey periods, between 6 July, 1973, and 11 July, 1974. The channel shift from its old course occurred during the peak flow period of the rainstorm flood, when the main portion of the Schei River was deflected during channel

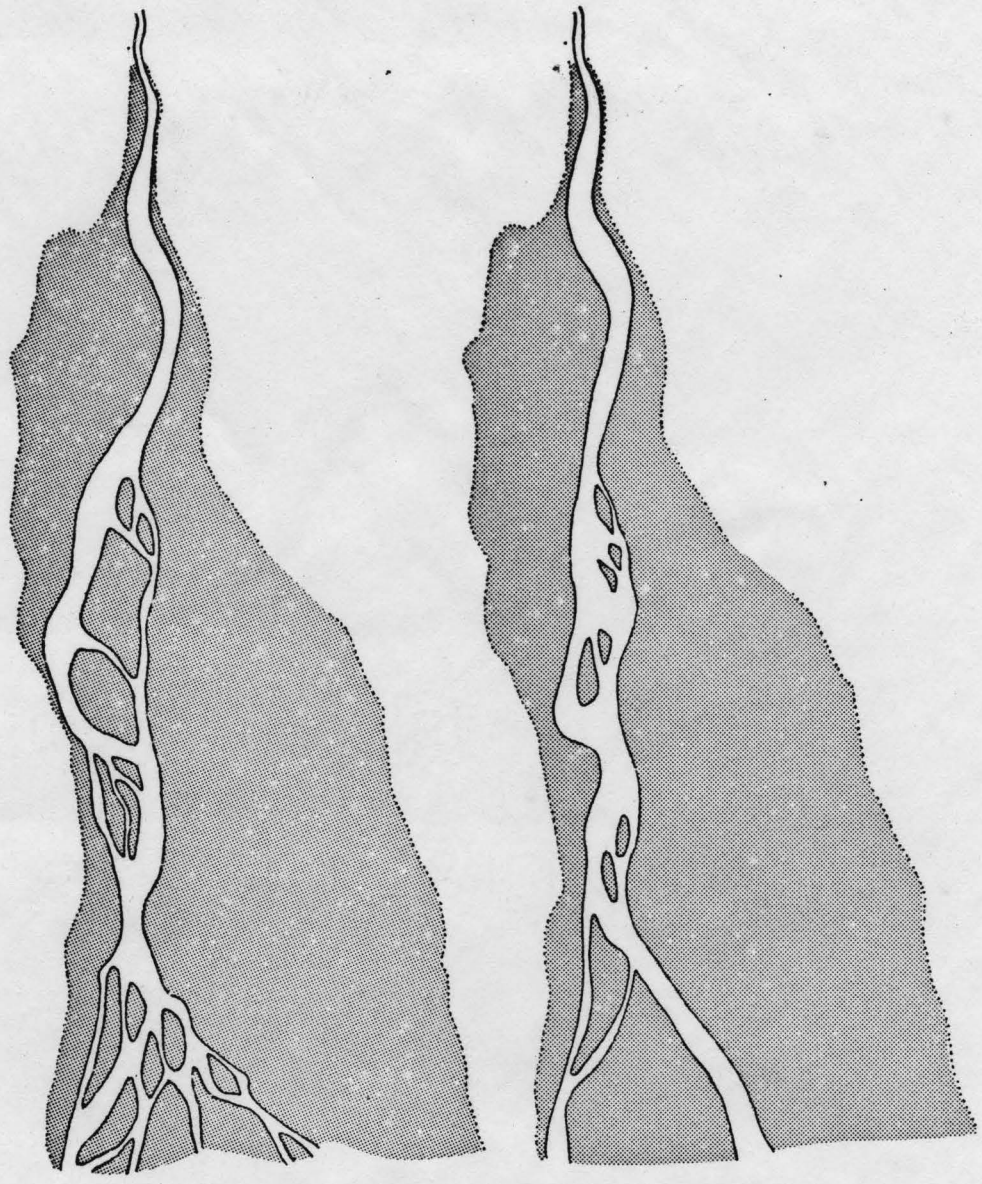

CHANGE IN CHANNEL NETWORK IN UPPER SANDUR PROXIMAL ZONE

note only main channels shown

Figure 5.10 Channel pattern change between 6 July, 1973 and 11 July, 1974.

adjustments. The former main channel zone may have partially been built up above the adjacent areas on its own sediments, leading to avulsion as a mode of channel shifting. More probable was the occurrence of an overloading in the calibre of the sediment load, exceeding the competence, and resulting in an unloading and diversion of flow into a new pattern. The channel filled probably during the final stage of the flood event, dumping a considerable amount of coarse bed load material on the bed which was then infilled with sand size sediment carried in suspension (Fig. 5.11).

Shifts in the main channel, whether minor or considerable, are usually associated with flood events, which although variable, appear to occur on the Schei River on a number of occasions during the course of the runoff season. Large portions of the active surface area of the sandur are inundated for short periods over the summer. This reflects the regular occurrence of the spring flood, and with warm climatic periods of considerable duration, the occurrence of the late season glacial runoff peak. Highly variable extreme rainfall flood events, and in the special case of the Schei River, ice ponding and release floods, also provide an impetus for sediment reworking and channel pattern changes over the sandur.

The braided stream system of the Schei sandur reveals a pattern whereby a single channel carrying the bulk of the sediment-water load in the proximal area (see p.123), transforms into a

Main channel prior to lateral shift due to the 22 July, 1973, rainstorm flood event. View looking downstream, adjacent to cross profile C1.

a.

Channel fill deposit of coarse sand and gravel. The main channel was slightly less than 1 m. deep.

b.

Figure 5.11 Lateral shift and channel fill of the main channel in the proximal portion of the Schei sandur.

detailed complex pattern in the medial zone and eventually rejoins into a more distinct pattern of one, or several, main channels in the distal zone.

The variability of the channel network over the sandur during the 1973 and 1974 seasons can be illustrated by comparing low altitude aerial photographs taken in July of both years (Figs. 5.12 and 5.13). The greatest change in channel pattern occurred during the 22 July rainstorm flood in 1973. In the upper proximal zone, the areas affected are usually immediately adjacent to the main active channel area. The medial zone appears to be an area where considerable reworking of sediment during high flow conditions affects almost the entire active surface. Highly complex braiding and minor channel fanning begins at the head of the medial zone, and reveals the greatest alteration in a complete channel pattern change and redistribution of material. In comparing the 1973 and 1974 aerial photographs, it can be seen that channel shift in the upstream area has forced an alteration and shift in the downstream channel segments of the medial portion of the sandur, although the lower distal region appears to be relatively unaffected by these pattern changes. The rapid modifications are more inherent in the smaller channel bars and channel segments of the medial zone. This complex pattern at low stage levels, reflects hydraulic adjustments during high flow conditions. The greater preponderance of minor channels,

SCHEI SANDUR : scale approximately 1:10000. uncorrected photo. flown July, 1973.
photograph number A30858-15. National Air Photo Library. Surveys and Mapping Branch. D.E.M.R.

Figure 5.12 Schei sandur : showing the channel pattern in July, 1973 at low flow.
Discharge approximately 2 $m^3 s^{-1}$

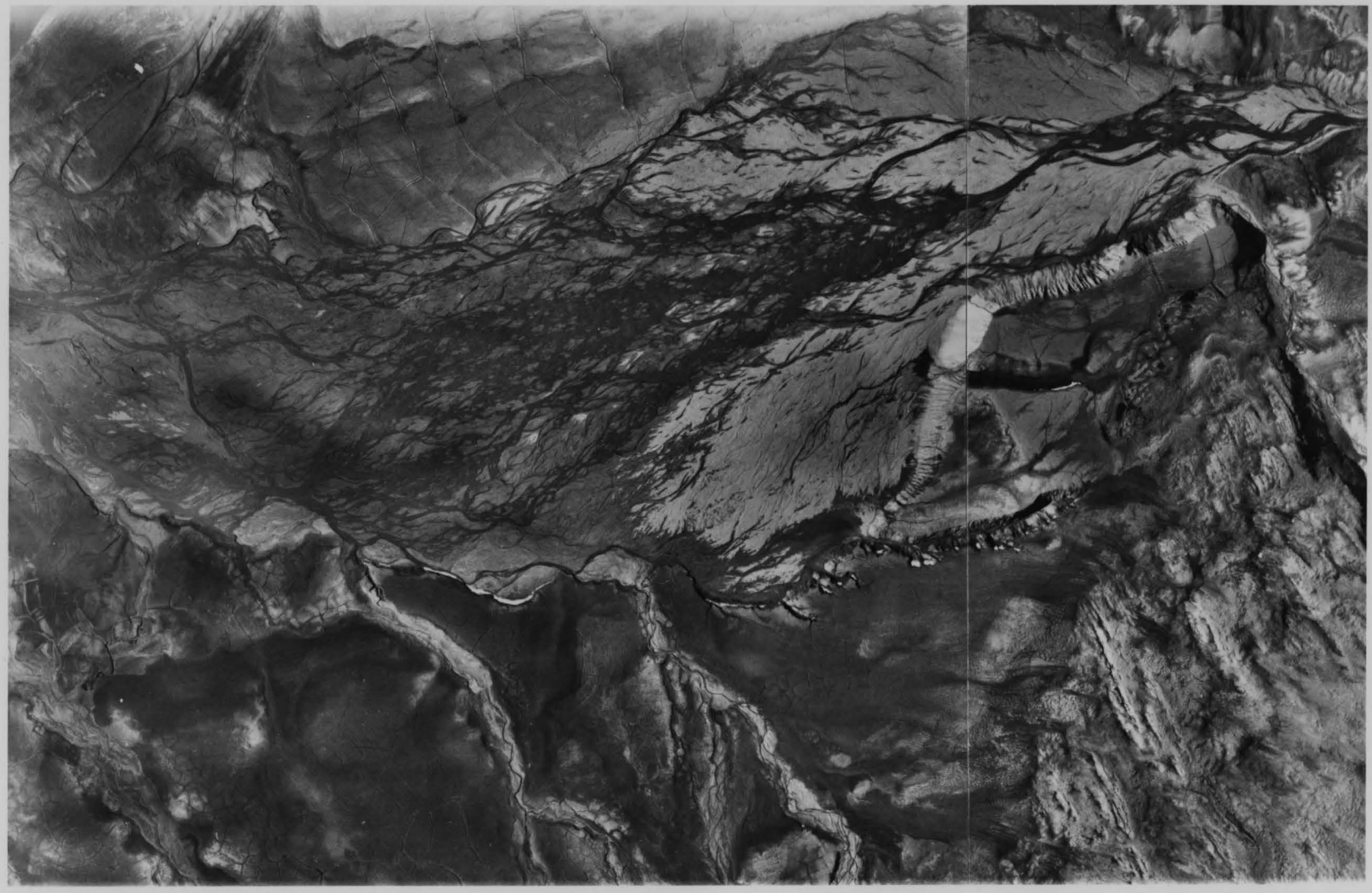

SCHEI SANDUR : scale approximately 1:10000. uncorrected photo. flown July, 1974.
photograph number A23942-152 & 3. National Air Photo Library. Surveys and Mapping Branch. D.E.M.R.

Figure 5.13 Schei sandur : showing the channel pattern in July, 1974 at moderate flow.
Discharge approximately 12 m^3s^{-1}

and a lack of well developed major channels, suggests that the establishment of complex minor channels is an equilibrium network adjusted to the higher sediment-water conditions during the flood period, with the subsequent readjustments of a number of major channels in this zone not fully developed. This present pattern should be viewed as a temporary network, where the minor complex channel segments were developed at flood conditions, with a higher total resistance to flow determined by the size of the bed and bank material and slope, but more efficient to carry the imposed sediment and discharge loads. Geometry adjustments and associated change in resistance conditions, with possible deposition of material (depending on the state of flow and load conditions), gives rise to braiding processes and the re-distribution of material over the sandur, and hence an altered channel pattern.

The main channel zone axis has now shifted towards the southern margin of the sandur, and may possibly continue this trend in the near future, although the upstream control of the channel pattern in the proximal zone, morphologically may enhance a restriction of lateral channel movement, and hence possibly restrict lateral channel development in the lower medial zone. The downstream control in the distal zone similarly reveals a restriction in lateral channel movement due to older terraced material.

5.6 LONG PROFILE ANALYSIS

Long profile measurements of the Schei River were surveyed in 1973 and 1974, with heighted points at 20 to 50 m intervals. Water surface elevations were obtained from the Schei-Sverdrup confluence to the lower part of the gorge in the Upper Schei River in 1973. Inability to traverse through this upper gorge of the Schei River prevented further extension of the profile line. Both measurements of water surface and stream bed elevations were taken in 1974. Figure 5.14 illustrates the results of the long profiles.

Analysis of the long profile of the sandur section, surveyed in 1974, reveals that this lower part of the Schei River is concave and can be approximated reasonably well by a simple exponential equation of the form:

$$Y = a_2 e^{a_1 x} \qquad (V.5)$$

Where Y is the height above sea level (masl) and x is the distance (m) from the Schei-Sverdrup River confluence.

The computed equation yielded:

$$Y = 0.995\, e^{.0004\, x} \qquad r = .97 \qquad (V.5a)$$

The exponent in the equation suggests a tendency towards a more linear form in this case.

The more complete profile surveyed in 1973 shows that different reaches exist along the entire river, with one reach

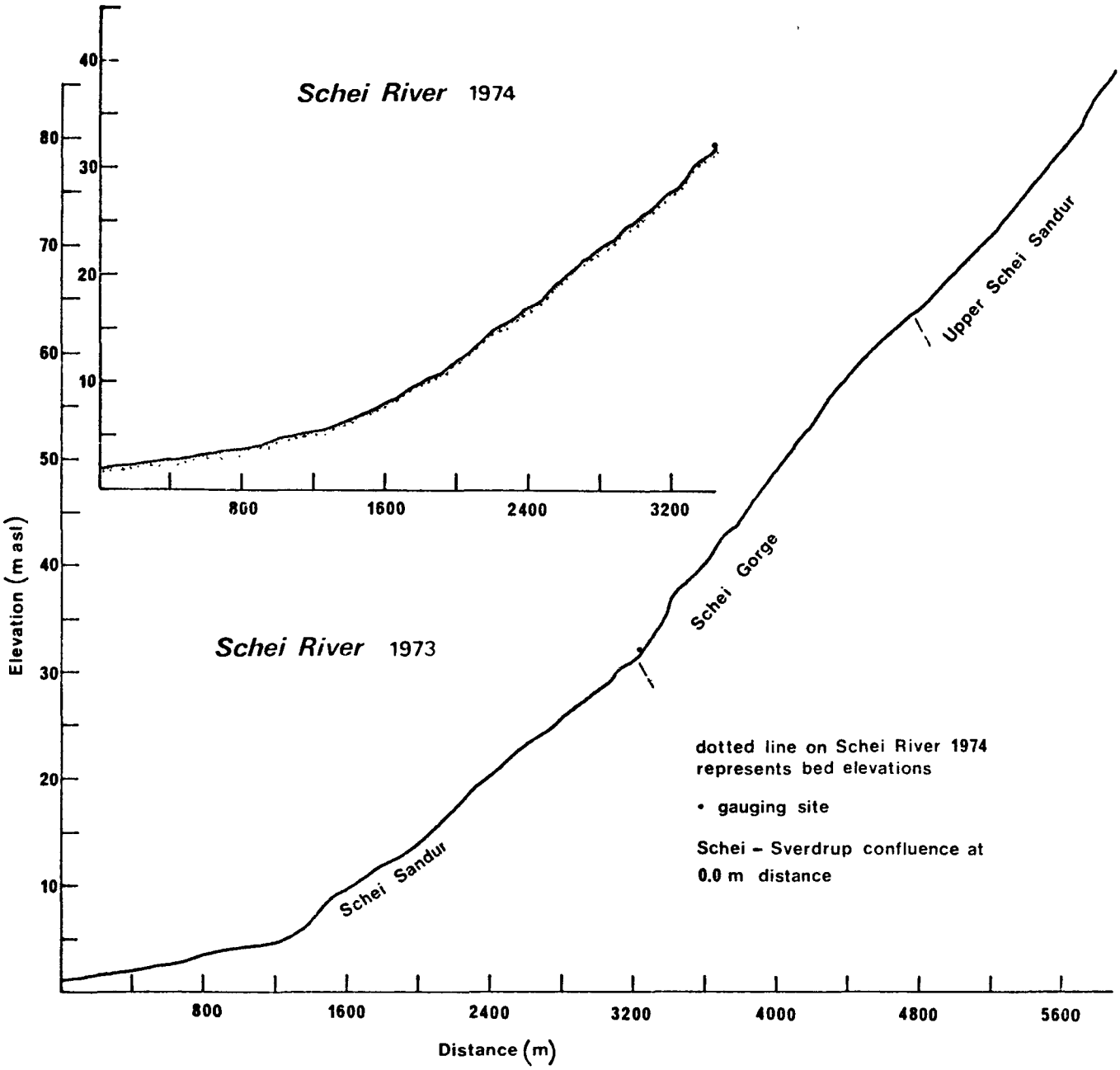

Figure 5.14 Longitudinal profiles of the Schei River surveyed in 1973 and 1974.

essentially being rectilinear in form. Upstream of the gauging site the river flows in a constricted single major channel, entrenched through a confining hogback ridge (distance 3200 to 4800 m). This linear reach of increased slope suggests that the Schei River is competent to carry the total sediment-water load supplied upstream through this section of bedrock outcrop, and will continue to remain a stable segment under the present conditions. This section should show a restricted particle size decrease downstream, as suggested by Mackin (1948), (for a more complete discussion see Church, 1972).

Upstream and downstream of this constrained reach a change in flow pattern occurs, as flow is braided in wide, shallower channels. These reaches appear to have a more exponential form and a reduction in slope downstream, although the effect is not as clear for the lower section of the long profile in 1973.

The difference between the exact form and horizontal length of the lower segments, surveyed in 1973 and 1974, is due to a radical alteration in the channel pattern during the concentrated flood event which occurred between the two years. The major channel of the sandur reach which was followed in the long profile surveys, occupied a more direct and shorter route to the Sverdrup confluence in 1973. A definite break occurs in the lower portion of this segment where the major channel is eroded into older terrace and/or estuarine deposits.

The nature of the material and vegetation probably accounts for increased channel stability and differing sediment transport characteristics through this segment, resulting in the break and increased slope, and hence a local departure from an exponential profile. The major channel as surveyed in 1974 was not only longer but followed a distinctly different route over the active sandur surface. The exponential form suggests that flow divergence in the braided channels and decreasing total load would result in coarse materials being preferentially and systematically deposited downstream, and lead to a concave long profile. Although a change exists in the actual characteristics of the long profile in the lower braided depositional reach, the similar forms over both years indicates that the profile is apparently stable.

5.7 FORM OF THE SANDUR SURFACE

The sandur surface is largely composed of gravel and cobble sized material with a considerable sand matrix. The surface (see Fig. 5.12) shows actively braiding channels and bar areas, with no vegetation occurring in the active portions of the sandur. Minor channels become more numerous but less well defined towards the lower fan area. Braiding also becomes more complex, and subsurface seepage evident in the lower fan area. Former channel traces are more distinct in the mid-fan and upper fan portions of the sandur.

Krigstrom (1962) subdivided a sandur surface into three zones, based on differences in the nature of the deposits and braiding behaviour:

1. The proximal zone, characteristic of a few main channels which tend to be relatively deep and well-defined.
2. The intermediate (medial) zone, possessing numerous braiding wide and shallow shifting channels, typifying channel behaviour in a sandur.
3. The distal zone, which is characterized by a shallow sheet flow of water to the sandur delta area, with a few deeper main channels occurring. By definition, the distal zone does not occur at the

lower segment of the Schei sandur and is taken to represent in this context the lower portion of the sandur where the flow is carried by a number of deeper main channels in sand and gravel material over a relatively shallow surface gradient.

The sandur surface long profile is concave, similar to that of the water surface and bed profiles of the river (see Figure 5.14). This simple exponential form may be approximated by an equation of the form

$$Y = a_2 e^{a_1 x} \qquad \text{(from V.5)}$$

The long profile of the Schei sandur is similar to that reported by Fahnestock (1963) on the White River dalsandur, Church (1972) on the Lewis River sandur, and the Hoffellssandur (Sundborg, 1954).

The cross profile of the Schei sandur is relatively level in the proximal zone below the hogback ridge, but becomes more upwardly convex in the mid-sandur and, to a lesser degree, lower sandur areas. This is due to the greater freedom of the channels to migrate laterally and build up the central part which is occupied most frequently by the major channels. This process eventually leads to avulsion and a shift in the channel pattern. The major channel area presently occupies the central portion of the sandur along the convex axis. Up to 1.5 m difference in height can occur between the central portion and margins of the Schei sandur, due to the channel sediment buildup.

5.8 DISTRIBUTION AND TREND CHARACTERISTICS OF THE SANDUR SURFACE

Church (1972) suggested that a number of sediment characteristics change down-sandur. Conceptually, changes which should occur include a reduction in the size of the surface material, related to a downstream change in the gradient from decreasing competence, and an increase in sorting due to abrasion and selective transport.

In order to investigate and distinguish any systematic change in the sediment distribution pattern over the active outwash surface (see Fig. 5.15), the mean size of the coarse materials and the local topographic elevation were examined on a comparative basis. These aspects, resulting from transport processes occurring under an arctic sandur environment, were studied from the proximal to distal portions of the Schei sandur.

Fahnestock (1963) and Boothroyd (1972) have both reported a relationship between particle size and slope plotted in a downfan direction; Fahnestock for a dalsandur, and Boothroyd for a slattlands-sandur.

The local topographic elevations and mean size of the surface materials of the Schei sandur were measured at 53 sample sites in a predetermined, systematic, orthogonal grid pattern, superimposed

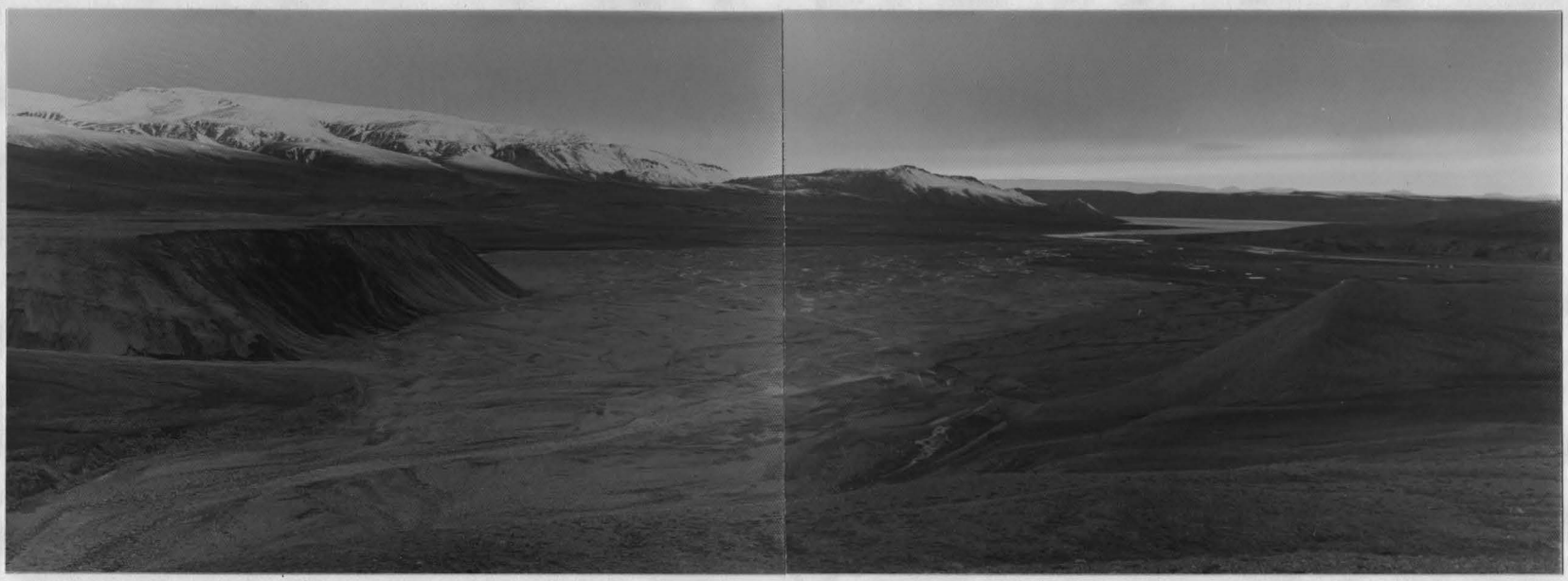

Figure 5.15 View of the Schei sandur where the sediment distribution study was undertaken. View looking west and downfan, towards Vendom Fiord.

over the sandur surface (see Fig. 5.16 for the sample locations). The sampling network consists of approximate 200 m intervals downfan, and 100 m intervals in a transverse direction. Minor variations in the sample site positions across the fan were due to the original site being occupied by an active channel. In these cases sites were selected as close as possible to the original location on surficial deposits adjacent to the channel.

The elevations of the sites were surveyed using a Kern level, and referenced to sea level. The mean size of the coarse sediments were obtained from measurements of clast size on photographs taken of the sandur surface, defined by an approximate 1 m square quadrat frame placed on the surface at each sample site. (See appendix A for a discussion of the technique used). This procedure was adopted as a suitable alternative for obtaining the mean size of coarse material, to the normal method of sample collection and principal axis measurement of clasts at each site, according to a randomized procedure such as Wolman's (1954) method. Each surficial deposit was assumed to be homogenous, with the surface sediment corresponding to the underlying material under investigation (i.e. no population difference). "Coarse" clasts were taken to represent material greater than 8 mm b- axis length. This division between coarse and fine material was adopted to reduce the number of clasts to be counted and measured at this lower limit, and thereby allow the sampling field procedure to be brief.

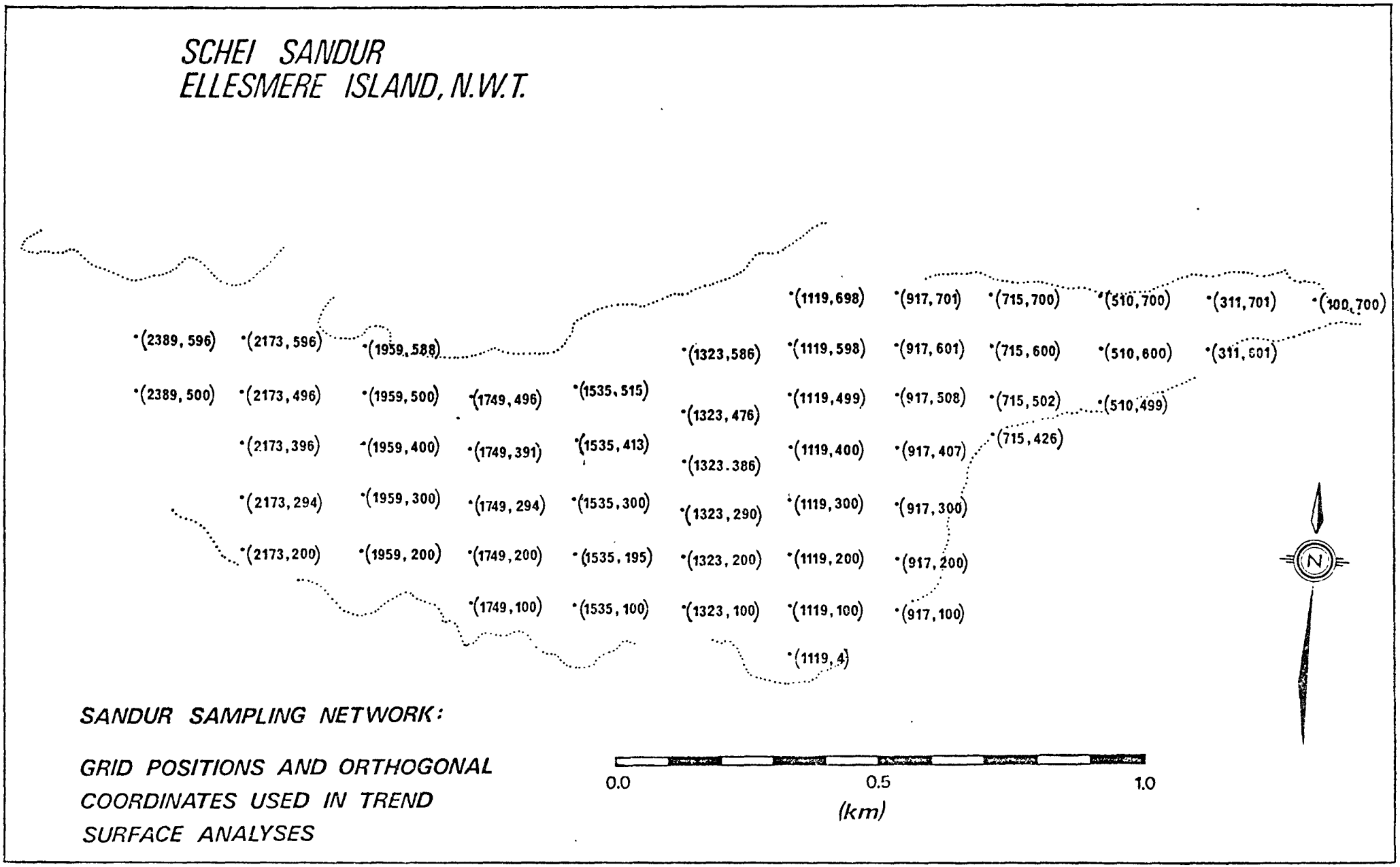

Figure 5.16 Schei sandur sampling grid.

The overall mean of the 53 mean sample sizes for the entire sandur is 20.1 mm, with a standard deviation of $\pm$ 4.8 mm. The means of the individual samples ranged from 13.4 mm in the distal portion of the sandur to 35.0 mm in the proximal end. Although this range in the mean size of the coarse materials over the sandur is not overly large, a considerable range occurs in the size of the largest cobble found at each site. This varied from 30.0 mm, in the sample with the smallest mean size in the distal area, to 210.0 mm in the sample with the largest mean size in the proximal zone. Large relict boulders are also common in the proximal area at the apex of the sandur. (Fig. 5.17).

Trend surface analysis was applied to the elevation and sediment data in order to separate the regional and local components of these parameters. The analysis involves regressing the dependent variable Z on two independent variables X and Y, which are the discrete location coordinates of the map area. In equation form the trend surface is of a modified form (Krumbien and Graybill, 1965):

$$Z_{ij} = \alpha (X_i, Y_j) + e_{ij} \qquad (V.6)$$

Where Z_{ij} is the observed value of the dependent variable at location (X_i, Y_j), $\alpha (X_i, Y_j)$ is the trend, and e_{ij} is the residual.

The fitting process involves finding the parameters of the trend, in satisfying the least squares criterion. First, second, and third order surfaces were generated.

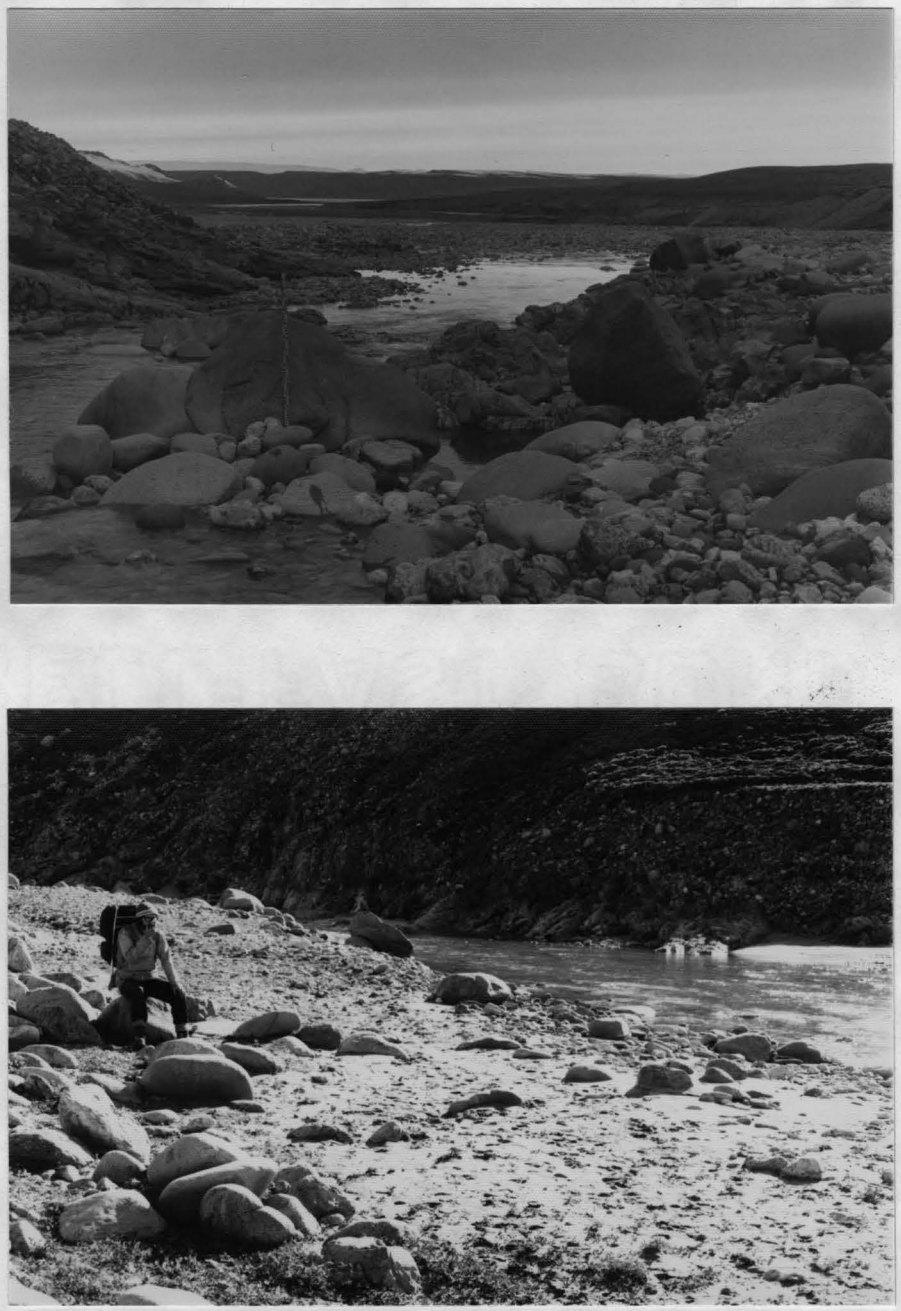

Figure 5.17 Large boulders at the headward portion of the Schei sandur.

Significant trends were found for both first order surfaces of the elevation and mean grain size data. Figure 5.18 illustrates the result of the first order surface of the sandur elevations, and as might be expected, reveals a highly significant linear trend. The general surface gradient trend decreases downfan, approximately paralleling the downstream channel directions in the medial portion of the sandur. The first order equation is given by:

$$E = 24.45 - 0.11 \times 10^{-1} X + 0.69 \times 10^{-2} Y \qquad r = .98 \qquad (V.7)$$

Where E is the elevation (masl) and X and Y are the location grid values (m).

Elaboration on this pattern is given by the second order fit which reveals a concave upward surface which exponentially decreases downstream (Fig. 5.19), and strongly decreases in a manner parallel to the channels from the proximal to distal zone. This apparent correlation suggests that the morphology of the sandur is controlled by migration and branching of the sandur channels, linked possibly to fluvial avulsion processes (see p.113). The second order equation is as follows:

$$E = 26.38 - 0.17 \times 10^{-1} X + 0.16 \times 10^{-1} Y + 0.29 \times 10^{-5} X^2 - 0.46 \times 10^{-5} XY - 0.78 \times 10^{-5} Y^2 \qquad r = .99 \qquad (V.8)$$

The second order surface shows only a slight increase in the variance reduction over the first order linear form, and together accounts for 99.8 per cent of the variation explained. The residuals from the second order trend show an area with positive peaks approximately

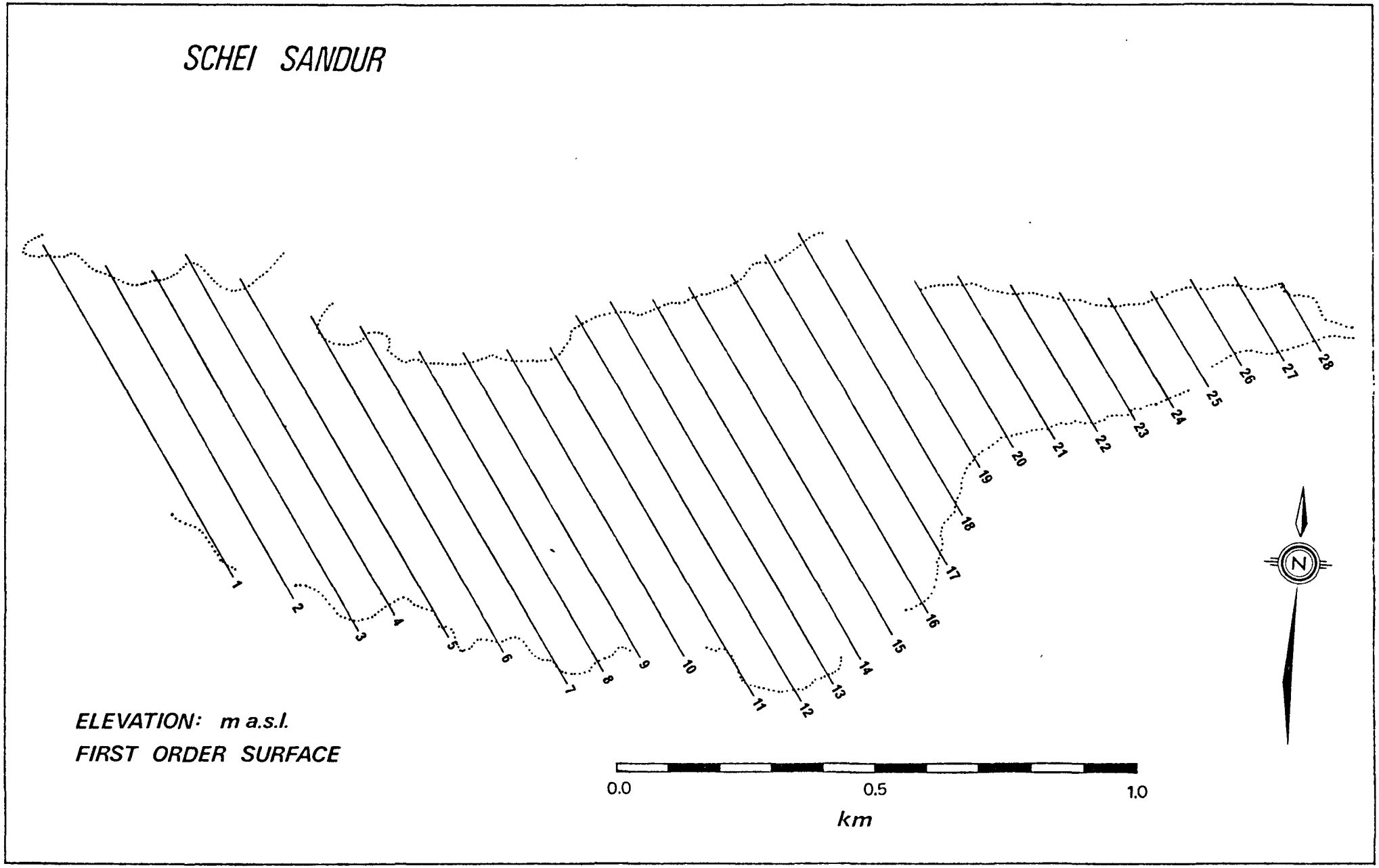

Figure 5.18 First order trend of the surface gradient of the Schei sandur.

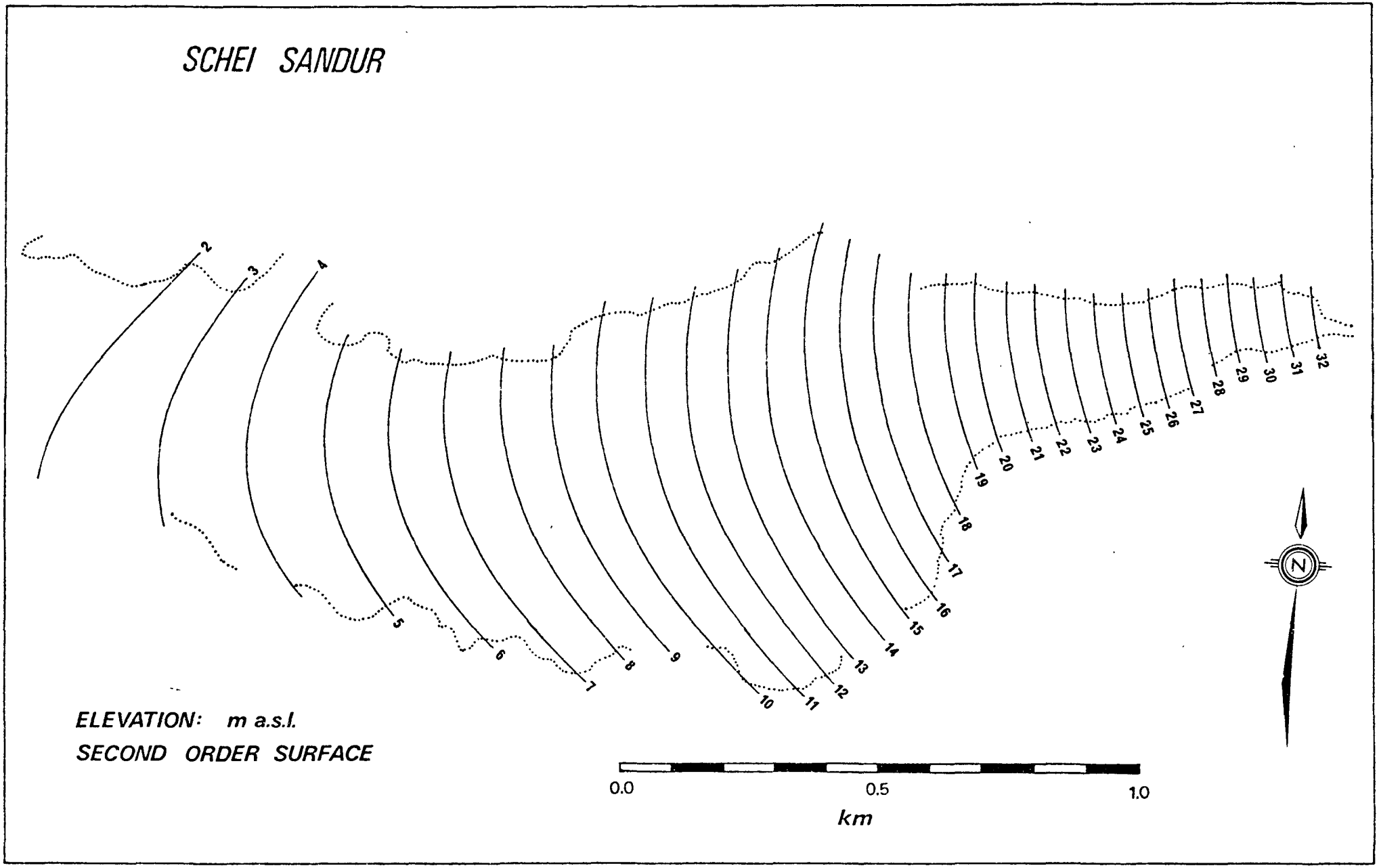

Figure 5.19 Second order trend of the surface gradient.

600 to 800 m downfan, and a negative peak along the north margin of the sandur 1700 m downfan. A weak oscillatory trend appears evident down-valley, although no explanation can be ascertained for this residual pattern.

Figure 5.20 shows the first order trend for the mean size of the coarse materials over the sandur. The mean grain size decreases downfan in a similar manner to the elevation trend, although slightly oblique. However, the linear trend of the mean grain size is not as highly a significant trend as the surface gradient tendency. The linear equation is given by:

$$\overline{B} = 28.05 - 0.65 \times 10^{-2}X + 0.17 \times 10^{-2}Y \qquad r = .81 \qquad (V.9)$$

Where $\overline{B}$ is the mean cobble size (mm) and X and Y are the location grid values (m).

The general trend implied reveals a decrease in the mean grain size from 29 mm to 13 mm b-axis length in spreading across the sandur to the distal region. This mean size tendency can be elaborated upon by the second order surface, given by:

$$\overline{B} = 22.58 - 0.86 \times 10^{-3}X + 0.80 \times 10^{-2}Y - 0.10 \times 10^{-5}X^2 - 0.56 \times 10^{-5}XY + 0.20 \times 10^{-5}Y^2 \qquad r = .82 \qquad (V.10)$$

The first and second order surfaces together account for 66.9 per cent of the variation explained. Generally the pattern correlates fairly closely again with the direction of the sandur channels. The second order trend (Fig. 5.21), in addition to showing a downfan decrease

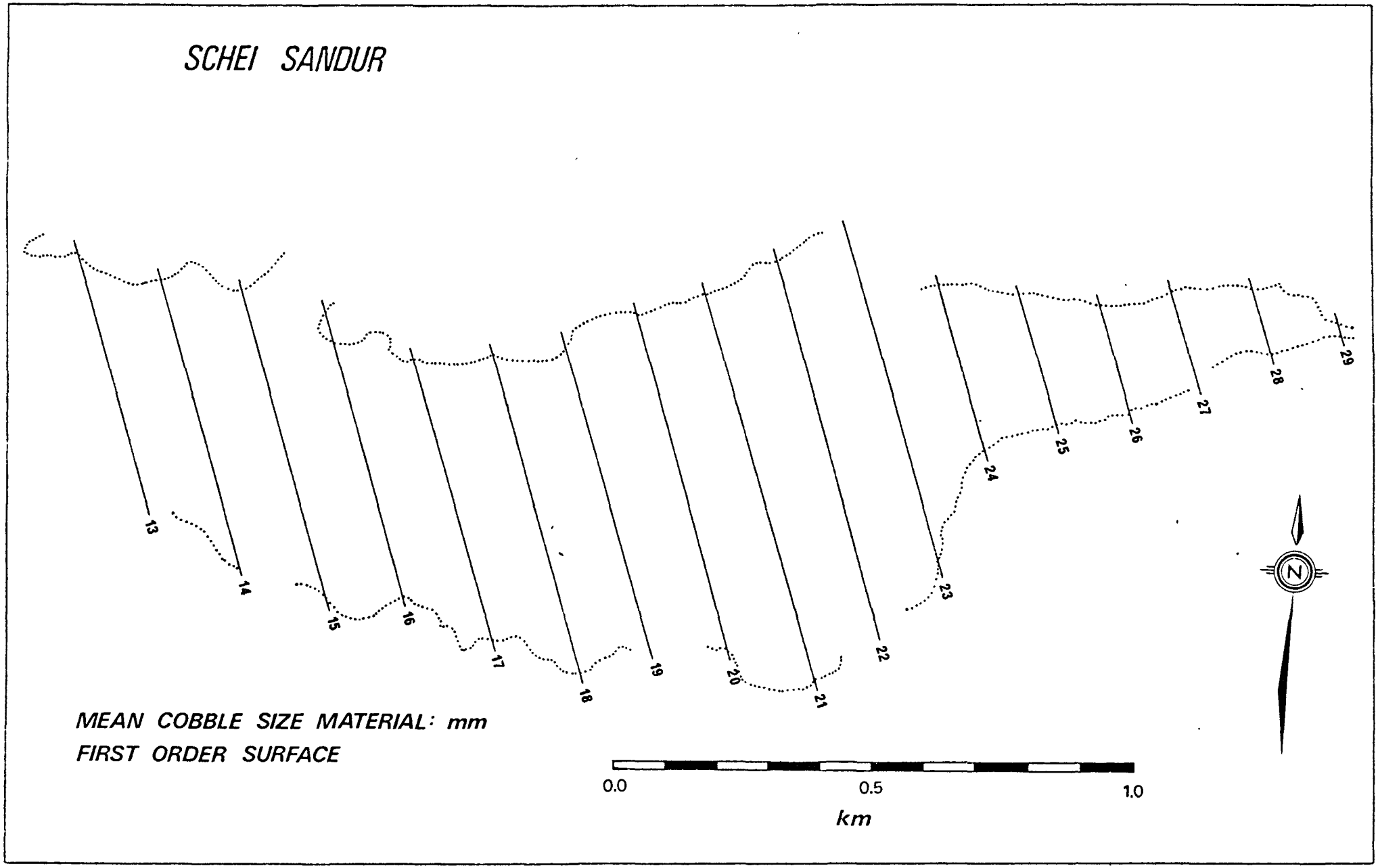

Figure 5.20 First order trend surface of the mean grain size of the coarse materials.

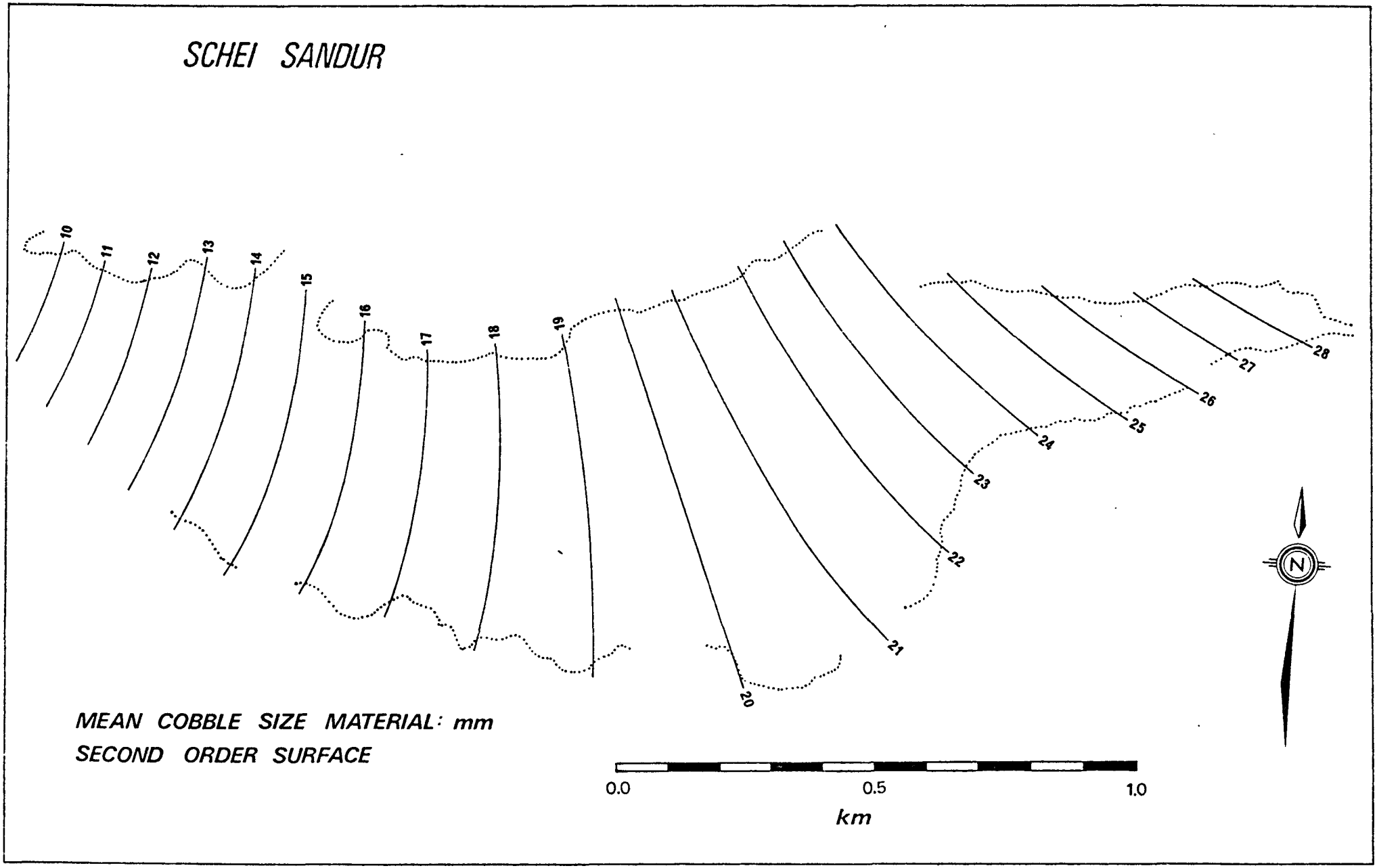

Figure 5.21 Second order trend surface of the mean grain size of the coarse materials.

in grain size due to decreasing competence of the river, also shows an inclination away from the north margin of the sandur in the proximal zone. The residuals from the second order trend exhibit alternating peaks of positive and negative values down sandur and show no discernible pattern. This is probably due to the technique used in acquiring the mean grain size data of the coarse materials over the sandur. It is suggested that the tendency for the mean size of the materials to decrease obliquely towards the southwest in the proximal region is due to the occurrence of coarser materials on the north margin of the sandur being delivered to the surface from older terraced alluvial material. Although the trend shows slight variations in mean grain size across the sandur, the cross sandur tendency is generally uniform.

The surface form of the sandur and mean grain size variation generally show a linear trend downfan, closely related to the channel pattern network. Although these features are variable over the sandur, the apparent correlation with the sandur channels emphasizes the influence of channel processes on the morphology and grain size of the sandur. The systematic and decreasing trends of elevation and mean grain size are also reflected by the form of the river long profile (see p. 119). Although this form is exponentially decreasing downstream, the profile indicates a tendency towards a linear decrease, as given by the exponent in the equation.

CHAPTER VI

CONCLUSIONS

The following are the major findings of this study:

(1) Surface runoff is highly variable in a glacierized basin and is dependent on snowmelt, glacial melt, and summer precipitation. Pronounced temporal variations in summer climatic conditions strongly affected the hydrologic regime. This influenced the sources of runoff, with summer precipitation and glacial melt being the more variable of these sources.

(2) Diurnal discharge variations are related to diurnal fluctuations in available energy. Such variations are accentuated by the shallow active layer, which minimized groundwater storage, and by the considerable basin relief. Short term irregular discharge variations were produced by temporary ice marginal ponding and release effects. These factors are important in their influence on sandur channel river mechanics.

(3) Due to the substrate characteristics mentioned above, a rapid response of surface runoff to rainfall events was evident. An average lag of 5 hr was noted, but this value probably increased over the summer runoff season due to changing discharge characteristics within the basin.

(4) The hydrologic regime strongly influenced temporal variations in the channel hydraulics, with differences in the mode of adjustment due to differing channel characteristics. At stable channel sections a greater adjustment to discharge may be expected through velocity adjustments, with depth and surface width changes being more conservative. This is associated with a rapid change in flow resistance. These factors imply rapidly changing sediment loads with discharge.

(5) Considerable material is entrained, transported, and deposited over the sandur during the runoff season. Generally sediment supply is abundant. River mechanics operating in the stream channels affect the rates and amount of sediment movement. The estimates of the sediment transported yielded the following results:

- The dissolved load is transported continuously but its magnitude is small in comparison with bedload and suspended load.
- The suspended load is significant, with high loads occurring frequently.
- Bedload transport, though sporadic, is important in regards to sandur development and processes.

Large variations in the distribution and the amount of material carried by each component of the total load can occur with different runoff seasons and within a given season. Flows above

the competence level of the sandur material affected the channel network stability. These flow conditions can occur relatively frequently over a runoff season.

(6) Different forms of the longitudinal profile reflect differing hydraulic conditions. On sandur deposits the exponentially decreasing form of the channel reflects a downstream gradation from systematic deposition. In this case, the tendency towards a straight line is also reflected in the strong linear trends in the sediment size and morphology of the sandur surface which probably controls the channel long profile.

(7) Diagonal and spool bars constitute the common bar forms of the sandur channels. These bars were part of a pool-bar sequence and reflected a response to hydraulic conditions, showing rapid erosional and depositional modifications. They have considerable influence on form resistance and flow patterns, and hence influence channel alterations.

(8) Trend surface analyses summarized the downstream and the cross sandur variations of the sediment size and morphology of the sandur surface and revealed the strong influence of channel processes on these features.

REFERENCES

Adams, W. P., 1966. Ablation and Runoff on the White Glacier, Axel Heiberg Island, Canadian Arctic Archipelago. Axel Heiberg Island Res. Rep. Glac., No. 1, McGill Univ., 77p.

Allen, J. R. L., 1965. A review of the origin and characteristics of recent alluvial sediments. Sedimentology, 5, 89-191.

Andrews, J. T., 1970. A Geomorphological Study of Post-Glacial Uplift with Particular Reference to Arctic Canada. Institute of British Geographers, 156p.

Arnborg, L., 1955. Hydrology of the glacial river Austurfljot, chp. 7 of the Hoffellssandur - a glacial outwash plain. Geog. Ann., 37, 185-201.

_____, Walker, H. J. and Peippo, J., 1967. Suspended load in the Colville River, Alaska, 1962. Geog. Ann., 49A, 131-44.

Ballantyne, C. K., 1975. Geomorphological and hydrological investigations in a high arctic glacierized drainage basin (M.Sc. thesis, McMaster Univ., in preparation).

_____. Suspended sediment transport and supply in a high arctic drainage basin. Unpub. paper presented to a C.A.G. meeting, Ottawa, 1975, 9 p.

Bird, J. B., 1967. The Physiography of Arctic Canada. John Hopkins Press. 336p.

Blatt, H., Middleton, G. and Murray, R., 1972. Origin of Sedimentary Rocks. Prentice-Hall, Inc., 634p.

Blench, T., 1966. Mobile-Bed Fluviology. Dept. of Tech. Ser., Technical Illustrating Division, Univ. of Alberta, 300p.

Boothroyd, J. C., 1972. Coarse-grained sedimentation on a braided outwash fan, northeast Gulf of Alaska. Tech. Rept. No. 6-CRD, Geography Programs, Office of Naval Research, U.S. Government, 127p.

Briggs, L. I. and Middleton, G. V., 1965. Hydromechanical principles of sediment structure formation. In Middleton, G.V., Ed., Primary Sedimentary Structures and their Hydrodynamic Interpretation. Sec. Econ. Paleontologists and Mineralogists. Spec. Publ. No. 12, 5-16.

Brush, L. M., 1965. Sediment sorting in alluvial channels. In Middleton, G.V., Ed., Primary Sedimentary Structures and their Hydrodynamic Interpretation. Soc. Econ. Paleontologists and Mineralogists. Spec. Publ. No. 12, 25-33.

Chein, N., 1954. Meyer-Peter formula for bed-load transport and Einstein bed-load function. M.R.D. Sediment Series, No. 7 Corps of Engineers, Missouri River Division, Neb., 23p.

Church, M., 1967. A relatively painless method of obtaining mean cobble size data on coarse clastic surfaces. Unpub. manuscript, U.B.C., 17p.

_____, 1972. Baffin Island sandurs: a study of Arctic fluvial processes. Geol. Surv. Can., Bull. 216, 208p.

_____and Kellerhals, R., 1970. Stream gauging techniques for remote areas using portable equipment. Inland Waters Branch, D.E.M.R., Tech. Bull. No. 25, 89p.

Cogley, J. G., 1971. Hydrological and geomorphological observations on a high latitude drainage basin : "Jason's Creek", Devon Island, N.W.T. Unpub. M.Sc. Thesis, McMaster Univ., 131p.

_____and McCann, S.B., 1975. An exceptional rainstorm in the Canadian High Arctic (in preparation).

Cook, F. A., 1967. Fluvial processes in the high Arctic. Geog. Bull., 9, 262-68.

Davar, K. S., 1970. Peak flow-snowmelt events. In Gray, D. M., Ed., Handbook on the Principles of Hydrology. Canadian National Committee for I.H.D., 9.1 - 9.12.

Doeglas, D. J., 1962. The structure of sedimentary deposits of braided streams. Sedimentology, 1, 167-90.

Embleton, C. and King, C. A. M., 1968. Glacial and Periglacial Geomorphology. MacMillan, 608p.

Fahnestock, R. K., 1963. Morphology and hydrology of a glacial stream, White River, Mt. Rainier, Washington. U.S. Geol. Surv., Prof. Paper 422-A, 70p.

_____and Bradley, W. C., 1973. Knik and Matanuska Rivers, Alaska : a contrast in braiding. In Morisawa, M., Ed., Fluvial Geomorphology. 4th An. Geomorphology Symposium, State Univ., New York, 220-50.

Falconer, G., Ives, J. D., Løken, O. H. and Andrews, J. T., 1965. Major end moraines in eastern and central Arctic Canada. Geog. Bull., 7, 137-54.

Folk, R. L. and Ward, W. C., 1957. Brazos River bar : a study in the significance of grain size parameters. Jour. Sed. Petrol., 27, 3-27.

Gray, D. M. and Wigham, J. M., 1970. Peak flow-rainfall events. In Gray, D. M., Ed., Handbook on the Principles of Hydrology. Canadian National Committee for I.H.D., 8.64 - 8.102.

Gustavson, T. C., 1974. Sedimentation on gravel outwash fans, Malospina Glacier Foreland, Alaska. Jour. Sed. Petrol., 44, 374-89.

Hack, J. T., 1957. Studies of longitudinal stream profiles in Virginia and Maryland. U.S. Geol. Surv., Prof. Paper 294-B, 96p.

Harms, J. C. and Fahnestock, R. K., 1965. Stratification, bed forms, and flow phenomena (with an example from the Rio Grande). In Middleton, G.V., Ed., Primary Sedimentary Structures and their Hydrodynamic Interpretation. Soc. Econ. Paleontologists and Mineralogists. Spec. Publ. No. 12, 84-115.

Hein, F. J., 1974. Gravel transport and stratification origins, Kicking Horse River, B.C., Unpub. M.Sc. Thesis, McMaster Univ., 135p.

Hjulstrom, F., 1955. The ground water, chp. 9 of the Hoffellssandur - a glacial outwash plain. Geog. Ann., 37, 234-45.

_____, Arnborg, L., Jonsson, J. and Sundborg, A., 1954-57. The Hoffellssandur - a glacial outwash plain. Geog. Ann., 36-38, 10 chp.

Hodgson, D. A., 1972. Landscape and late-glacial history, head of Vendom Fiord, Ellesmere Island. Report of Activities, part B, 1972-1973. Geol. Surv. Can., Paper 73-1, part B, 129-36.

Hollingshed, A. B., 1971. Sediment transport measurements in a gravel river. Proc. Amer. Soc. Civil Engineers, Jour. Hydraulics Division, 97, No. HY11, 1816-34.

Knight, J., 1971. Distributional trends in the recent marine sediments of Tasiujaq Cove of Ekalugad Fiord, Baffin Island, N.W.T. Maritime Sediments, 7, 1-18.

Krigstrom, A., 1962. Geomorphological studies of sandur plains and their rivers in Iceland. Geog. Ann., 44, 328-46.

Krumbein, W. C. and Graybill, F. A., 1965. An introduction to Statistical Models in Geology. McGraw-Hill Book Co., 475p.

Leopold, L. B., 1970. An improved method for size distribution of stream bed gravel. Water Resources Research, G., No. 5, 1357-66.

_____and Maddock, T. Jr., 1953. The hydraulic geometry of stream channels and some physiographic implications. U.S. Geol. Surv., Prof. Paper 252, 57p.

_____, Wolman, M. G. and Miller, J. P., 1964. Fluvial Processes in Geomorphology. Freeman, 522p.

Maag, H., 1969. Ice dammed lakes and marginal glacial drainage on Axel Heiberg Island, Canadian Arctic Archipelago. Axel Heiberg Island Res. Rep., McGill Univ., 147p.

Mackin, J. H., 1948. Concept of the graded river. Geol. Soc. Am. Bull., 59, 463-512.

McCann, S. B. and Cogley, J. G., 1972. Hydrological observations on a small arctic catchment, Devon Island. Can. Jour. Earth Sci. 9, 361-65.

_____, Howarth, P. J. and Cogley, J. G., 1972. Fluvial processes in a periglacial environment : Queen Elizabeth Islands, N.W.T., Canada. Trans. Inst. Brit. Geogr., 55, 69-82.

_____, Cogley, J. G., Woo, M-K and Blachut, S. P., 1973. Hydrological studies, south central Ellesmere Island. Unpub. report to Glac. Div., Water Resources Branch, Dept. of Environment, 153p.

_____, James, W., Cogley, J. G. and Taylor, R. B., 1972. A hydrological and coastal reconnaissance of south central Ellesmere Island. Unpub. report to Glac. Div., Water Resources Branch, Dept. of Environment, 125p.

McDonald, B. C. and Banerjee, I., 1971. Sediments and bed forms on a braided outwash plain. Can. Jour. Earth Sci., 8, 1282-1301.

Norris, A. W., 1963. Upper Vendom Fiord. In Fortier, U.O., et al., Geology of the north-central part of the Arctic Archipelago, N.W.T., (Operation Franklin). Geol. Surv. Can., Memoir 320, 338-54.

Novak, I. D., 1973. Predicting coarse sediment transport : the Hjulstrom curve revisited. In Morisawa, M., Ed., Fluvial Geomorphology. 4th An. Geomorphology Symposium, State Univ., New York, 11-25.

Østrem, G. and Stanley, A., 1969. Glacier mass balance measurements: a manual for field and office work. Inland Waters Branch, Dept. of Environment, Reprint Ser. 66, 119p.

_____, Bridge, C. W. and Rannie, W. F., 1967. Glacio-hydrology, discharge and sediment transport in the Decade Glacier area, Baffin Island, N.W.T. Geog. Ann., 49A, 268-82.

_____, Ziegler, T. and Ekman, R. S., 1970. Slaintransportunder-sokelser i Norkse Bre-elver 1969. Norges Vassdrags og Elektrisitetsvesen, Rapport 6/70, 68p.

Pissart, A., 1967. Les modalites de l'ecoulment de l'eau sur l'ile Prince Patrick (76° lat. n., 120° long. o., Arctique Canadien). Buil. Peryglac. No. 16, 217-24.

Rapp, A., 1960. Recent development of mountain slopes in Karkevagge and surroundings, northern Scandinavia. Geog. Ann., 42, 65-200.

Raudkivi, A. J., 1967. Loose Boundary Hydraulics. Pergamon Press, 331p.

Rudberg, S., 1963. Geomorphological processes in a cold, semi-arid region. In Muller, F., Ed., Axel Heiberg Prelim. Report 1961-62. Jacobsen-McGill Axel Heiberg Exped. McGill Univ., 139-50.

Sundborg, A., 1956. The River Klaralver - a study of fluvial processes. Geog. Ann., 38, 127-221.

Tarr, R. S., 1897. Rapidity of weathering and stream-erosion in the arctic latitudes. Am. Geol., Feb., 1897, 131-36.

Thorarinsson, S., 1939. Hofellsjokull, its movements and drainage, chp. 8 of Vatnajokull - scientific results of the Swedish-Icelandic investigations, 1936-38. Geog. Ann., 21, 189-215.

Thorsteinsson, R., 1972. Geology, Strathcona Fiord, District of Franklin. Geol. Surv. Can., Map 1307A.

_____ and Tozer, E. T., 1960. Summary account of structural history of the Canadian Arctic Archipelago since Precambrian time. Geol. Surv. Can., Paper 60-7, 25p.

Tricart, J., 1969. Geomorphology of cold climates (Watson, E., Trans.) MacMillan, 320p.

Sellers, W. D., 1965. Physical Climatology. The Univ. of Chicago Press, 272p.

Smith, D. G., 1973. Aggradation of the Alexandra-North Saskatchewan River, Banff Park, Alberta. In Morisawa, M., Ed., Fluvial Geomorphology. 4th Geomorphology Symposium, State Univ. New York, 201-19.

Smith, N. D., 1974. Sedimentology and bar formation in the Upper Kicking Horse River, a braided outwash stream. Jour. Geol., 82, 205-23.

Wigham, J. M., 1970. Sediment transportation. In Gray, D. M., Ed., Handbook on the Principles of Hydrology. Canadian National Committee for I.H.D., 11.5 - 11.25.

Williams, P. P. and Rust, B. R., 1969. The sedimentology of a braided river. Jour. Sed. Petrol., 39, 649-79.

Wolman, M. G., 1954. A method of sampling coarse river-bed material. Am. Geophys. Union Trans., 35, 951-56.

_____ and Brush, L. M., 1961. Factors controlling the size and shape of stream channels in coarse, non-cohesive sand. U.S. Geol. Surv., Prof. Paper 282-6, 28p.

Yalin, M. S., 1973. Research contributions to mechanics of sediment transport. In Fluvial Processes and Sedimentation. Hydrology Symposium No. 9, Univ. of Alberta, 698-711.

APPENDIX A

DISCUSSION OF METHOD USED FOR OBTAINING COARSE SIZE DATA OF SURFICIAL SEDIMENTS OVER THE SCHEI SANDUR

The following represents a summary and discussion of a technique devised by M. Church for acquiring mean cobble size data in coarse gravel and cobble deposits. Usage of the method has been employed without the original author's knowledge or consent. Any errors, alterations, or shortcomings in the application of the method to the Schei sandur must be attributed to the writer and not the original author. Description of the method originally appeared as an unpublished manuscript under the title of "A Relatively Painless Method of Obtaining Mean Cobble Size Data on Coarse Clastic Surfaces".

The method used in obtaining the mean size of coarse material, involved randomly placing a quadrat frame on the surface of a pre-determined sampling site and photographing the quadrat from as near vertically overhead as possible. Subsequent analysis for each quadrat photograph involved counting the number of coarse clasts within the quadrat and converting this result to a mean size for the sample, based on a relationship between the number of clasts counted and the mean sample size (control curve). This control curve relationship was

obtained by using ten control samples from the field study, initially assumed to represent the complete mean grain size variation of the coarse material over the sandur surface.

Figure A.1 illustrates two of the control samples used, showing the clast size variation in the proximal and medial portions of the sandur.

Each control sample was initially photographed at the sampling site, and then the b-axis lengths of all the clasts within the quadrat likely to be counted on the photograph, were measured.

The mean size of each control sample was determined by the size distribution of the coarse material, derived from phi groupings of the b-axis diameters. Figure A.2 illustrates the cumulative grain size distributions for the Schei sandur control samples, plotted as cumulative percent coarser by number. The grouped data was analyzed by the number of clasts, instead of the weight, to reduce any influence on the determined mean by the petrology of the clasts. The derived means from the size distributions were based on Folk and Ward's (1957) graphic mean, where:

$$M = \frac{\emptyset 16 + \emptyset 50 + \emptyset 84}{3} \qquad (A.1)$$

Note that the distributions are constrained at the lower limit, due to the 8 mm b-axis length used as the distinction between coarse and

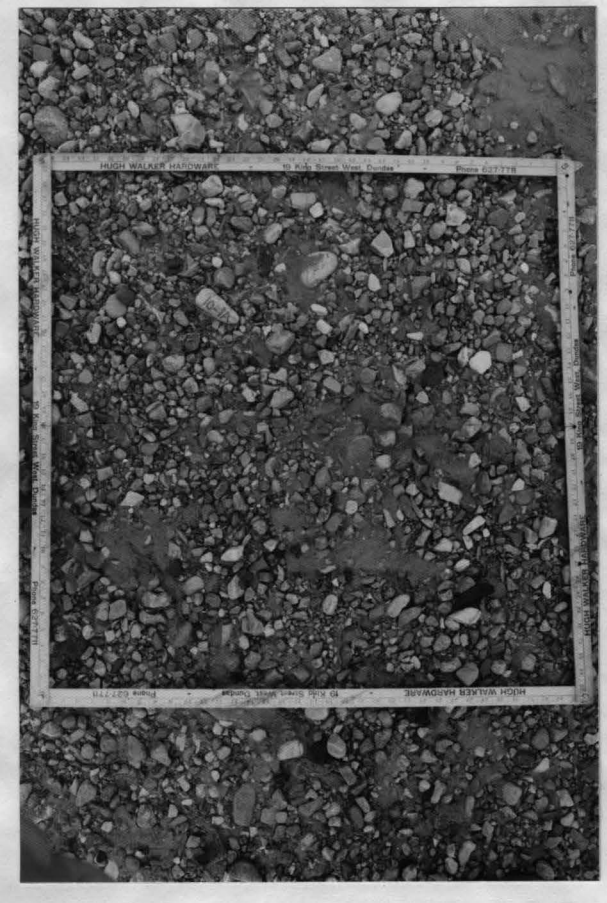

Quadrat 10-1a
Sampling Position (1959,588)

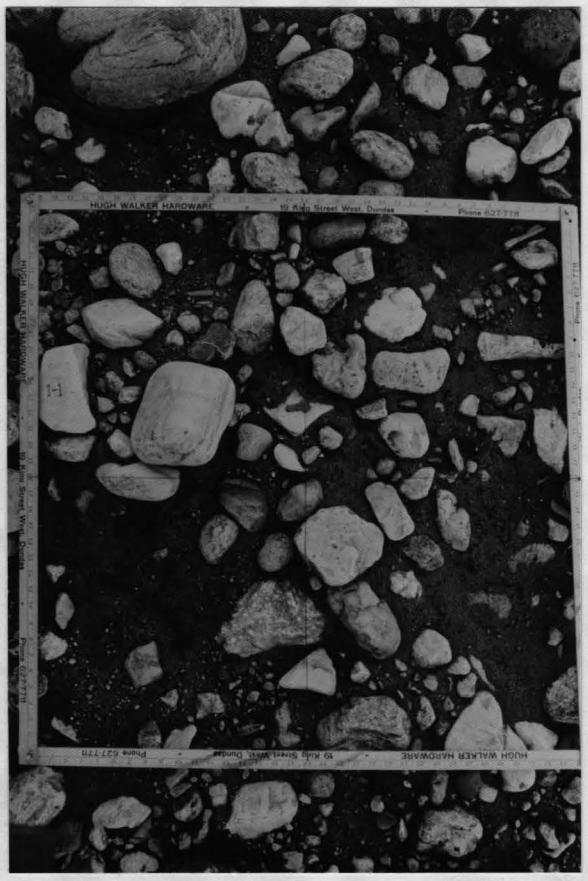

Quadrat 1-1
Sampling Position (100,700)

Figure A.1 Two control examples from the Schei sandur showing fairly homogeneous samples of cobbles of different mean size.

The quadrat is slightly less than one metre square. The photographs are smaller than the size used in the analysis.

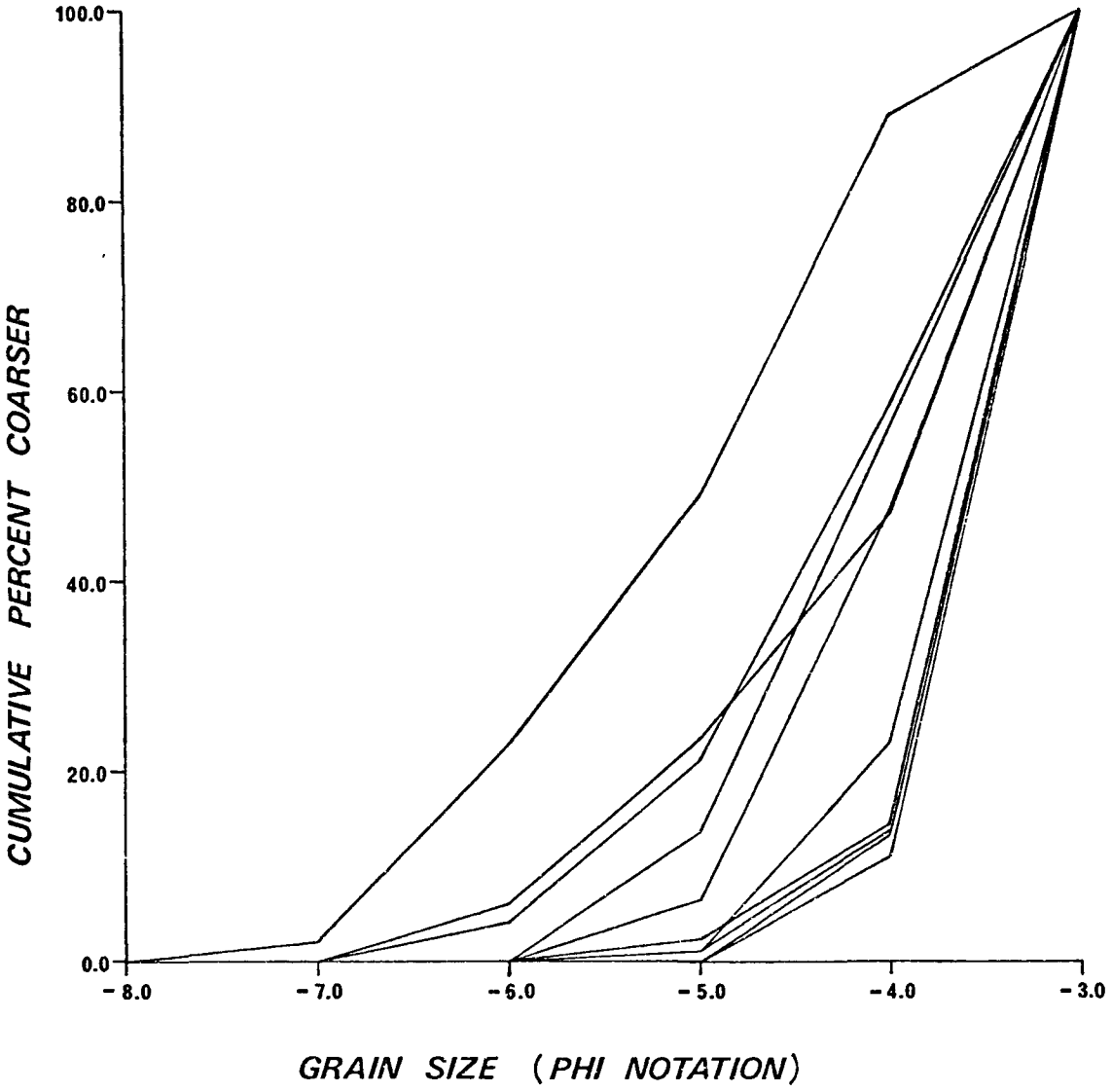

Figure A.2

Control sample cumulative distributions of grain size for the coarse materials on the Schei sandur.

fine materials. The range of the sampled coarse materials varied from 8 mm to 210 mm in b-axis length, corresponding to a -3 phi to -7 phi variation in grouped data. Table A.1 shows the control sample data calculated for the Schei sandur.

The relationship between the mean coarse clast size and the number of clasts counted is based on the fact that the larger the mean size, the fewer the number of clasts appearing within a given area, or the quadrat. As fine matrix material (less than 8 mm size) inevitably is present in all the samples, the coarse clasts appearing in the quadrat will not completely occupy the total area of the quadrat, and hence the number of clasts counted must be adjusted to give an equivalent number of similar size clasts which would be counted if no fine material were present, and the quadrat were fully occupied. This adjustment factor required is a ratio of the total quadrat area, divided by the area covered by clasts, or the percentage of clast material within the quadrat. The adjustment factor for the control samples and the remaining samples over the sandur was calculated by using a regular point grid laid over each photograph and computing the clast percentage by a point count technique of approximately 200 points.

This correction factor applied to the number of clasts counted, preserves the relationship between the mean size of the coarse material and the number of counted clasts in the quadrat.

TABLE A.1

CONTROL SAMPLE DATA FROM THE SCHEI SANDUR

Quadrat Number	Total Point Count	Cobble Point Count	Adjustment Factor	Number of Cobbles Counted	Adjusted Number of Cobbles Counted	Number of Cobbles Measured	Calculated Mean Cobble Size (mm)	Mean Cobble Size (mm)
1.1	196	83	2.36	159	375.2	173	28.3	35.0
2.1	196	109	1.80	256	480.8	654	24.6	20.4
4.1	196	85	2.31	268	619.1	597	21.3	21.0
5.4	196	48	4.08	194	791.5	529	18.5	19.3
6.4	196	64	3.06	318	973.1	933	16.5	17.4
10.3A	196	70	2.80	333	932.4	239	16.9	13.6
10.3	196	37	5.30	309	1637.7	213	12.3	13.8
10.2A	196	39	5.03	251	1262.5	181	14.2	14.8
10.2	196	31	6.32	209	1320.9	181	13.9	13.9
10.1A	196	96	2.04	626	1277.0	254	14.1	13.8

Total quadrat space is assumed utilized in the adjustment, with a packing coefficient not introduced into the adjustment. A factor affecting the complete space utilization of the quadrat (especially in relatively coarser sized material) occurs with clasts partially lying outside the quadrat, exceeding the quadrat space, and increasing the mean size of the clasts. This situation was dealt with by accepting a clast in the count only if more than half of that clast lay inside the quadrat.

It can be seen in Table A.1 that discrepancies occur between the number of clasts measured in the field and the number of clasts counted. This is due to clasts concealing each other in the photograph, possible poor resolution effects, measuring clasts in the field which do not appear on the photograph, or counting errors of the clasts (especially in the relatively finer coarse materials). Generally the number of clasts measured in the field show no relationship to the mean size (a relationship will only occur if the measured clasts are corrected by an adjustment factor to preserve the relationship).

The control sample data for the Schei sandur was found to fit the following relationship of the form:

$$Y = aX^{b} \qquad (A.2)$$

The derived regression for the control data yielded

$$\overline{B} = 804.55\ N^{-0.565} \qquad r = -.90 \qquad (A.2a)$$

Where $\overline{B}$ is the nominal clast diameter and N the number of clasts counted on the photograph.

This relationship was used to construct the control curve illustrated in Figure A.3, which determines the mean size of the coarse materials for the remaining sample photographs. Data for the remaining samples is listed in Table A.2, except for samples in the distal portion of the sandur where the mean size was calculated from grain size cumulative distribution curves of the coarse materials. Figure A.4 shows the distributions of these samples, with the mean grain size of the samples presented in Table A.3.

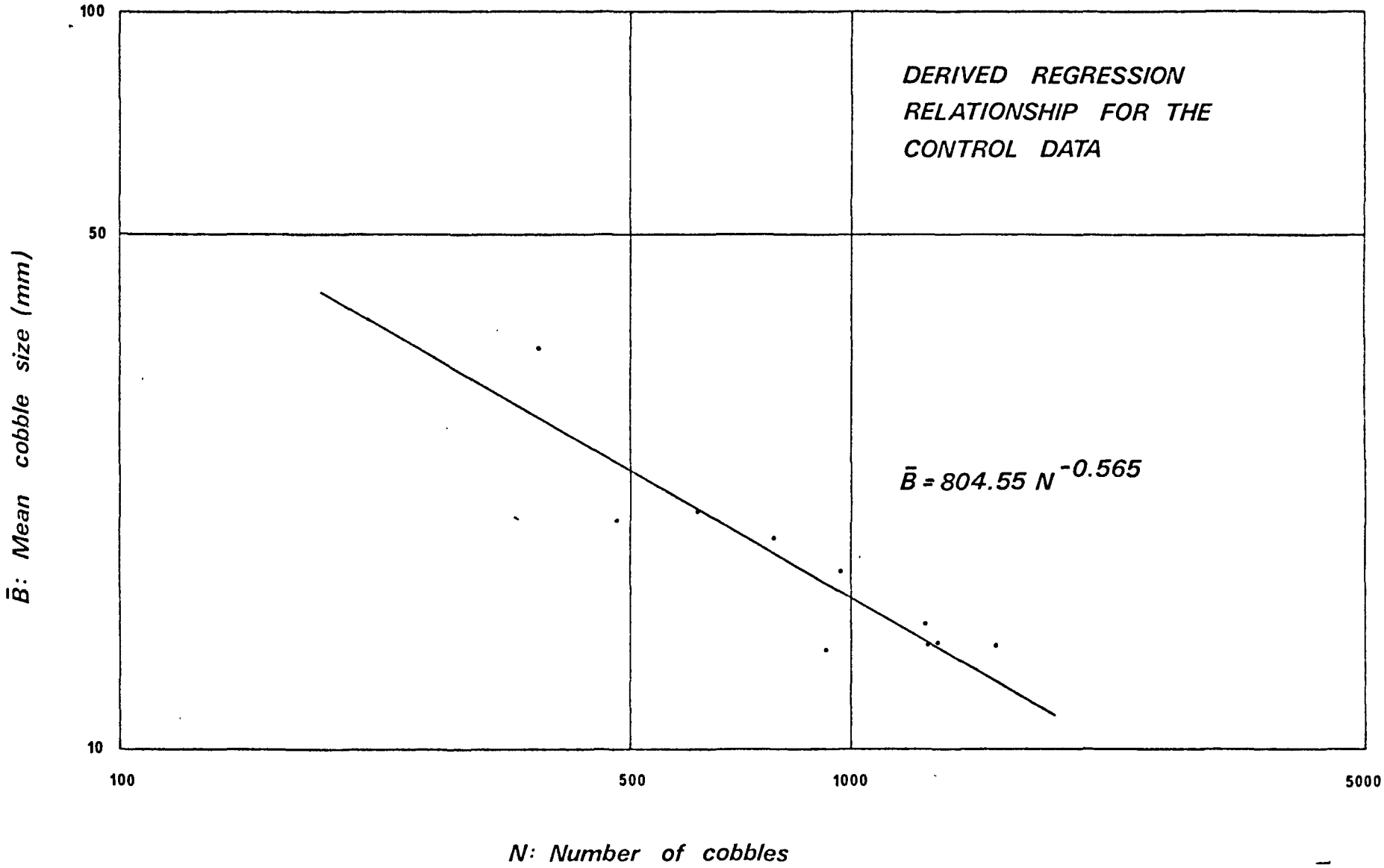

Figure A.3 Plot of the regression of the data used in the operational control curve.

TABLE A.2

CALCULATED MEAN COBBLE SIZE FOR SAMPLES OVER THE SCHEI SANDUR IN THE PROXIMAL AND MEDIAL PORTIONS

Quadrat Number	Total Point Count	Cobble Point Count	Adjustment Factor	Number of Cobbles Counted	Adjusted Number of Cobbles Counted	Calculated Mean Cobble Size (mm)
2.1A	196	82	2.39	138	329.8	30.4
3.1	196	77	2.55	142	362.1	28.8
3.1A	196	74	2.65	204	540.6	23.0
3.2	196	83	2.36	205	483.8	24.5
4.1A	196	85	2.31	288	665.3	20.4
4.2	196	79	2.48	239	592.7	21.8
4.2A	196	48	4.08	142	579.4	22.1
5.1	196	62	3.16	115	363.4	28.8
5.1A	196	91	2.15	304	653.6	20.6
5.2	196	107	1.83	311	569.1	22.3
5.2A	196	44	4.45	126	560.7	22.5
5.3	196	70	2.80	189	529.2	23.3
5.3A	196	78	2.51	208	522.1	23.4

TABLE A.2

CALCULATED MEAN COBBLE SIZE FOR SAMPLES OVER THE SCHEI SANDUR IN THE PROXIMAL AND MEDIAL PORTIONS

Quadrat Number	Total Point Count	Cobble Point Count	Adjustment Factor	Number of Cobbles Counted	Adjusted Number of Cobbles Counted	Calculated Mean Cobble Size (mm)
6.1	196	86	2.28	169	385.3	27.8
6.1A	196	63	3.11	235	730.9	19.4
6.2	196	53	3.70	147	543.9	22.9
6.2A	196	55	3.56	181	644.4	20.8
6.3	196	86	2.28	210	478.8	24.6
6.3A	196	55	3.56	197	701.3	19.8
6.4A	196	40	4.90	142	695.8	19.9
7.1A	196	62	3.16	240	758.4	19.0
7.2	196	44	4.45	142	631.9	21.0
7.2A	196	30	6.53	90	587.7	21.9
7.3	196	61	3.21	171	548.9	22.8
7.3A	196	70	2.80	192	537.6	23.0
7.4	196	48	4.08	143	583.4	22.0

TABLE A.2

CALCULATED MEAN COBBLE SIZE FOR SAMPLES OVER THE SCHEI SANDUR IN THE PROXIMAL AND MEDIAL PORTIONS

Quadrat Number	Total Point Count	Cobble Point Count	Adjustment Factor	Number of Cobbles Counted	Adjusted Number of Cobbles Counted	Calculated Mean Cobble Size (mm)
8.2	196	59	3.32	191	634.1	21.0
8.2A	196	59	3.32	217	720.4	19.5
8.3	196	39	5.03	157	789.7	18.6
8.3A	196	35	5.60	186	1041.6	15.9
8.4	196	34	5.76	198	1140.5	15.1
9.2	196	53	3.70	200	740.0	19.3
9.2A	196	31	6.32	164	1036.5	15.9
9.3	196	56	3.50	165	577.5	22.1
9.3A	196	40	4.90	132	646.8	20.8
9.4	196	25	7.84	79	619.4	21.3

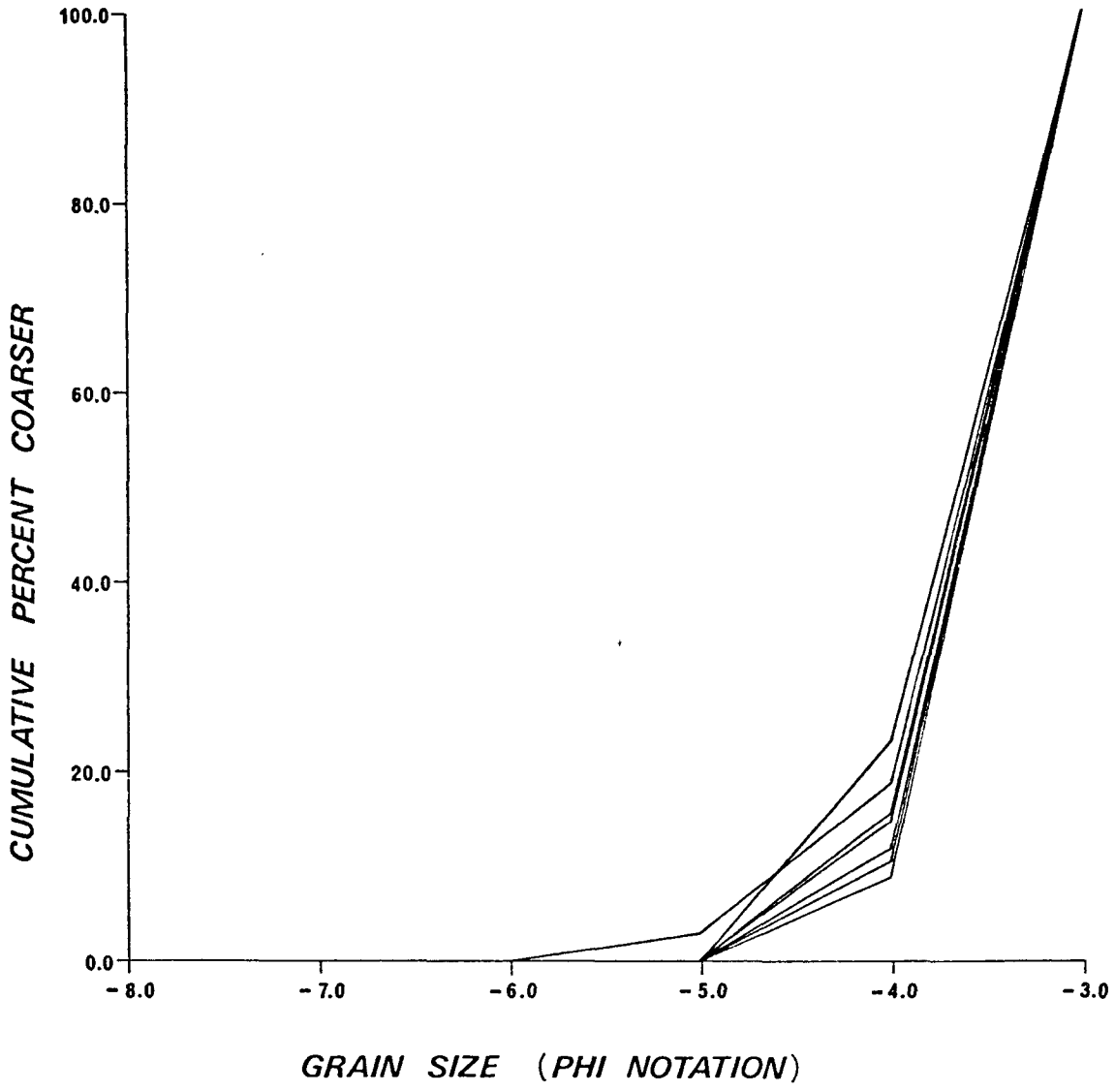

Figure A.4 Sample cumulative distributions of grain size for the coarse materials in the distal end of the Schei sandur.

TABLE A.3

MEAN COBBLE SIZE FOR SAMPLES
IN THE DISTAL PORTION OF THE SCHEI SANDUR

Quadrat Number	Mean Cobble Size (mm)
11-1A	13.6
11-2	13.8
11-2A	13.6
11-3	14.2
11-3A	13.9
12-1A	13.4
12-2	14.4

Limitations and operational problems in the use of the method include the following:

1. Rapid variations in the size of the coarse materials adjacent to a sampling site. An assessment was made to determine if the position of the quadrat was obviously anomolous, after dropping the quadrat frame near a sampling site. This may have introduced bias in the ideal of random sampling, although the field procedure involved dropping the quadrat frame within 3 m of a sampling site in what was deemed fairly homogenous material typical of the sandur surface at that site.

2. When the size of the coarse materials approach the size of the quadrat, errors will arise in the determination of the mean size. Although this problem exists in the method, coarse materials of a size approaching the limitations of the quadrat were not encountered on the Schei sandur.

3. The method should be used only if the size characteristics of the coarse materials is required. No information can be gained on the skewness, kurtosis, sorting, or shape of the coarse materials, although the use of colour film would allow petrologic information to be gained.

4. 35 mm SLR cameras with a moderate wide angle lens were preferred for the photography. A normal lens would not allow a photograph to be taken from a near vertical position over the quadrat, and hence influences the final product because a considerable number of clasts might be obscured. Distortion by a wide angle lens was found to be minimal, and has no significant influence on the analysis.

5. For larger values of N (the number of cobbles counted), the control difference (the difference between the counted clasts and the clasts measured in the field) becomes larger, but reflects a smaller change in the mean derived clast size and hence tends to balance the control difference effect.

The method as defined by Church and described here is considered to be a relatively accurate and fast procedure for obtaining mean grain size data of sandur-type deposits.

APPENDIX B

STAGE-DISCHARGE RATING CURVE DERIVED FOR THE 1974 SEASON